LUND UNIVERSITY

MASTER THESIS

Estimation of the absorbed dose to patients treated with ^{177}Lu-Dotatate with regards to the long-term retention and radionuclide impurity in the form of ^{177m}Lu

Dissertation of Edita MJEKIQI

Supervisors:
Katarina Sjögreen Gleisner - Associate Professor
Erik Larsson - PhD
Medical Radiation Physics

ABBREVIATIONS

PRRT	Peptide Receptor Radionuclide Therapy
RNT	Radionuclide Therapy
NaI(TI)detector	Sodium Iodide (Thallium) detector
HPGe detector	High Purity Germanium detector
PMT	Photomultiplier Tube
ADC	Analogue to Digital converter
AE	Auger electrons
MCA	Multi-channel Analyzer
IT	Isomeric Transitions
A_{tot}	Total Activity
λ	Decay constant
As	Specific Activity
c.a	carrier added
TB	Total Body
ϵ	Photo-peak Efficiency
FWHM	Full Width at half-maximum
CPS	Counts per Second
ROI	Region of Interest
RNP	Radionuclide Purity
CT	Computed Tomography
SPECT	Single Photon Emission Computed Tomographic images
AUC	Area under the curve
3D	Three dimensional
ICRP	International Commission on Radiological Protection
MIRD	Medical Internal Radiation Dose Committee
D	Absorbed Dose
$\overline{D}$	Mean Absorbed Dose
$\tilde{A}$	Total Cumulated Activity
F	Specific Absorbed Fraction
DFs	Dose Factors

Table of Contents

ABSTRACT

The use of radio-labeled somatostatin analogs, such as ^{177}Lu-labelled DOTATATE, in PRRT, has based on the studies performed until now, shown to be promising for RNT disseminated neuroendocrine tumors [1]. In this regard, the aim of treatment is to assure the delivery of the highest possible absorbed dose to the tumor cells, while saving the normal tissues [1], meaning, to achieve a higher activity uptake in tumors with neuroendocrine origin while assuring the lowest possible radio-toxicity in normal organs [2].

The key challenge associated with the absorbed dose distribution in the body upon administration of PRRT using ^{177}Lu-DOTATATE is the absorbed dose to the kidneys, as being the dose limiting organs in PRRT [7]. The main excretion route of ^{177}Lu-DOTATATE is through urine, where >65% of the total administered activity is excreted. This has lead us to investigate the long time retention of ^{177}Lu in the total body, and also to estimate the absorbed dose given by possible radionuclide impurities.

According to the declaration from the producer, a sample of ^{177}Lu contains less than 0.05% of ^{177m}Lu. In order to investigate whether the ^{177m}Lu contribution to the absorbed dose is as low that it can be tolerated or even neglected, spectroscopy measurements have been performed on patients receiving therapy with ^{177}Lu-DOTATATE at Skåne University Hospital [15]. Prior to performing these measurements, the spectroscopy equipment has been carefully calibrated. The data obtained from patient measurements have been analyzed using different methods, and have been combined with imaging based data, obtained as part of the routine dosimetry performed at Skåne University Hospital.

INTRODUCTION

In radionuclide therapy (RNT), a radioactively labeled pharmaceutical is used for patient treatment. The underlying idea of RNT is that the pharmaceutical is designed to accumulate in the target tissue, e.g. the tumor. The radioactive label is thus carried to the tumor, and at decay by particle emission an absorbed dose is delivered for the internal radiation treatment.

The administered therapy activity of ^{177}Lu-Dotatate is excreted through urine, and a concern is therefore the retention of ^{177}Lu activity in the kidneys, with possible renal damage as side effect of the treatment.

Currently, a clinical patient trial is being performed at the clinic of Oncology, Skåne University Hospital, where patients with disseminated neuroendocrine tumors are being treated with ^{177}Lu-[DOTA0,Tyr3] Octreotate (also termed ^{177}Lu-DOTATATE). The radionuclide ^{177}Lu disintegrates by beta-decay and emits electrons that are used for induction of the absorbed dose. ^{177}Lu also has gamma-emissions, allowing for external measurement of the radiopharmaceutical distribution, using a gamma camera. By imaging at several times after injection, the radiopharmaceutical distribution over time is measured.

Production of ^{177}Lu can be performed in two ways, both involving neutron activation. One of the production paths also produces a small amount of metastable ^{177m}Lu. Owing to the small amount of ^{177m}Lu, the absorbed dose induced by ^{177m}Lu is normally not considered in the calculation of the absorbed dose. However, considering the physical half-lives of ^{177}Lu and ^{177m}Lu, which are 6.7 and 160.4 days respectively, there may be a non-negligible contribution from ^{177m}Lu.

In the standard procedures for patient dosimetry, the long-term retention of ^{177}Lu /^{177m}Lu -DOTATATE is not measured. Instead, it is extrapolated from imaging measurements performed during the first week after administration.

The aim of this study is to investigate some of the research questions coupled with renal dosimetry of patients treated with ^{177}Lu-DOTATATE.

The specific aim is to investigate the long-term retention of ^{177}Lu /^{177m}Lu -DOTATATE, by using gamma spectrometry measurements during the first or second months after administration, as a complement to routine imaging-based studies. Furthermore, the project aims to make dosimetric conclusions based on these new long-term data.

For this purpose, a method for the estimation of the activity at different time points and determination of the absorbed doses has been developed.

A methodology for the estimation of TB Activity has been established using NaI(TI) and HPGe detector systems. A well defined calibration geometry for measurement of reference sources of ^{57}Co and ^{137}Cs has been established because these radionuclides emits gamma energies close to the gammas of ^{177}Lu at 208 keV and ^{177m}Lu at 378 keV, 418 keV, respectively. Careful measurement of the background and subsequent subtraction has been also performed. Spectral data analysis was performed both automatically, using the Maestro spectrometry software, and manually using Excel, values of the number of counts versus the channel number. Here, the detector efficiency and the energy resolution were determined.

A brief introduction to PPRT and the detector systems will be described. The production routes of ^{177}Lu and its decay scheme as well as the decay scheme of ^{177m}Lu will also be presented. As the aim of the study is associated with the activity determination of ^{177}Lu at different time points and the contribution of ^{177m}Lu *(based on the decay scheme)*, a detailed observation on the outcomes will be presented. The results obtained will be further discussed under the chapter ***Results*** and a comparison on the Activity determination outcomes using the internal radiation dosimetry will also be addressed.

I. Radiation Therapy/Peptide Receptor Radionuclide Therapy

The use of radio-labeled somatostatin analogs in PRRT, has shown to be promising for the RNT treatment of neuroendocrine tumors [1]. The main challenge associated with this kind of treatment is to assure the delivery of the highest activity in the tumor cells, while saving the normal tissues [1]. The aim is to achieve a higher uptake from tumors with neuroendocrine origin while assuring a lowest possible radio-toxicity in normal organs [2]. The ^{177}Lu-DOTATATE has shown a high level of absorption in tumor tissue with a very high affinity [3].

In PRRT the excretion from the body is mainly done through the kidneys, leading to the concern that kidneys are the main organ at risk with a high retention of radioactivity considered to be a dose limiting organ for the PRRT use. By evaluating the absorbed dose to the kidneys, it is believed that renal damage from the radiation therapy can be reduced [7, 1].

II. Gamma – Ray Spectroscopy

The γ-ray, an electromagnetic radiation produced by nuclear reactions, is characterized by a high energy and short wavelength in the electromagnetic spectrum. This high energy may cause damage when it is absorbed by living cells.

The electromagnetic nature of γ-ray photons, enables a strong interaction with the charged electrons in the atoms of matter. Therefore, the detection of γ-rays depends on the interaction process of γ-ray photons, which causes a trasnfer of all or part of the photon energy to the electrons, withing the absorbing material. The electrons created as a result of γ-ray interactions will be characterized with an equal E_{max} to that of γ-ray photons. During the interaction process, they will loose some energy and as a result will slow down. The energy loss is as a result of the excited atoms and Bremstrahlung emission withing the material. Finally, as a result the released charge by electrons will be collected by the PMT and detector electronics, and an electronic pulse is generated with a height that is proportional to the deposited radiation energy. This thus enables identification of the gamma energy [39].

At β- decay of a radioactive isotope, it eventually reaches the ground state of the daugter isotope. It may decay to excited states, which upon deexcitation causes a subsequent release of energy by emission of γ-rays. The γ-ray energies can be detected and measured by employing a suitable detector system which is useful for γ-ray energy detection as well as the determination of the activity of the source [38,39].

There are several factors associated with the impact and choice of the detector system to be used: particle range, energy resolution, efficiency, count rate performance and price.

For the purpose of this study two different types of detector systems for γ-ray spectroscopy have been used: the standard NaI(Tl) detector system and a HPGe detector system (which has a high energy resolution and lower background noise).

II.1 NaI(TI) Scintillation Detector System

For this project a NaI(TI) solid state scintillation detector system has been used. The crystal is bounded with a reflective material to minimize the loss of scintillation light. A layer of Aluminum is also used for protection of the sensitive crystal and also because of the hygroscopic behavior of NaI (a salt). The crystal is optically coupled to a PMT. The PMT consists of a photocathode followed by a series of dynodes ending at the anode. In the photocathode through the photoelectric absorption of photons, the release of electrons is caused in the vacuum of the PMT [27, 38, 39].

The γ-rays may deposit energy when interacting with the scintillator and the pulse size from the detector depends on the γ-ray energy that has been deposited in the scintillator. The points of photon interaction within the detector crystal are homogenously distributed for higher photon energies. For lower energies, the interactions mostly are in the front side of the crystal volume [38, 39]. The interaction of γ-rays with the NaI(TI) crystal can undergo different interaction processes: [38, 39]

- *Photoelectric absorption* – an interaction of a photon with the absorber atom, the photon vanishes and an energetic electron is ejected and the overall contact is made with the atom as a whole.
- *The Coherent Scattering* - during the interaction process of the incident γ-ray photon with the matter, causing an excitation of the atom, which then scatters. *The Compton Scattering* characterized as a process of the interaction of incident γ-ray with an orbital electron, and giving part of its energy to the orbital electron [38,39]. This process causes the ejection of the electron, and scattering of γ-ray photon (which carries radiation energy away from the detector material). Thus, the deposited energy in the crystal is smaller than for the photoelectric absorption process, and results in the detected energy spectrum as a continuous count distribution. When gamma photons are scattered in an angle approximately 120^0 – 180^0, more gamma energy is transferred to the electron, and as a result more energy is deposited within the crystal material. This is called the *Backscatter Peak* [9, 38, 39].

In our experiments Lead (Pb) was used as a shielding material by surrounding the detector system in order to minimize the effects of background γ radiation. In Pb collimator the photoelectric absorption occurs which leads to detection of *Characteristic X-Rays.* This is a result of the de-excitation of atoms in exited states, which exist only for a short time period when the orbital electrons change their configuration. When the atom reaches the lowest energy state, the energy is released in the form of Characteristic X-Rays or Auger electrons [39]. Furthermore, the characteristic X-rays can also be produced in NaI(Tl) scintillation detector, as a result of x-ray escape resulting to a peak at a lower energy at about 30 keV.

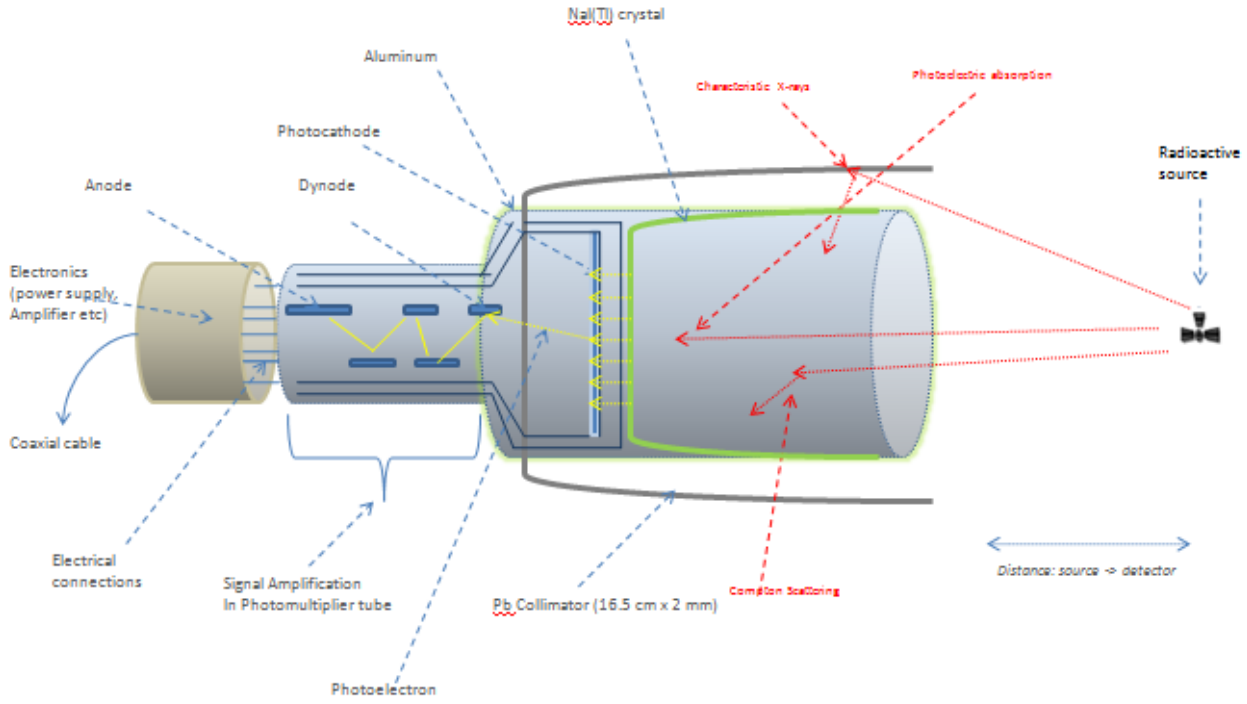

Fig. 1, Schematic illustration of NaI(TI) detector and γ-ray interaction processes during measurements

When the released electrons pass through matter they lose their kinetic energy as given by the stopping power: [38, 39]

$$S_p = -\frac{dE}{dx} \qquad (1)$$

A transformation of the deposited electron energy into light (photons) occurs since upon de-excitation light is produced. This light is reflected towards the photocathode of the PMT. The

scintillation photons passing through the photocathode eject electrons by the photoelectric effect, and then in a continuous process, the electrons pass through the chain of dynodes. In the PMT the electrons are accelerated by a strong electric field, causing the release of other electrons when they collide with the dynodes. When the last dynode is reached the electron cascade is transferred to the anode collector which is connected to the charge preamplifier which enables the conversion of the collected charge into a voltage pulse [38, 39]. As a final process the pre-amplified pulse through the linear amplifier is shaped and amplified. The number of photons detected in the scintillation crystal is proportional to the amount of γ-ray energy which is absorbed in the NaI(Tl) crystal [38.39]. The pulse decay time is about 0.25 microseconds in NaI(Tl) detector and the convertion into a pulse is 0.5 microseconds. In the analog-to-digital converter the pulse height is registered as counts corresponding to a specific deposited photon energy, which is displayed in the MCA [27, 38, 39].

The NaI(Tl) detector system used for conducting experiments was 3” x 3” Harshaw/Fllrol type 12S12/3A Serie CP-488 (660 V).

II.2 The HPGe Detector System [9, 10, 38, 39, 44]

The HPGe detector with high capacitance is used for detection of γ-rays. The Germanium crystal serves as a semiconductor, where an electronic signal is transmitted via mobile or "free" electrons and holes. If the crystal is doped with a small amount of impurity atoms the number of charge carriers increases. When a doped semiconductor can contain excess holes, it is then called a p-type detector. When it contains excess free electrons it is known as n-type detector.

When doped Ge and n-doped is put together, an electric field occurs in a small region near the joining, due to diffusion of electrons and holes. This region is called the depletion layer.

By putting a reversed voltage, meaning to couple the negative voltage to p-type region and positive voltage to n-type region, the depletion layer can be enlarged up to the Zener-limit. It is this layer which is used for detection of γ-rays. Due to the high purity Ge a relatively large voltage can be applied, creating a relatively large detector volume.

If not cooled, the excited electrons in the Ge crystal are followed by further excitation as a result of thermal energy. The HPGe detectors are mainly cooled by liquid nitrogen (LN_2)- in a thermal contact which allows cooling it at around -200^0 C, in order to reduce the thermal charge carrier generation (background noise) to a reasonable level. Their operation is thus mainly at low temperatures.

There are several types of HPGe detectors, depending on the configuration, energy range to be detected, shape of Ge crystal, applied voltage and γ-ray charge collection, for instance: ultra LEGe, Low energy Ge, broad energy Ge, coaxial Ge, reverse electrode and XrRa.

The incoming γ-rays gives their energy to electrons and during the trajectory of the electrons, inelastic collisions with atomic electrons will cause excitations of the electrons in the valence band to the conduction band. Secondary electrons thus create a bunch of electron hole-pairs during their trajectory in the detector. These are collected using an electric field producing a charge which is collected by the pre-amplifier. The holes travel in the opposite direction and can also be measured. The pulse size is proportional to the collected charge which is proportional to the deposited energy. The results are generated in the form of spectroscopic

data. Since the energies of γ-rays are known, this can provide useful information on the composition of an unknown sample.

The principles of operation thus includes the collection of the charge by the high voltage from the pre-amplifier, the produced charge from γ-radiation (from sample to the detector), amplifies it and produces a pulse “with amplitude proportional to the total charge”. The amplifier takes the pulse signal from pre-amplifier filters and shapes it in order to enhance the signal to noise-ratio. This also helps in avoiding the overlapping between the produced pulses. After the production of the analog signal from the detector by the amplifier, it will be converted into a digital signal using the ADC (analogue-to-digital converter) and finally it will be registered in the MCA software. The high-power voltage supply applied for HPGe detector system ranges from +1000-5000 V.

The most important characteristics for these kinds of detectors are the energy resolution for detection of small mass energy samples, data analysis with high level of precision and tolerance against high count-rates.

The HPGe detector used for our experimental purpose is an- ORTEC Detective DX, a p-type HPGe detector with coaxial construction, with crystal nominal dimensions of 50 mm diameter and 30 mm deep. It was cooled with electricity.

The crystal shielding material is from steel with dimension of 5mm, and the Input power from 10 to 17 V DC 30 W, and operation temperature ranges from 0°C up to 40° C.

III. Decay of ^{177}Lu and ^{177m}Lu

The radionuclide ^{177}Lu labeled to DOTATATE is used in clinical trials for in vivo therapy of neuroendocrine tumors. [2, 14, 16, 19]. Because of its nuclear decay characteristics and chemical properties [16], ^{177}Lu has shown impact on the renal toxicity [7] but in comparison to other available radionuclide, such as ^{90}Y it is considered to be a radionuclide which is better tolerated by the kidneys [10, 15].

The half life is 6.64 days [6, 18, 20] whereas other reported 6.734 days [17, 21], it emits β- particles with maximum energy of 498.3 keV with a penetration range of 2mm [13, 21] and decays to stable ^{177}Hf (through excited states of ^{177}Hf). The decay scheme is shown below: [14,15, 18 20].

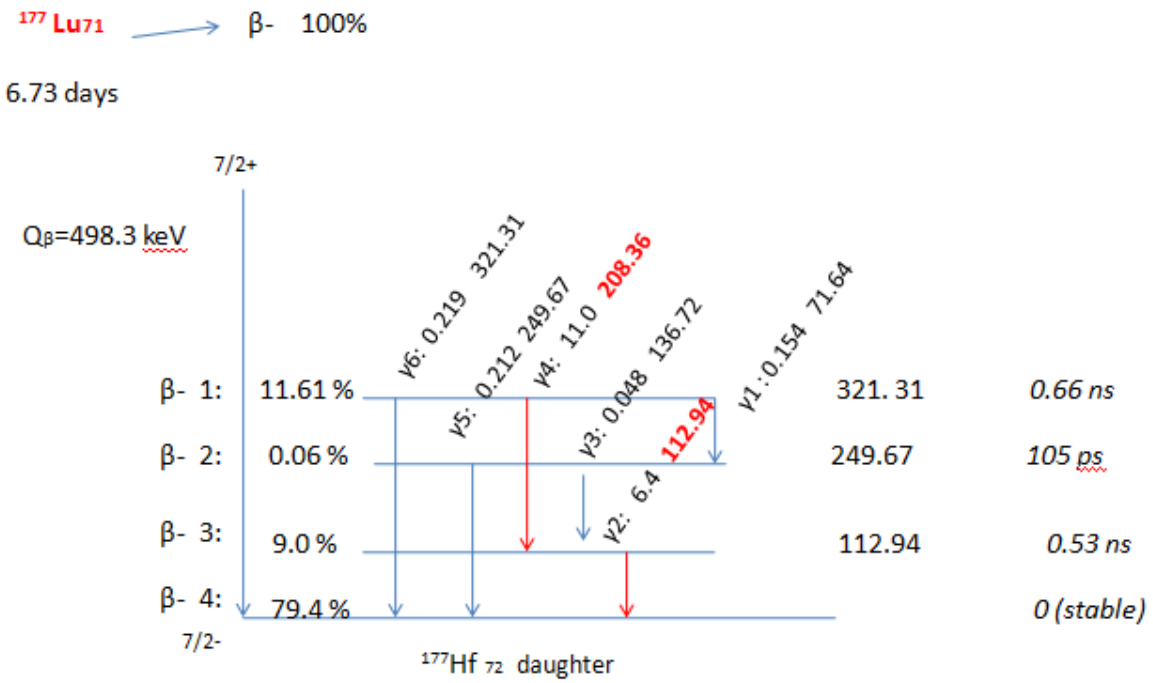

Fig.2, Reproduced decay scheme of ^{177}Lu from Nuclear Decay Data Scheme [42]. *(Marked in red color are the gamma-energies used for measurement).*

As seen from the decay scheme, its disintegration is mainly done by β- emission in 79.4% to the ground state of ^{177}Hf with maximum β- energy of 498.3 keV. Moreover, there is also a β- emission in 11.61% to 321.31 keV, in 9.0% to 112,94 keV while only a small fraction of 0.06% to 249.67 keV. As consequence of de-excitation of the excited states, gamma-radiation is emitted

and the most intense gamma rays are at energies of 112.94 keV and 208 keV, with abundances of 6.4% and 11%, respectively [6, 12, 13, 16, 18, 42]. These are useful for imaging purposes which enables a proper monitoring of in vivo localization of the injected ^{177}Lu-DOTATATE as well as reliable dosimetric estimations [12, 14, 18, 20, 42].

As it decays by β- decay it emits electrons which have a short path length, i.e they deposit their energy locally thus giving a high absorbed dose [13].

The manufacturer specification for the ^{177}Lu radionuclide purity is >99%, while <0.05% is ^{177m}Lu and 0.01% of other impurities with a specific activity of 7400 MBq at the calibration time [22]. For this purpose the decay scheme and further investigation of the ^{177m}Lu activity within the ^{177}Lu sample, has been made [15]. The decay scheme of ^{177m}Lu is shown below:

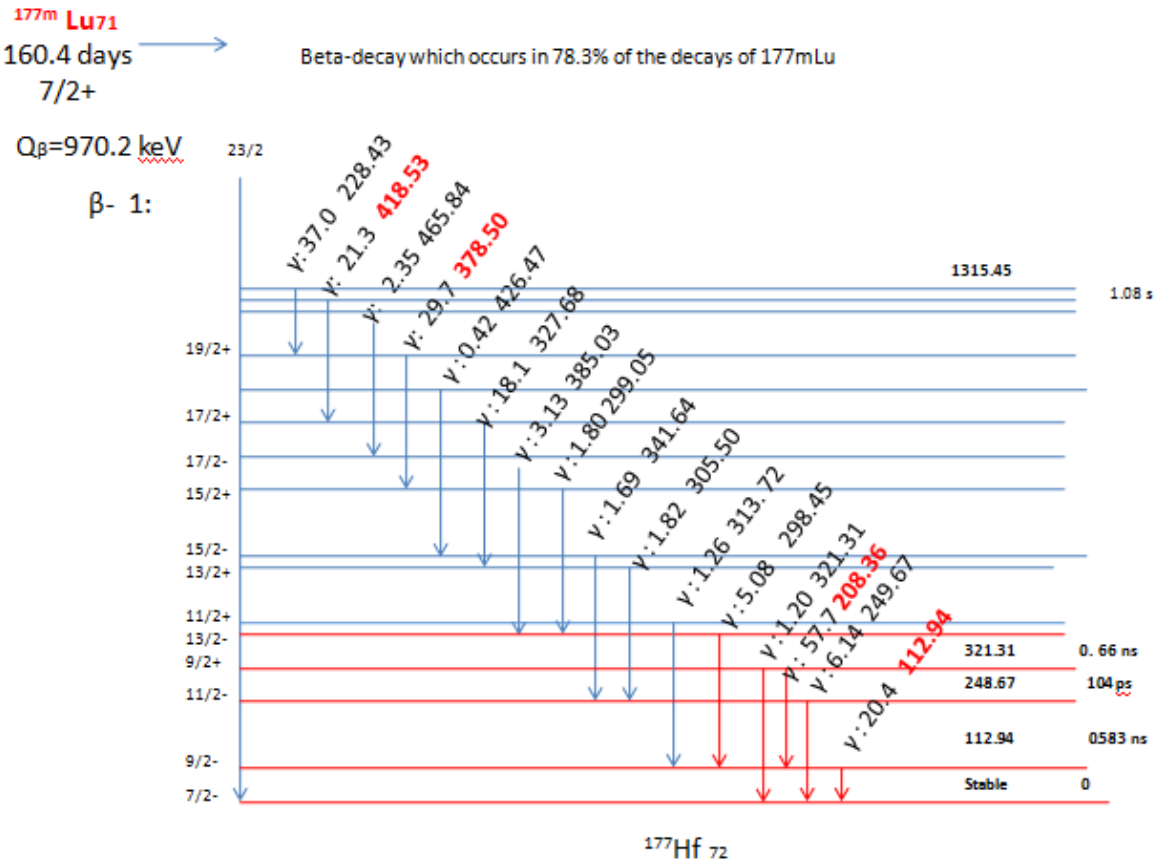

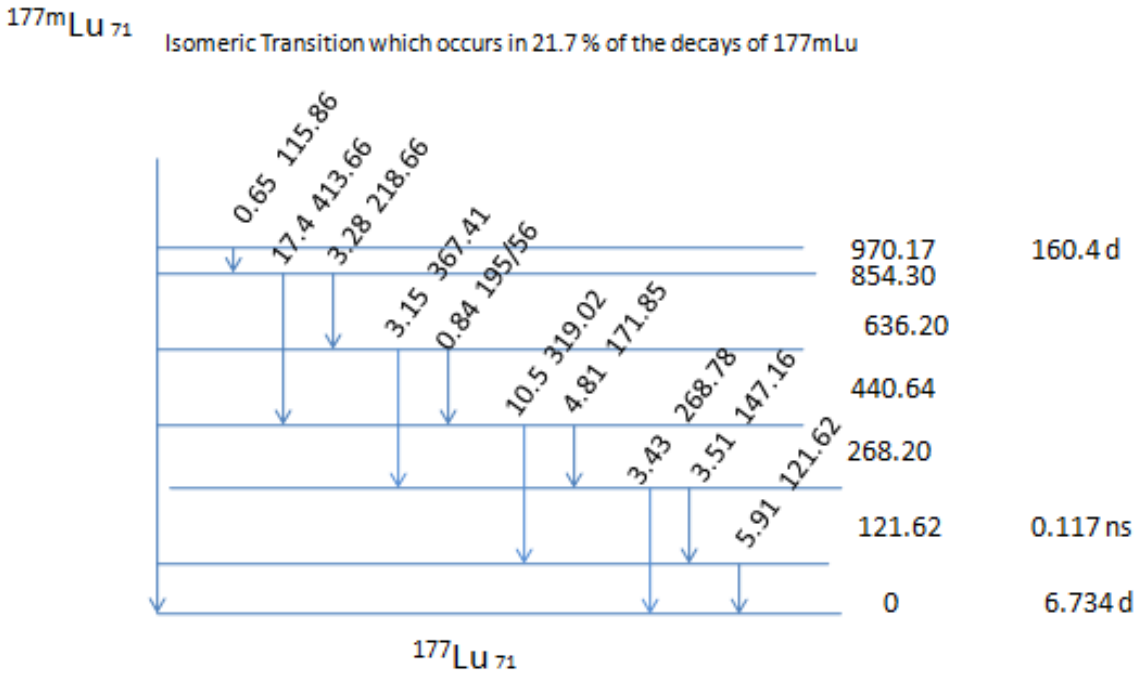

Fig. 3, Decay Scheme of ^{177m}Lu reproduced from Nuclear Data Decay Scheme [42]. *(Marked in red are the gamma energies used for measurement).* Note that the daughter product of the isomeric transition is ^{177}Lu which in turn decays through the scheme depicted in Figure 2, to ^{177} Hf.

Therefore, the administered activity contains both ^{177}Lu and ^{177m}Lu at unknown relative amounts. ^{177m}Lu decays partially to ^{177}Lu at 21.7% by isomeric transition through γ-emission, and partially at 78.3% by β-decay to ^{177}Hf which also is the decay product of ^{177}Lu. The half-life of ^{177m}Lu is 160.4 days.

The ^{177m}Lu can be used for γ-ray efficiency calibration purposes as a standard manner because of its emission probability [10]. Its half life of 160.4 days is considered to be relatively long and by the isomeric transition ^{177}Lu is also produced at decay.

Thus, ^{177m}Lu decays partially through β-decay to ^{177}Hf, with a long half-life of 160.4 days and partially through γ-emission, towards the ^{177}Lu ground state which subsequently decays to stable ^{177}Hf through β-decay. As a result of the decay of ^{177m}Lu, the amount of ^{177}Lu is thus built-up. The total activity (A_{Total}) as a function of the time that *(t)* has passed after radionuclide production (t) can be written as: [18]

$$A_{Total}(t) = A_{177Lu,1}(t) + A_{177mLu,}(t) + A_{177Lu2,}(t) \qquad (2)$$

where $A_{177Lu,1}(t)$ and $A_{177mLu,}(t)$ are the activities of ^{177}Lu and ^{177m}Lu that are directly produced at radionuclide production, and $A_{177Lu2,}(t)$ is the ^{177}Lu activity that is decay product of ^{177m}Lu.

The Activity of ^{177}Lu, as being built-up during the decay of ^{177m}Lu, is given by the equation for serial decay [19, 46].

The total Activity is thus given by:

$$A_{Total}(t) = A_{177Lu1,0}\, e^{-\lambda_{177Lu}t} + A_{177mLu,0}e^{-\lambda_{177mLu}t} + A_{177Lu2}(t) = A_{177Lu1,0}\, e^{-\lambda_{177Lu}t} + A_{177mLu,0}e^{-\lambda_{177mLu}t} + \frac{0.217\, A_{177mLu,0}\, \lambda_{177Lu}}{\lambda_{177Lu}-\lambda_{177mLu}} \left(\exp(-\lambda_{177mLu}t) - \exp\left(-\lambda_{177Lu}t\right)\right) \quad (3)$$

where λ_{177Lu} and λ_{177mLu} are the physical decay constants and $A_{177Lu1,0}$ and $A_{177mLu,0}$ are the activities of ^{177}Lu and ^{177m}Lu, respectively, directly after radionuclide production. The factor 0.217 in the last term is the probability for the isomeric transition in the decay scheme of ^{177m}Lu (fig.3).

It is important to note that because of the complex decay scheme, the decay of ^{177m}Lu needs to be well characterized and also γ-ray emission to be accurately determined [19].

III.1 Production Routes of ^{177}Lu

Depending on the required Specific Activity *(As)* , two production routes are applicable for the production of ^{177}Lu, both involving neutron activation processes: [15, 16]

1) The **direct production route** based on neutron irradiation of Lutetium targets [16]. This is an easier production path of ^{177}Lu, and is used for production of the ^{177}Lu that is labeled to peptides in the activities from 7GBq to 9GBq [22];
2) The **indirect production route** , necessitating a chemical separation of ^{177}Lu from the target [16]

Which method is used for the production of ^{177}Lu depends on the required Specific Activity, *As.* The chemical impurities may affect the efficiency of the radiopharmaceutical labeling process and it can therefore lead to a decreased radiopharmaceutical labeling efficiency [16]. Thus, with higher *As* the radio-labeling of the tumor specific antibodies or peptides can be more efficient, resulting in smaller amounts administered substance, which assures that the tumor uptake is not saturated due to filled binding sites for the tracer in the tumor cells [16]. Therefore, the chemical purity can be important for the radionuclide used for therapeutic purposes.

1) The direct production route involves the nuclear reaction with neutron bombardment of ^{176}Lu, as follows: [6, 14, 15, 16]:

$$^{176}\text{Lu}(\text{ n, }\gamma)\text{-> }^{177}\text{Lu} \qquad (4)$$

This method for the production of ^{177}Lu, enables higher *As* for the radionuclide [14], while only a small amount of impurity in the form of ^{177m}Lu and small fraction of impurity of ^{176m}Lu (half-life 2.64 h) is generated [6, 15]. For this production route there is a need for enriched target material because of natural abundance of approximately 2.6% of the ^{176}Lu. The only limitation associated with this production route is the c.a of ^{177}Lu preparations which can be obtained, because of the stable isotopes of ^{176}Lu.

2) The indirect production route of ^{177}Lu involved the nuclear reaction of ^{177}Yb which is produced by the bombardment of ^{176}Yb by a chemical separation in order to produce a higher As of ^{177}Lu, as follows [8, 16]:

$$^{176}\text{Yb}\ (n,\gamma)\ ^{177}\text{Yb} \rightarrow (\beta^{-})\ \ ^{177}\text{Lu} \qquad (5)$$

^{177}Lu is thus obtained free c.a from β-decay of ^{177}Yb, produced by the neutron capture of ^{176}Yb (which has low cross section), in the nuclear reactor. In order to obtain the n.c.a. ^{177}Lu with maximum As, Lutetium should be chemically separated from the Yb target [16].

The indirect production route is based on the neutron irradiation of Ytterbium followed by the radiochemical separation of ^{177}Lu from the Ytterbium isotopes [16]. The requirements for the separation of ^{177}Lu includes: Reduce the Yb amount to approximately < 100 ng; High chemical and radionuclide purity of ^{177}Lu , to be obtained from the radiopharmaceuticals (LuCl3 in 0.05 M HCl) [16]. A fast and reliable separation method should be performed. There are several separation processes but will not be discussed in this report at this stage [16].

IV. Internal Radiation Dosimetry

The radioisotope used for medical depends on its purposes: [39]

- *Diagnostic purposes* (high γ-rays yield which can penetrate out from the body and as a result are detected/imaged; Also minimizes the radiation dose to tissues in patients; γ-rays with *E*=50-350 keV and minimal emission of particles is associated.
- *Therapeutic purposes* (mainly particles emitters for instance β- particles so they can deliver at a high localized radiation dose to the tissues adjacent to the decay for example tumors accumulating the radio-labeled tracer. Emission of γ-rays allows for imaging and dosimetry.

The determination of the tumor uptake of ^{177}Lu and absorbed dose to the tumors and risk organs require knowledge of patient specific time-variated biodistribition of the activity in the body [3]. In order to obtain accurate dosimetric calculations the individual renal volume, dose rate and fractionation play an important role and this enables the prediction of risk for renal function difficulties [35]. Doses are based on the volume and the average activity uptake values over the ROI, using the planar imaging conjugate view method. With this method the only possible outcome is the mean dose to the organ (by fitting the time activity curve to the ROI data) and using the resulting cumulated activity as an input for dosimetry calculation (for instance, OLINDA dosimetry computer code), in order to obtain the organ dose estimations and the dose distributions [10, 36]. For this purpose, the Gamma Camera for the WB imaging and SPECT and CT is used at Lund Hospital University, as illustrated below:

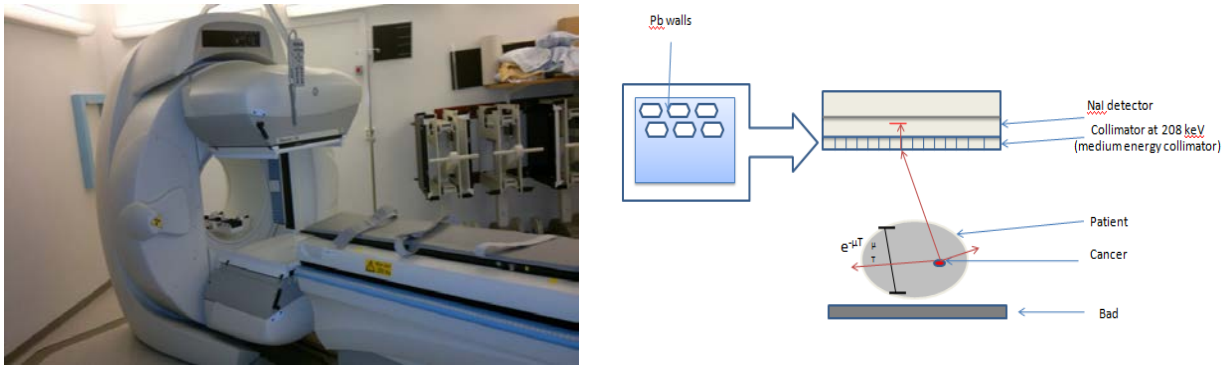

Fig. 4, Gamma Camera

The technical specifications for this gamma camera are as follows: [45]

GE Millennium Discovery VH, CT Hawkeye, which enables the measurement at different angles from 90° – 180° detector rotation in order to achieve a good scanning efficiency. The camera has two detector heads. The scintillation detectors are flat NaI(Tl) crystals 40cm x 50cm (which register the number of counts in the energy window. These detectors have an energy range 40 keV-520 keV and a crystal thickness of 1" (25.4mm). There are 59 PM tubes. The camera is equipped with different collimators, which are used depending on the radionuclide gamma energy: for measurement of ^{177}Lu a medium energy collimator is used as suitable for 208 keV. The camera allows for planar whole-body scanning in anterior and posterior views, as well as SPECT (Single-Proton-Emission-Computed Tomographic) scanning.

The x-ray CT image is used to delineate the patient anatomical structure and creating the attenuation maps used for attenuation correction purposes. The x-ray tube generates x-rays on Tungsten targets which are filtered by 0.5 mm copper. The data acquisition is conducted by remote control equipment, and the patient table allows the adjustment of the patient position and scanning of anterior and posterior WB scans.

The main purpose for Gamma Camera imaging is to determine the radioactivity distribution within different organs. The function of the Gamma Camera is to register the number of counts resulting to an image. Only a small fraction of the emitted radiation is detected [41]. During the image acquisition process some of the photons will be able to penetrate through the collimator (via holes) and registered in NaI(Tl) detector as a number of counts. Thus, the photon energy hits the NaI(Tl) crystal and the PM tube collects and positions the pulses. There are also photons that scatter.

The medical images are taken with 2D planar WB scanning for determining the specific activity distribution (with resolution 5-10mm) [4]. The method for image acquisition and data analysis also includes the use of SPECT/CT images which allows 3D measurements of the activity uptake [8,10].

The x-ray equipment is used in this context for determining the transmission of x-rays through the patient. Generally for an absorbing material with thickness *X* (cm), the transmitted amount of photons, N in relation to the incoming number of photons N_0, can be described as:

$$\frac{N}{N_o} = e^{-\mu X} \qquad (6)$$

where μ is the linear attenuation coefficient (1/cm) valid for a particular photon energy and absorber material. The CT equipment makes an image that reflects the distribution of μ in the patient, and can thus be used to correct the gamma camera image for photon attenuation. A whole body planar x-ray image can also be acquired, a so called scout image, which is used for attenuation correction of the whole-body scans from the gamma camera measurement.

The quantitative images are sufficient for defining an accurate localization of the activity in organs of interest and modeling, in order to obtain the cumulated activity within ROI and be able to estimate the absorbed dose [30]. The dosimetric calculations for activity determination of the absorbed dose by using models and data, remains essential.

The Absorbed Dose is the energy *(E)* deposited per unit mass *(m)* and is measured in the unit of Gray (Gy) with 1Gy=1J/kg [39]. The Absorbed Dose is defined as:

$$D = \frac{dE}{dm}\left[\frac{J}{kg} = Gy\right] \qquad (7)$$

According to MIRD which has developed the model for the Absorbed Dose used in internal dosimetry is equal to the integral of Dose Rate ($\dot{D}$) over period of time (t), meaning that it varies with Activity (A) which varies with time (t): [29]

$$\overline{D} = \int_0^\infty \dot{D}(t)dt = \int_0^\infty A(t) \cdot DF\ (T \leftarrow S)dt = \tilde{A} \cdot DF(T \leftarrow S) \qquad (8)$$

where $\overline{D}$ is the mean absorbed dose (Gy), $\tilde{A}$ is the total cumulated activity (MBq-h), DF is the mean absorbed dose to the target tissue T per unit cumulated activity (Gy/MGq-h) in an activity located in source tissue S [29]. In the MIRD nomenclature DF is instead called S-factor: DF is the same value but in this report termed according to OLINDA dosimetry software. Term $\tilde{A}$ covers the metabolic factors and physical decay and depends on the source organ and biological elimination of ^{177}Lu by the source organ. DF factor depends on the emission characteristics

from the physical decay of radionuclide, the range of emitted radiation and size of organ [29]. The values of DF are determined for standard phantom geometries specific for gender and age. They are defined as:

$$DF(T \leftarrow S) = \frac{\sum_i y_i E_i \Phi_{(T \leftarrow S)}}{m_T} \qquad (9)$$

where y is the emitted number of radiation particles, E is the particle energy, and Φ – absorbed fraction of the emitted energy i.e. the absorbed energy in target tissue T from decay in source tissue S.

Thus the absorbed dose is calculated through the MIRD schema [21]. The activity in different organs is calculated using the images obtained from Gamma Camera. The time-activity curves for different organs allow for calculation of the cumulated activity by curve fitting [21] and subsequent integration over time. The estimates of the Absorbed Dose are obtained using LUNDADOSE software, which has the kinetic curve fitting and DFs for patients, based on gender and age [21,33].

From SPECT/CT images, the absorbed dose rate can be calculated more accurately. The principle for estimation of the absorbed dose is similar to that described above. However, since the planar scans provide information that is not resolved in the depth dimension, whereas SPECT provides 3D information, the SPECT based information is superior.

At Lund University Hospital 4 planar scans are acquired after the administration of ^{177}Lu – DOTATATE and calculations performed using LUNDADOSE. Also SPECT/CT imaging is performed at 24 hours after administration.

The protocol for patient measurements used at using gamma camera is as follows:

- ✓ 20% energy window centered over the 208 keV photo-peak in the energy spectrum
- o Whole body scans performed at four time points. The details below:
    - Scan length: 200 cm
    - At day 0 (0.5 h after the administration): Scan speed 20 cm/min, acquisition time, 12 min

- At day 1 (24 h after the administration): Scan speed 10 cm/min, acquisition time: 24 min
- At dat 1 (24 h after the administration): SPECT/CT imaging
- At day 4 (96 h after the administration): Scan speed 10 cm/min, acquisition time: 24 min
- At day 7 (168 h after the administration): Scan speed 10 cm/min, acquisition time: 24 min

The Absorbed Dose in kidneys is determined based on a combination of the time series of time-activity obtained from planar whole-body scans, and the dose rate determined from SPECT/CT on one occasion (24 hours). The TB activity is determined from the whole-body scans.

V. Experimental Geometry, Methodology and Data Analysis

The experiments have been carried out in a laboratory at the Department of Medical Radiation Physics, Lund University using the experimental set up system of NaI (TI) 3" x 3" (74mm x 74mm scintillation crystals) detector system at Voltage at 750 V, with a construction described in a Chapter II.1 above. For some of the measurements the HPGe detector system was also used in order to make a comparison of the Activity results. In the figure below an illustration of used detector system, is presented. Both detectors, NaI(TI) and HPGe detector were aligned to the MCA software configuration, for data acquisition for further analysis [23].

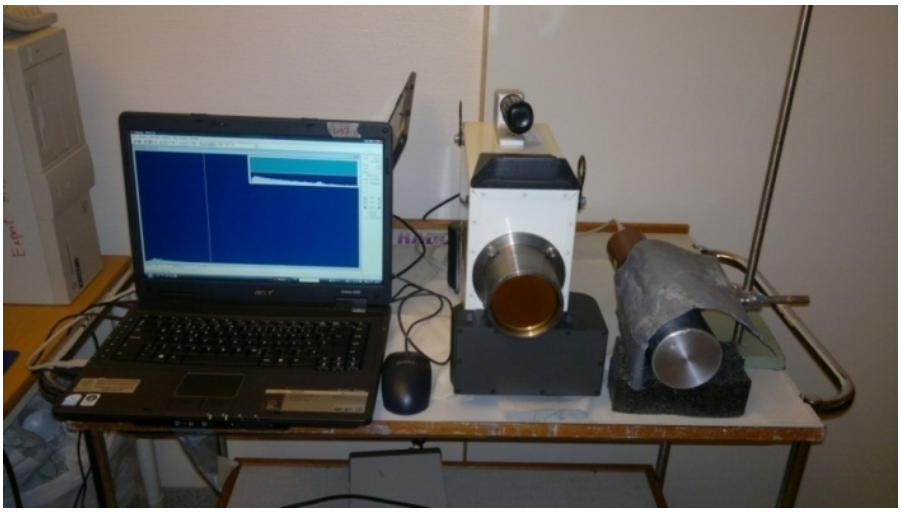

Fig. 5, Experimental Setup for patient measurements

For the NaI(TI) detector Lead (Pb) was used as a shielding material with length 16.5 cm and thickness 2 mm, in order to obtain a better angular resolution and less impact of Compton scattering in surrounding material, in the room. The measurement of γ-ray spectroscopy has been performed using a well defined geometry by setting an appropriate distance between the source and the detector crystal. The distance has an impact on the precision of the results from the analysis, and the uncertainty associated with the distance [9]. During the experimental work measurements of selected reference sources and ^{177}Lu samples have been performed at a source-detector distance of 74 cm. The data acquisition time was normally set to 300 *s*. Prior to every measurement the background was measured for 40 000 *s*, and its count rate has been subtracted from the count rate of source measurement. For instance, obtained spectra of ^{137} Cs are shown in the plot below:

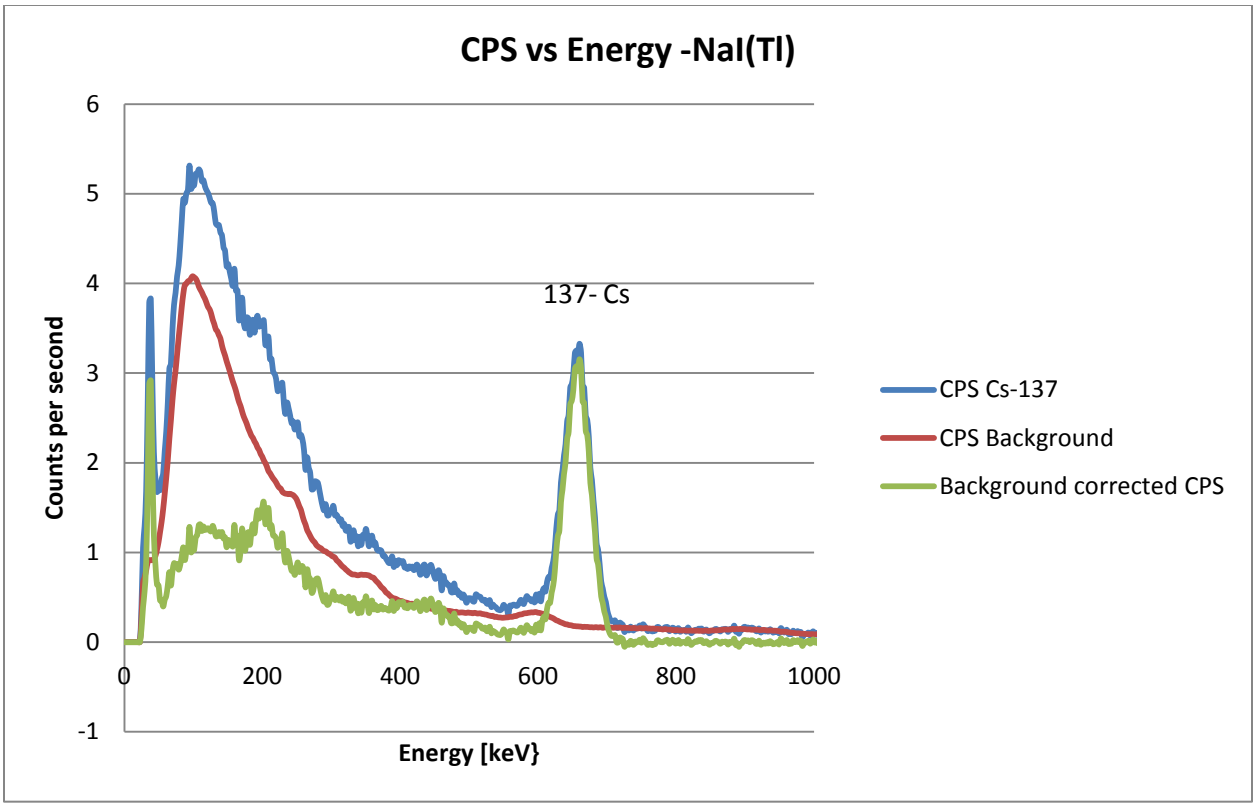

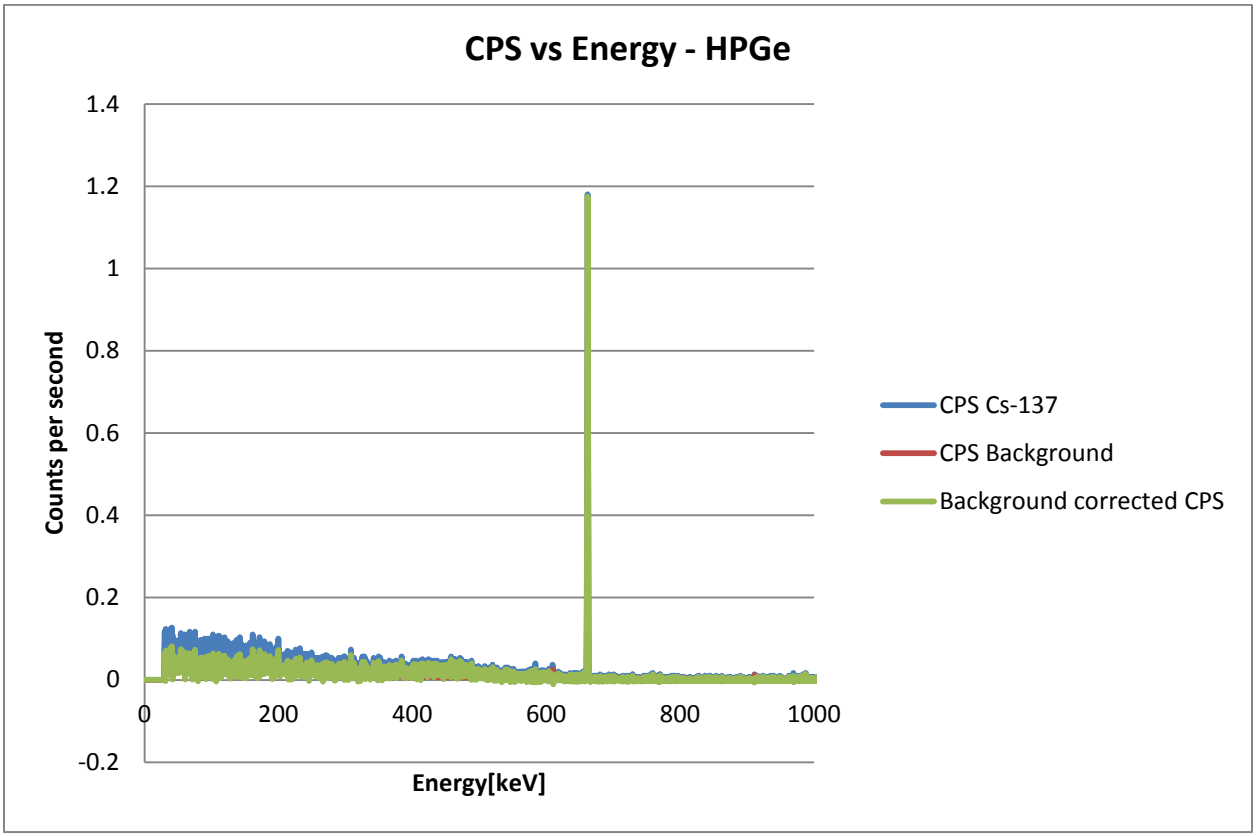

Fig.6, CPS vs Energy [keV] for ^{13}Cs with NaI(Tl)detector (upper panel) and HPGe detector (lower panel).

The measured count rate in background also has an impact on the results from the data analysis. The most prominent peak in the practically performed measurements was the γ-rays from Potassium (K) as a result from cosmic radiation (contribution to background), was detected at 1461 keV. This had no impact on the results from the data acquisition of reference sources and ^{177}Lu, because of its energy which did not interfere with the γ-peaks of the sources [9]. The identification of the γ-ray energies as a function of energy, more specifically, identification of the γ energies close to ^{177}Lu and ^{177m}Lu has been made, identifying the sources of: ^{57}Co, ^{133}Ba and ^{137}Cs to be the most appropriate to be used, in order to cover the range of γ-ray energies emitted by ^{177}Lu and ^{177m}Lu, at 113 keV, 208 keV for ^{177}Lu, and at 378 keV and 418 keV for ^{177m}Lu, respectively.

Measurements of the above mentioned reference sources were performed for determination of the Activity, detector photo-peak Efficiency for both detector systems. (*more information on the outcomes will be presented in a later chapter of this report*). Data analysis for each experiment has been made by two methods: automatically (*results obtained from Maestro analysis software*) and by manual analysis in Excel programme. The experimental data and a detailed table on gammas, beta energies and x-rays for each of the used radioactive sources are available in Appendix I and Appendix II, respectively at:

https://www.dropbox.com/s/zihjh3jtwbgocts/APPENDIX%20I%20%20DATA%20on%20Measurements.xlsx and https://www.dropbox.com/sh/x2eoyms55057or0/AMGh3Phu1J.

VI. Detector System Energy Calibration

The energy calibration of the detector system was performed by using the identified reference sources in order to obtain the channels in the MCA relative to the energy absorbed in the detector upon interactions by the photoelectric effect, by implying a linear relationship between the deposited energy and channel number [39]. The calibration of the NaI(Tl) detector system was performed by using the most suitable γ-ray energies of identified reference sources close to those emitted by ^{177}Lu and ^{177m}Lu [27]. For the purpose of energy calibration, the radioactive sources of ^{57}Co at 122 keV and ^{137}Cs at 662 keV were used, because these radioisotopes emit closer γ-ray energies to that of ^{177}Lu at 113 keV and 208 keV, and to that of ^{177m}Lu at energies 378 keV and 418 keV, respectively. Meanwhile, ^{133}Ba at 356 keV has been used for verifying the stability of the detector system. In some of the measurements the energy calibration proved to be *not* very stable, causing discrepancies in the peak values [27]. The spectra of the photo-peak at known energies have been acquired, caused by the photoelectric effect in the NaI(Tl) crystal. As already cited in this report the spectrum shape may also vary and be influenced by other possible effects/processes which might occur during the γ-ray energy absorption [28].

In the figure below a picture illustrating the sources used for measurements, using both detector systems, is presented:

Fig 7, *Reference sources and ^{177}Lu samples*

The Table of Radioactive sources for the three of above mentioned radioactive sources used, show the properties as follows: [9, 42]

- ✓ ^{57}Co with a half-life of 271,79 *d* at 122,06 keV (abundance 85,6%)
- ✓ ^{133}Ba with a half-life of 10,5 *y* at 80,99 and 356,01 keV (abundance 34,6 % and 62,05%)
- ✓ ^{137}Cs with a half-life of 30,07 *y* at 661,65 keV (85,1%)

From the known gamma-energies of the above listed radionuclides, the offset and slope were determined using the equations: [25]

$$Slope = \frac{662\ keV - 122\ keV}{peak\ channel\#_{662} - \ peak\ channel\#_{122}}\ \left[\frac{keV}{channel\#}\right]$$

Offset= Energy @ channel zero [keV] *(10)*

VII. Determination of Energy Resolution

The energy resolution for the detection process of γ-rays reflects an uncertainty in the determination of the γ-ray energy. It depends on random fluctuations in the γ-ray absorption and light emission, light collection in photocathode, production of photoelectrons, collection of photoelectrons and multiplication by PMT dynodes [24, 39].

The energy resolution is different for different photon energies. From the spectra analysis, the results show that the FWHM is smaller for HPGe detector comparing to NaI(TI) detector. Thus, the HPGe detector offers a very good resolution and is useful for nuclide identification even at small energies. The value for the FWHM corresponds to the resolution of the NaI(TI) and HPGe detectors. It describes how useful the detector is for separating between two energy peaks, in order to identify the nuclide (based on energy), particularly for HPGe detector. The higher the count rate the better energy resolution [27].

The basic parameters for the energy resolution of the detector are: the peak shape and Full Width at Half Maximum (FWHM) as a function of ϒ-ray energy [28]. The energy resolution (ΔE) of the detector has been determined by using the equation:

$$\Delta E = \frac{FWHM}{E} \cdot 100\% \qquad (11)$$

where E is the γ-ray energy. Theoretically, the determined γ-ray energy is governed by Poisson statistics. The uncertainty in the determined γ-ray energy, and thus the FWHM, is then proportional to $\sqrt{E}$, and the energy resolution to $\Delta E \sim \frac{\sqrt{E}}{E} = \frac{1}{\sqrt{E}}$. From a measurement of the energy resolution at one γ-ray energy, for instance for ^{137}Cs at 662 keV, giving ΔE_{662}, the energy resolution at another γ-ray energy (E) can be estimated as:

$$\Delta E_{model} = \Delta E_{662} \cdot \left(\frac{\sqrt{662}}{\sqrt{E}}, \right) \qquad (12)$$

For this purpose, three methods were used for the determination of the energy resolution for both detector systems:

1) Manual calculation (data obtained manually)

Here, the maximum number of counts in the photopeak energy window has first been determined. Then the scatter background in 3 channels immediately to the right and left of the photopeak energy window has been determined to be used for the determination of the average number of counts in scattered background and the peak height above the background. The counts at half maximum were then calculated. Finally, the width of the photopeak for the counts at half maximum was determined. For ^{57}Co and ^{137}Cs peak shapes allowed for identifying the FWHM, while for ^{177}Lu a linear interpolation of the counts versus energy data was performed particularly for the HPGe detector measurement where the energy peaks were narrow.

2) Maestro calculation (automatic data obtained by the Maestro software) and
3) ^{137}Cs as a reference/model calculation (taking into account that ^{137}Cs has the most appropriate shape as a full peak for this purpose).

The results obtained are shown in the plots below, resulting in some variability in the used methods, especially for Maestro calculation for 208 keV:

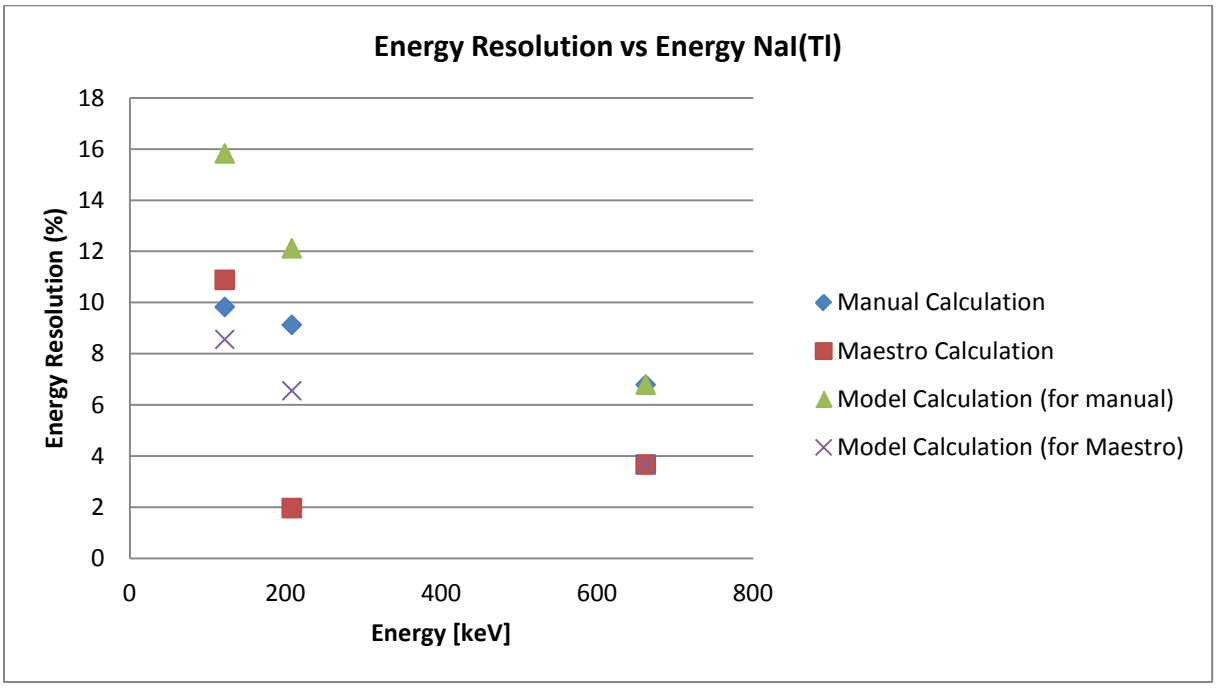

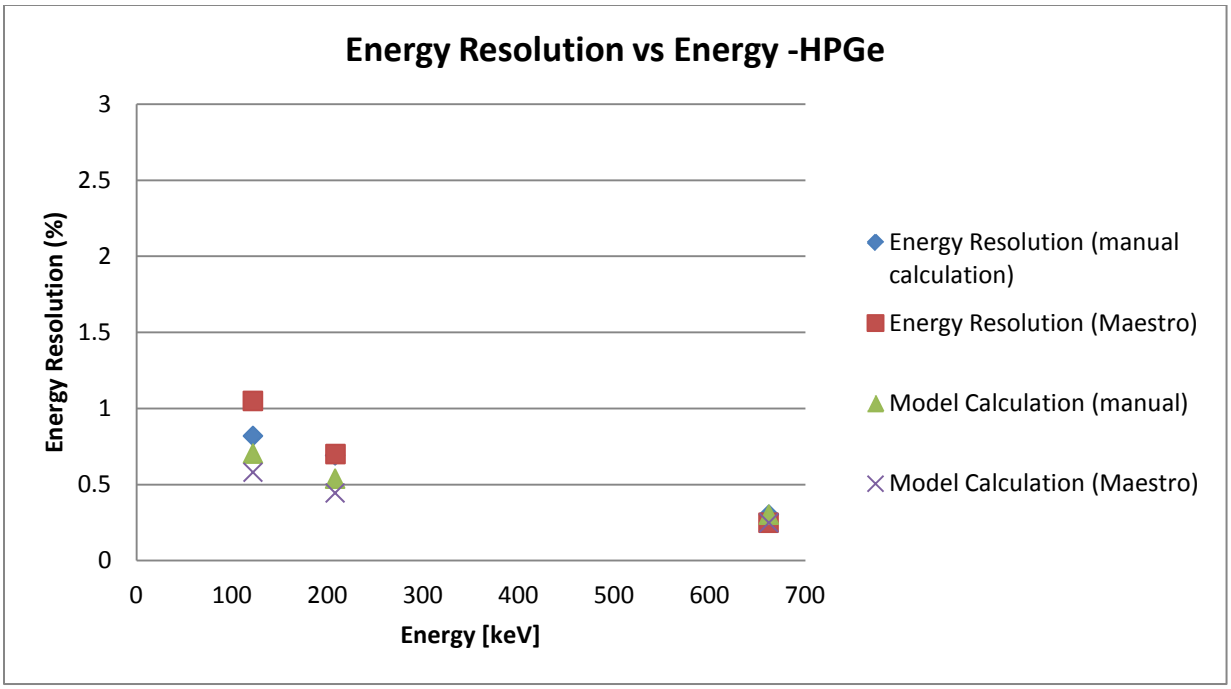

Fig, 8, Energy Resolution of the detector systems, a) NaI(Tl) detector, b) HPGe detector

The energy resolution for NaI(Tl) detector particularly for ^{177}Lu has encountered an error in the FWHM value resulting to be only 4.11 as an arbitrary value, resulting to a non-appropriative energy resolution of NaI(Tl) detector, particularly for ^{177}Lu at 208 keV, as shown in the plot above, under *a)*. By taking into account the interactions and amplifications as well as encountering the contribution from each peaks for expansion of the full energy peak at 208 keV, might have lead to this error result, in this particular sample. However, from the measurements of other several ^{177}Lu samples the FWHM value was reasonable, but still in this particular ^{177}Lu sample used in our experiment for determining the energy resolution, has lead to bringing the attention that such errors might occur, therefore special attention should be made for reaching the best possible FWHM value in order to avoid an inappropriate energy resolution determination.

The detailed results on the estimation of energy resolution for the both detector systems of the specific measured radionuclide are shown in the Appendix III.

VIII. Activity Determination for Reference Sources and ^{177} Lu samples

Measurement of radioactive reference sources in point source geometry have been performed at different occasions. The Activity of radioactive sources has been estimated using the equation:

$$A = A_0 * e^{-\lambda t} \text{ [Bq]} \qquad (13)$$

The activity for reference sources and several ^{177}Lu samples was determined, as shown in the table below:

Source	Original Activity	Original Date	Elapsed time	Measurement NaI(Tl) 15.05.2012 A(MBq)	Elapsed time	Measurement HPGe 26.06.2012 A(MBq)
^{57}Co	22.2 MBq	01.02.2006	2296 *d*	0.06	2338 *d*	0.06
^{133}Ba	4.31 MBq	25.03.2002	3705 *d*	2.21	3747 *d*	2.18
^{133}Ba	8.62 MBq	25.03.2002	3705 *d*	4.41	3747 *d*	4.37
^{137}Cs	346 kBq	8.2003	9.5 *y*	0.28	9.5 *y*	0.27

Radioactive source	A0 [MBq]	Original date	Elapsed time	A [MBq]
^{177}Lu	730 MBq	24.04.2012	1 *h*	726.82
^{177}Lu	730 MBq	24.04.2012	23 *h*	660.35
^{177}Lu	730 MBq	24.04.2012	43 *h*	605.21

Table no. 1, Activity determination for radioactive reference sources and ^{177}Lu samples

As indicated in the table above, measurements were performed at different time points, so that the activities used for measurements were slightly different. The Activity calculation sheet is attached to this report in Appendix IV.

In equation (3) we consider only the first two terms: the activities of ^{177}Lu and ^{177m}Lu and estimate them, on the basis of 7 days and one month after injection (which is normally one or two days after radionuclide production). Considering that the activity of ^{177m}Lu at the time of production, according to the producer is only a small fraction 0.05% of the total amount, for instance in a sample of 7400 MBq, where 0.05% is ^{177m}Lu, being 3.7 MBq one hour after the production, with ^{177}Lu there will be a drop to approximately 3597 MBq for ^{177}Lu one week after

the injection, but still the Activity for ^{177m}Lu will remain at a level of 3.6 MBq. The activity drop will be with different for ^{177}Lu and ^{177m}Lu, due to their half-lives.

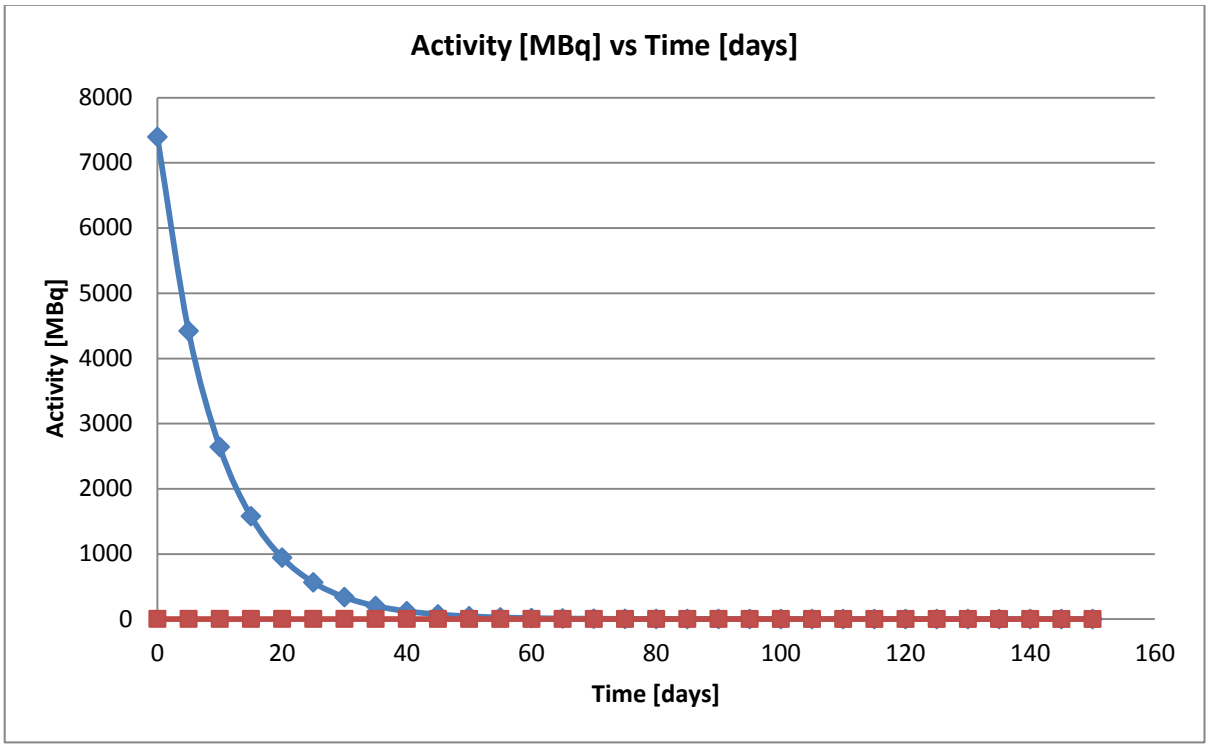

Fig. 9, Activity for ^{177}Lu and ^{177m}Lu at different time points after production

From the calculation data after one month from the production day, the activity of ^{177}Lu will be 304 MBq while for ^{177m}Lu, it will be 3.2 MBq. From the plot below one can see that the time point when ^{177}Lu "matches" ^{177m}Lu is at day 75, and this is the time point when the ^{177m}Lu starts to dominate.

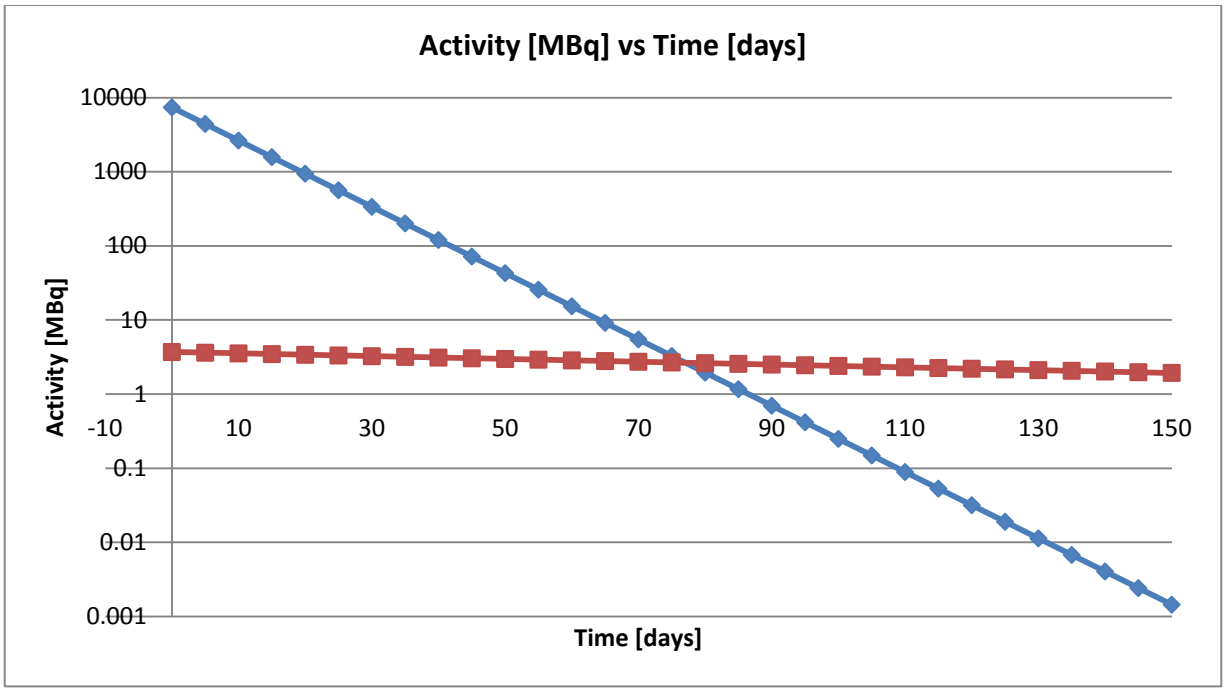

Fig. 10, Activity vs Time after production for ^{177}Lu and ^{177m}Lu in logarithmic scale

This estimation would help us compare at a later stage the TB Activity at different time points, as shown in Appendix V.

If we consider all three terms in equation (3) i.e ^{177}Lu1, ^{177m}Lu and ^{177}Lu2 and assume that the amount of ^{177m}Lu at the time of production is 0.05% then based on the decay data and their half-lives, one can see that the activities of the three components, normalized to the total activity, following the shape in the plot below:

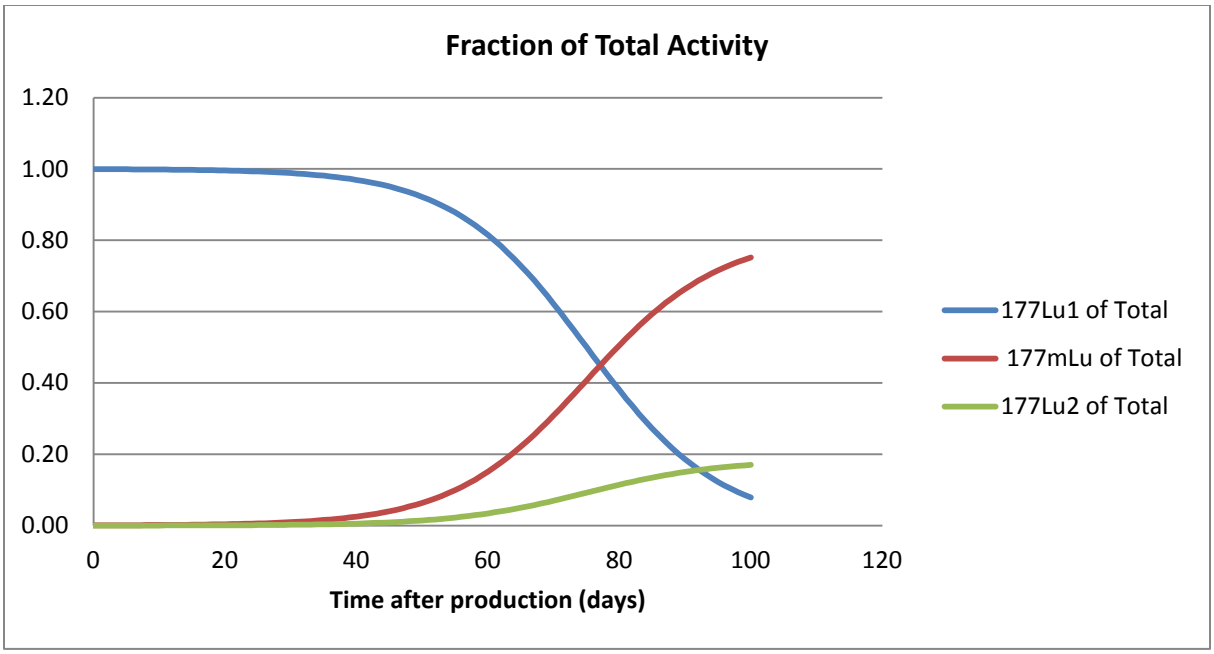

Fig. 11, Fraction of Total Activity including each of the contributing terms in equation (3), ^{177}Lu1, of total, ^{177m}Lu of total and ^{177}Lu2 of total.

If we for each of the contributing components in equation (3) insert the number of 208 keV gammas that are emitted for ^{177}Lu and ^{177m}Lu decays, which are 11% and 57.7%, respectively, then the amount of 208 keV gammas can be calculated. The fraction of the total number of 208 keV gammas that are emitted from each component is shown in the plot below:

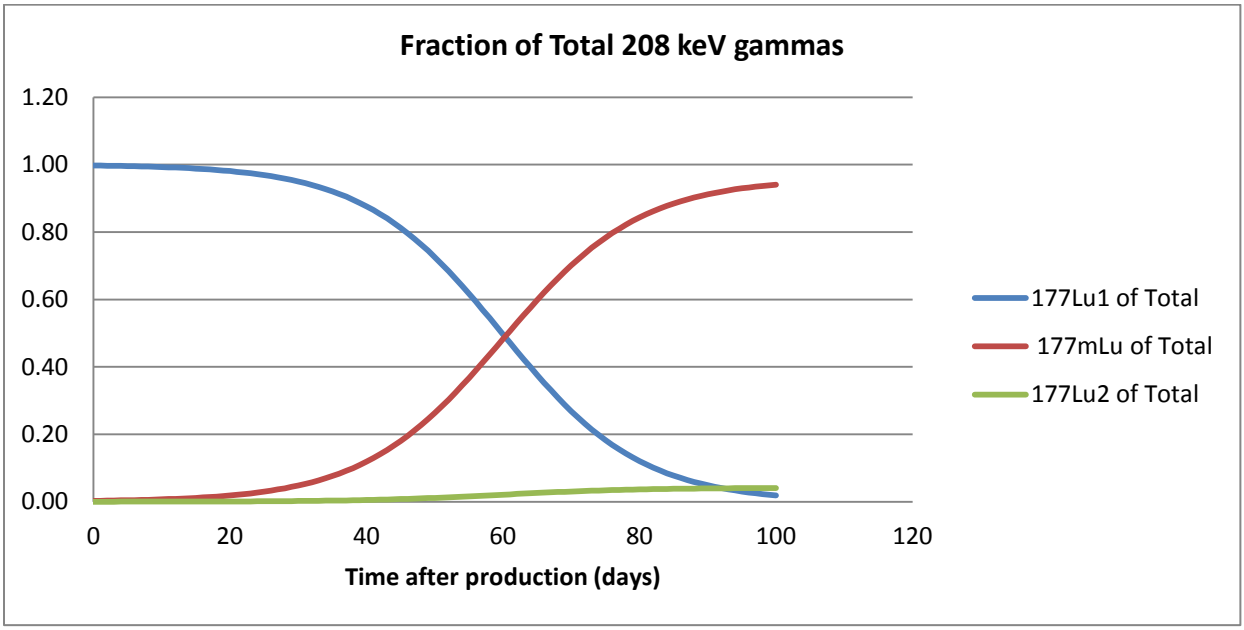

Fig. 12, Fraction of Total 208 keV gammas including each contributing terms ^{177}Lu1 of Total, ^{177m}Lu of Total and ^{177}Lu2 of Total

In order to determine the respective amount of ^{177}Lu and ^{177m}Lu from the spectra that were measured in patients, this has to be taken into account. The formulae for these considerations have been compiled by the supervisors and are given in Appendix VI. Measured spectra for a point source of ^{177m}Lu in air with both detector systems are shown below:

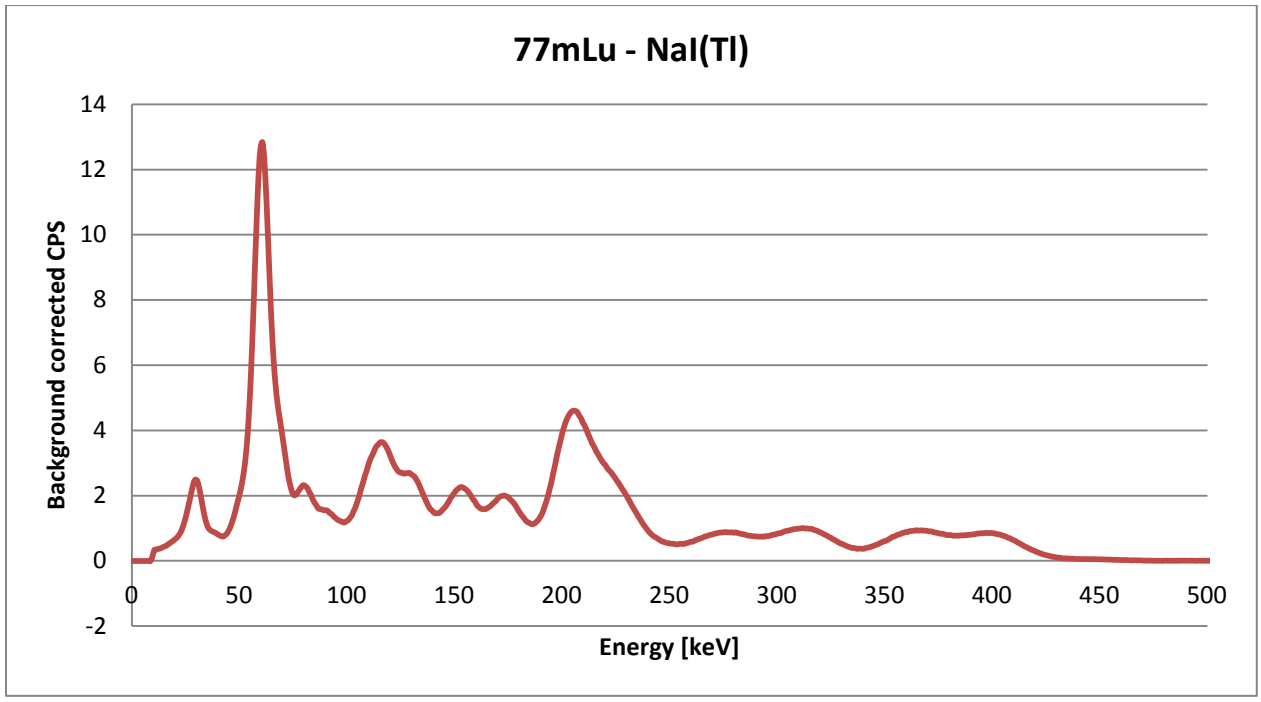

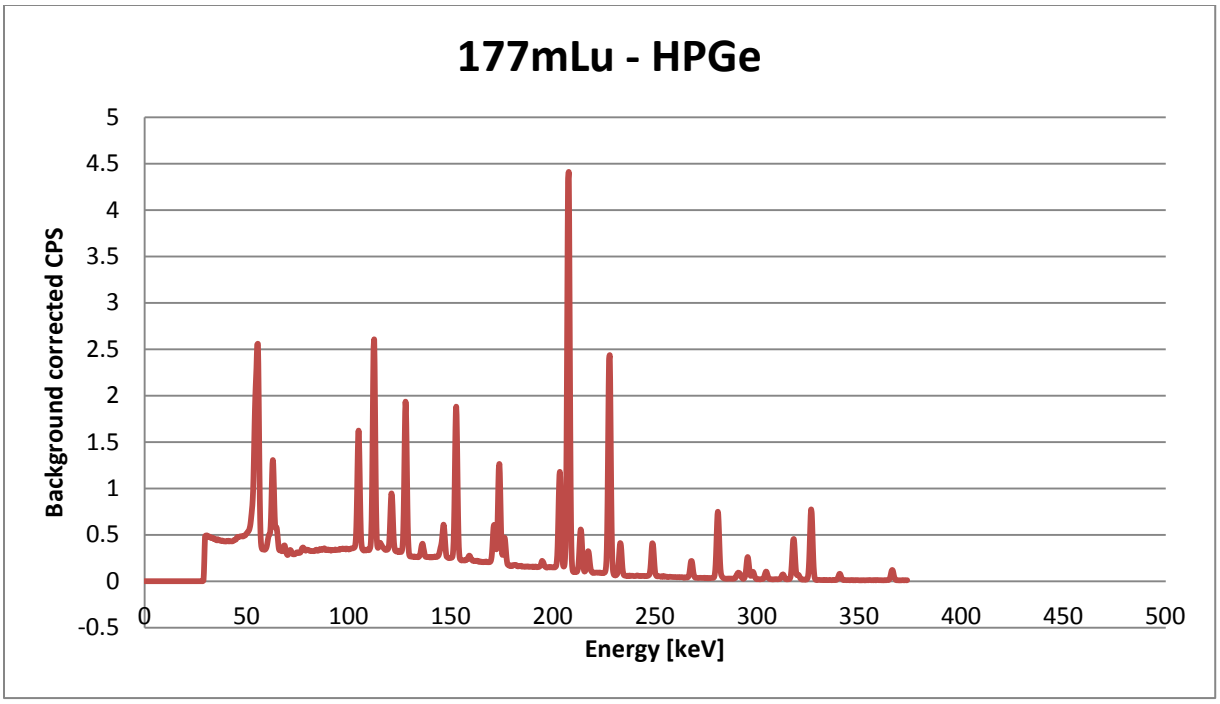

Fig. 13, 177mLu measurement with NaI(Tl) and HPGe detector systems

IX. Determination of Photo-peak Efficiency

The detector photo-peak efficiency describes the count rate obtained per photon that impinges to the detector and it varies with γ-ray energy. It was determined for measurements of reference sources, by identifying the γ-rays coming from the radioactive source [9]. The count rate analysis for all measurements has been performed by determining the detected count rate from the detector as: net area under the photo-peak divided by the measurement time, divided by the gamma fluence rate (which is the number of photons that impinges to the detector surface per unit time). The gamma fluence rate has been calculated from the source activity, as the number of emitted photons with the selected energy per decay, abundance of the γ-ray photon, the distance of the source from the detector, and the area of the detector front surface [38, 39]. Background measurements were performed prior to the source measurements and background count rate was subtracted.

More specifically, the determination of:

- ✓ ***Gross area CPS*** – *The sum of background corrected CPS under the photo-peak area*
- ✓ ***Average scatter background CPS (l &r)*** - Average count rate in 3 channels located to the left (l) and right (r) of the photo-peak.
- ✓ ***Scatter area*** - *Channels multiplied by the average scatter background CPS (l+r)/2*
- ✓ ***Net area CPS*** - Gross area minus scatter area (R_{peak})
- ✓ ***Energy Calibration*** – *used to determine the offset and slope as described above*

In order to calculate the Net Area CPS (R_{peak}) the scatter area (which is the sum of "triangle" and "rectangle") was subtracted from the gross area. An illustration as follows:

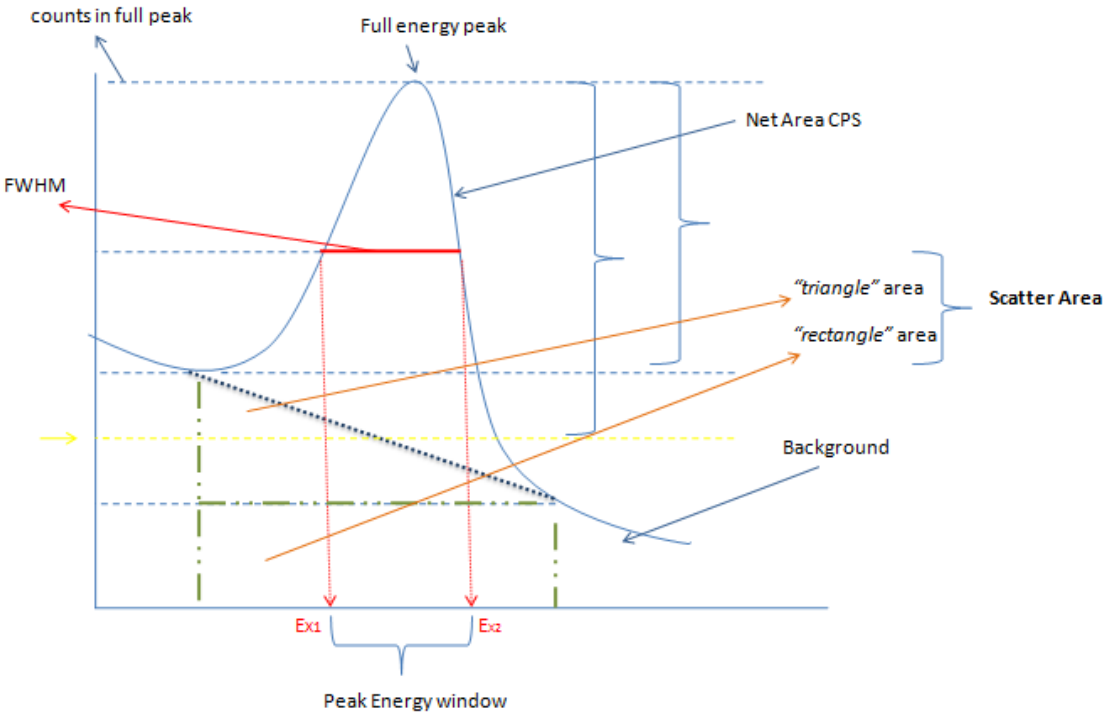

Fig. 14, Gross area CPS and Net area CPS.

The photo-peak efficiency (ϵ) determination has been calculated by using the net area CPS (R_{peak}) for the photo-peak of different radioisotopes, the source-detector distance (D), and specifications on n-gammas for each of the radioisotopes, activity (A), and front surface of the detector (S) using the equation: [38]

$$\epsilon = \frac{R_{peak}}{A \cdot n_{\gamma}} \frac{4\,\pi\,D^2}{S} \qquad (14)$$

The photo-peak efficiency (ϵ) valid for selected measurement geometry which is a point source at a relatively large source-detector distance. The results obtained on photo-peak efficiencies for both detector systems on measured radioactive sources are shown in the plots below:

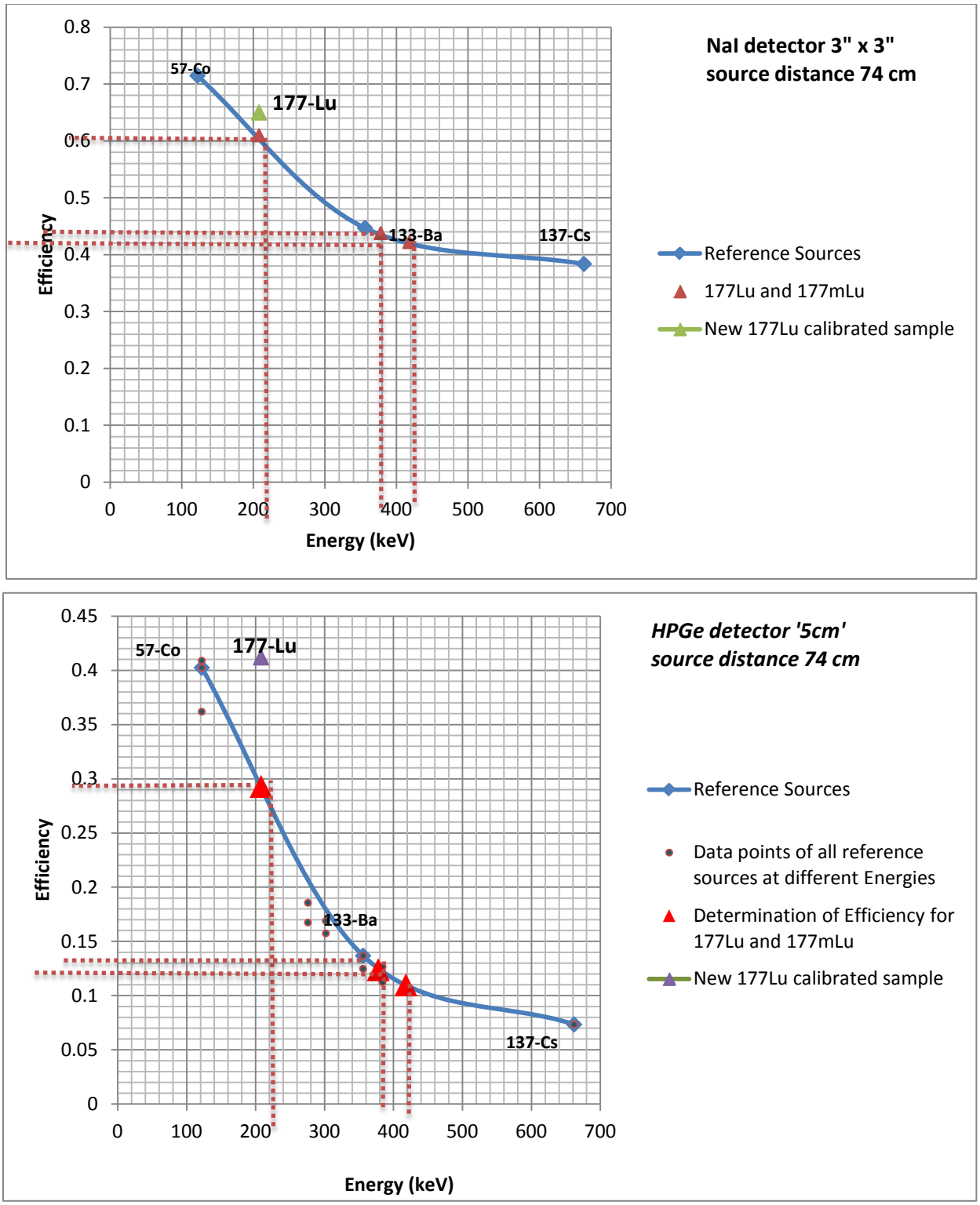

Fig.15, Plots on Efficiency determination for: *a)* NaI(TI) detector and *b)* HPGe detector determined for reference sources, for which the efficiency for gamma peaks of ^{177}Lu and ^{177m}Lu were estimated, as indicated by red dashed lines. At a later stage in the project a calibrated ^{177}Lu sample was obtained as indicated by 'New ^{177}Lu calibrated sample'.

As one can see from the plots above, there is a decrease in the photo-peak efficiency increasing with the γ-ray energy.

The HPGe detector shows to have a smaller efficiency comparing to NaI(Tl), due to the fact that NaI(Tl) has higher probability for the detection of γ-radiation. Even though NaI(Tl) has poor resolution it is more efficient comparing to the HPGe detector. Furthermore, the scitillation detection enables a high detection efficiency for different types of radiations, and capability to measure energy spectra with a high counting rate. Scintillators in γ-spectrometry provides a high detection of efficiency; large Z and large density of the crystal with a high light output [38, 39].

As indicated above the variation of the detectors efficiencies using different radioisotopes at different energies (keV) has been determined. Reference to this, an approximate determination of the detector system efficiency for detecting the ^{177}Lu and ^{17m}Lu has been determined.

The measurement of reference sources at different photon energies performed with the NaI(Tl) detector system, the results of the net area count per second (R) are shown in Appendix VII to this report.

The results of the efficiency for both detector systems in % are shown in the table below :

Radioactive source	Energy [keV]	Efficiency NaI(Tl)	Efficiency HPGe	Efficiency of new calibrated ^{177}Lu sample	
^{57}Co	122	0.690	0.276	NaI(Tl)	HPGe
^{133}Ba (1)	356	0.435	0.090	0.649	0.411
^{133}Ba (2)	356	0.444	0.094		
^{137}Cs	662	0.379	0.054		
^{177}Lu	208	0.61	0.293		
^{177}Lu	378	0.419	0.121		
^{177}Lu	418	0.41	0.11		

Table no.2, Efficiency of the radioactive reference sources and ^{177}Lu , ^{177m}Lu

X. Determination of Standard Deviation in Efficiency

The standard deviation $\boldsymbol{\sigma_\epsilon}$ shows the variation of the obtained efficiency from measurements as an average mean. The calculation of standard deviation for performed measurements has been evaluated using the expression, by derivation as shown in Appendix VIII.

$$\sigma_\epsilon^2 = \left(\frac{\epsilon}{AUC_{net}}\right)^2 \cdot \sigma^2_{AUC_{net}} + \left(\frac{2}{D} \cdot \epsilon\right)^2 \cdot \sigma_D^2 + \left(\frac{\epsilon}{A}\right)^2 \cdot \sigma_A^2 = \epsilon^2 \left\{\left(\frac{\sigma_{AUC_{net}}}{AUC_{net}}\right)^2 + \left(\frac{2\sigma_D}{D}\right)^2 + \left(\frac{\sigma_A}{A}\right)^2\right\}$$

The results for standard deviation are shown in the plot below for both detector systems. Results, indicates that the uncertainty in the efficiency is around 6%.

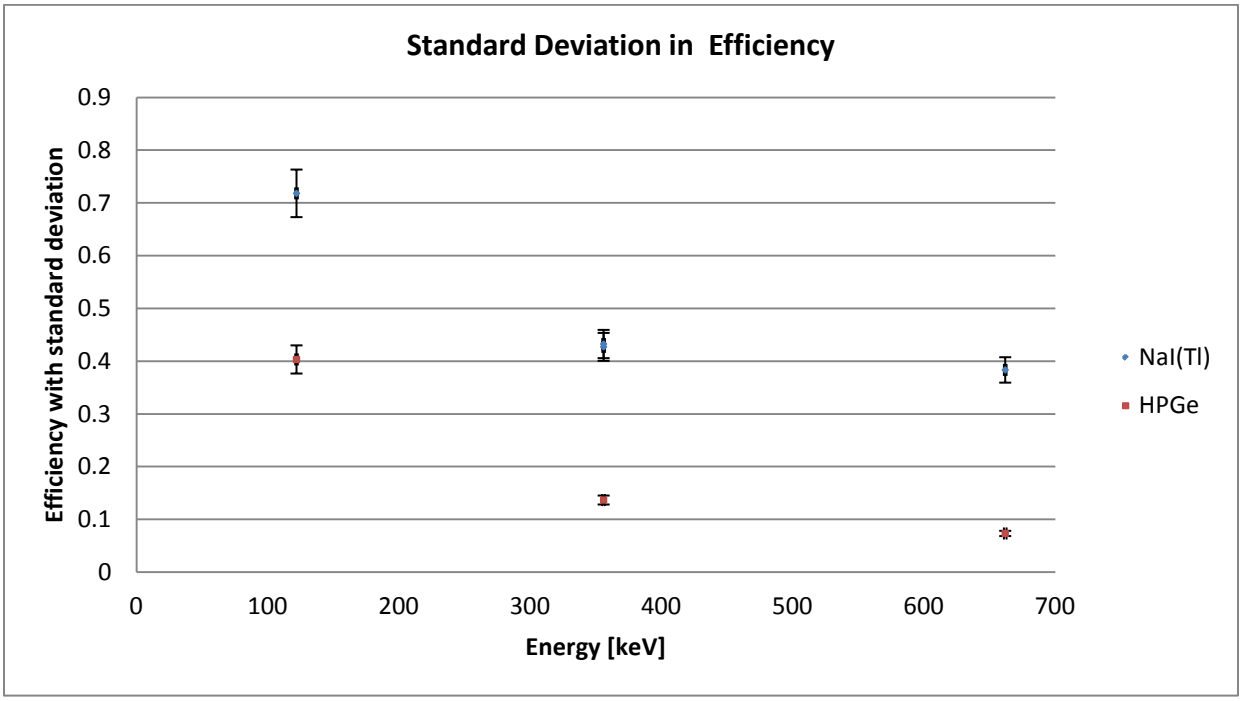

Fig. 16, Standard Deviation for both detector systems

The standard deviation estimates were obtained using: * the net area under curve from measurements, * the standard deviation in the net area from Maestro software, * the uncertainty in distance between source and detector which was estimated to ±2 cm (at 74 cm), * the uncertainty in activity given in the specification for reference sources to σ_A/A =3%. For NaI(Tl) detector the resulting standard deviation in efficiency is approximately ±0.03, while for HPGe it is ±0.02.

XI. Distance estimation for the measurements with NaI(TI) detector

Prior to initiating patient measurements, we wanted to estimate the patient-detector distance that would give a similar count rate for activities of ^{177}Lu and ^{177m}Lu, and also that would give a count rate which yielded a dead time less than 5%. For this reason, distance estimation was made by assuming that the photon emission probability can be obtained using the results from the determined activity and γ-ray spectroscopy, using the relation:

$$R_{peak} = A \cdot n_\gamma \frac{S}{4\pi D^2} \cdot \epsilon \Rightarrow \frac{R_{peak}}{A} = n_\gamma \cdot \frac{S}{4\pi D^2} \cdot \epsilon \left[\frac{CPS}{Bq}\right] \quad (15)$$

Thus, the determination of NaI(TI) detector efficiency for detecting ^{177}Lu at 208 keV, and ^{177m}Lu at 378 keV and at 418 keV was estimated, using the efficiency values previously obtained from reference sources, as shown in Appendix IX.

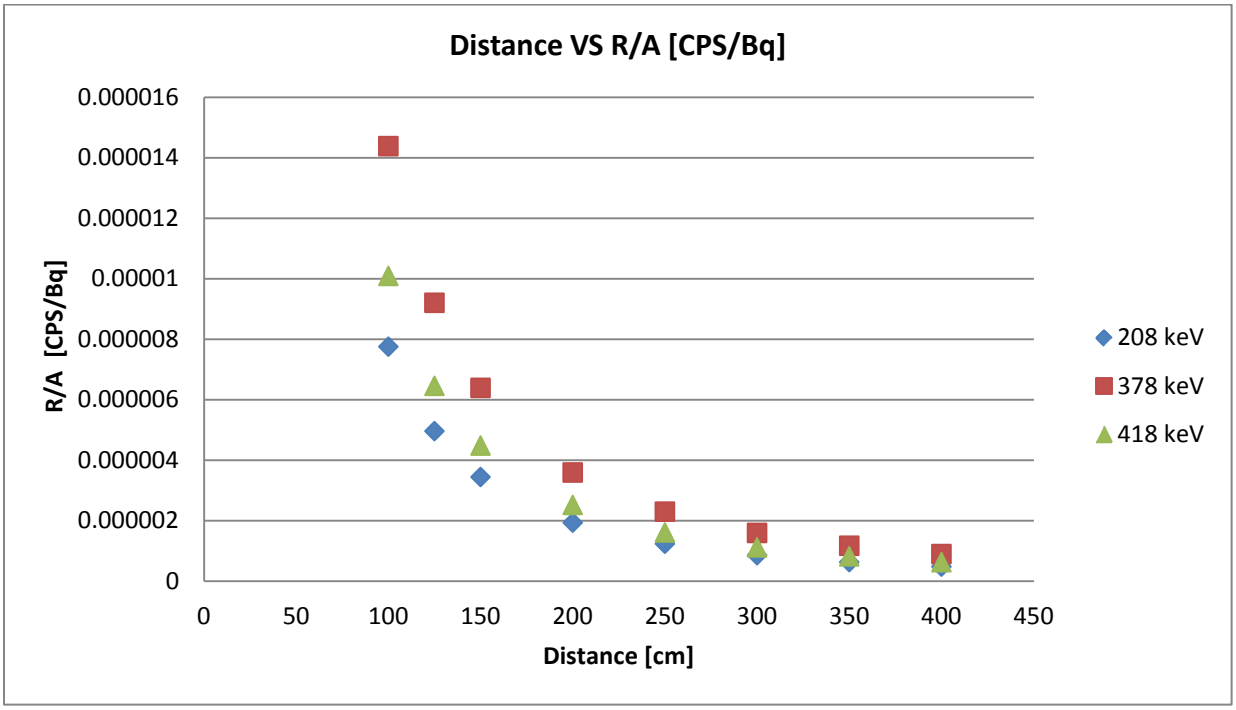

Fig. 17, Distance estimation for detector NaI(TI) efficiency activity detection of ^{177}Lu and ^{177m}Lu

Therefore, for the 1st time point the measurement was performed at a longer distance in order to obtain a sufficient count rate while keeping the dead time as low as possible (less than 5%), while at a later time the measurements were performed at closer distance geometry in order to obtain sufficient count rate, so the data analysis could be possibly performed.

XII. The Activity determination of a ^{177}Lu sample using the HPGe detector system

The γ-ray spectra analysis for the determination of the ^{177}Lu /^{177m}Lu ratio using HPGe detector system has been made and analyzed by APEX software. These measurements were practically performed prior to my involvement in the project. For practical purposes and familiarization with the energy peak determination by using APEX software a practical experiment has been performed by measuring a sample of ^{177}Lu. A practical examination of how well different peaks can be separated and detected by the detector system has been conducted. An illustration of the experimental setup is shown in the figure below:

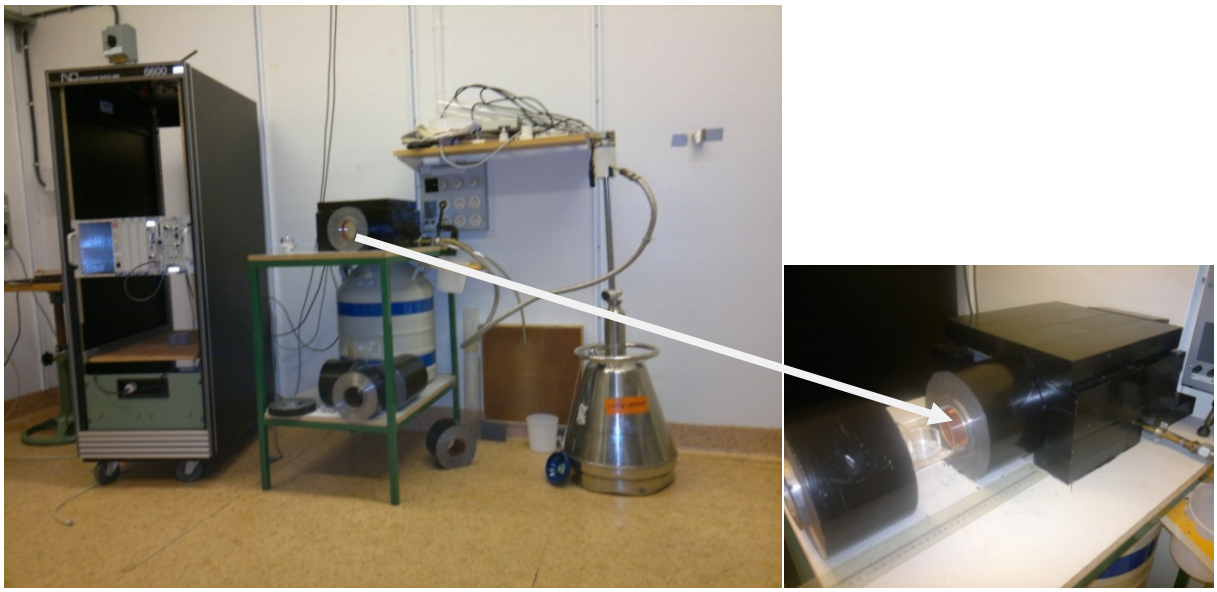

Fig. 18, HPGe detector system used for measurement of ^{177}Lu sample

In previous measurement three different samples of ^{177}Lu / ^{177m}Lu, consisting of cans of 60ml containing well-mixed radionuclide solutions, were placed in a close-detector geometry (2π). Different energy peaks were identified using a predefined radionuclide library was used (identifying the γ-ray energies, based on abundances, and the half-lives of the radionuclides). These measurements were performed on 20110912 and 20110928.

The HPGe detector energy was well calibrated, and its efficiency had been determined for different geometries by earlier measurements. The detailed γ-ray spectrum analysis reports have been used as a reference data for further analysis. Using the report information on peak identification as well as the data acquisition time, the measurement performed by different

detectors (mainly ADC2 and ADC3), were used for the determination of ^{177}Lu/^{177m}Lu activities. Please note that a detailed summary containing all relevant information on the samples and above mentioned parameters are presented in the table under Appendix X. The ^{177m}Lu activity for each of the energy peaks (keV) for all the samples, was determined. Furthermore, by using the information on the decay data for both ^{177}Lu and ^{177m}Lu, the γ's belonging to both ^{177}Lu and ^{177m}Lu, were quantified by using the information on the energy peaks from the reports on gamma ray spectra analysis:

Energy [keV]	Yield %
105.36	12.34
112.95	20.44
128.50	15.50
153.28	16.90
174.39	12.61
204.10	13.80
208.37	57.0
228.37	37.00
281.79	14.10
327.68	18.10
413.54	17.40
418.54	21.30

Table 3, Radionuclide library from APEX gamma ray spectra analysis report, valid for 177mLu

Since both ^{177}Lu and ^{177m}Lu have gamma energies at 112.95 keV and 208.37 keV, other gamma-peaks for ^{177m}Lu were used for activity determination. The efficiency was stated to be better determined for the higher energy range, and therefore the peaks at 281.79 keV, 327.68 keV and 418.54 keV, were used. The ^{177}Lu activity was then determined by subtraction of the ^{177m}Lu activity and correcting for the different half-lifes. Based on the measurements of one set of 3 samples, it was found that, in the examined samples, the amount of ^{177}Lu at radionuclide production was 0.025% thus in accordance with the values stated by the manufacturer of ^{177}Lu of being <0.05%. From the other set of 3 samples the activity determination was not possible because the measurements have been performed too late (at 171 days), i.e. when the activity of ^{177}Lu was under the detection limit of the detector system.

XIII. Patient Measurements

The methodology for patient measurements has been well defined on a basis of above mentioned principles in order to accurately determine the TB Activity.

In total 7 patients have been part of this study, 3 males and 4 females. After administration of ^{177}Lu-Dotatate on day 0, measurement 1 has been performed on day 7. This is the same day as the last image is taken for routine dosimetry purposes and is used for comparison with the TB activity determined from images. The 2nd and 3rd measurements have been performed when the patient return for a doctor visit at approximately 1.5 month, and before start of new treatment at approximately 2.5 months after administration. All of the patients have undergone at least 2 measurements at different time points. Four patients have undergone a 3rd measurement. Within this frame, the geometry using NaI(TI) detector system for all of the patient measurements was used, while for some of the measurements HPGe was also employed for comparison purposes. The HPGe detector system was used for two patients at 1st time point, four measurements on the 2nd session and one in the 3rd session.

Anterior and posterior measurements were performed and a detailed patient protocol on measurement has been maintained. The distance for patient measurement has been made to the center of the body and has varied for the different measurements. Generally, the patient-detector distance for the 1st time point measurement was approximately 2.90m-3.40m, giving a detector dead time of less than 5%. For later measurement time points the patient was positioned closer to the detector system, in order to obtain a sufficient count rate and keep the measurement time reasonably low (10min per view, in total 20min). The distance was approximately 1.20m-3.10m, respectively for the last measurement (3rd measurement) 1.51m-1.33m. Prior to every measurement, the background was measured at an appropriate time length at 40 000 *s*. The energy calibration for NaI(TI) detector was made using ^{57}Co and ^{137}Cs, while ^{133}Ba was used for verification purposes of the calibration stability, which showed slight variations in the energy scale. For this purpose, a manual energy calibration was also performed by a linear fitting of the channel versus γ energy data. A picture illustrating an anterior patient measurement is shown below:

Fig. 19, An illustration from Patient measurement session

The data acquisitions in Maestro were converted into the Excel program for further analysis. The CPS was determined as the number of counts divided by the live time of the detector measurement. The background subtraction was also performed, as illustrated from the patient 2 in anterior measurement, is shown in the plots below:

a) Patient Measurement – An example from Patient no.2 in anterior position using NaI(Tl) detector system, 1st measurement, 7 days after the administration date:

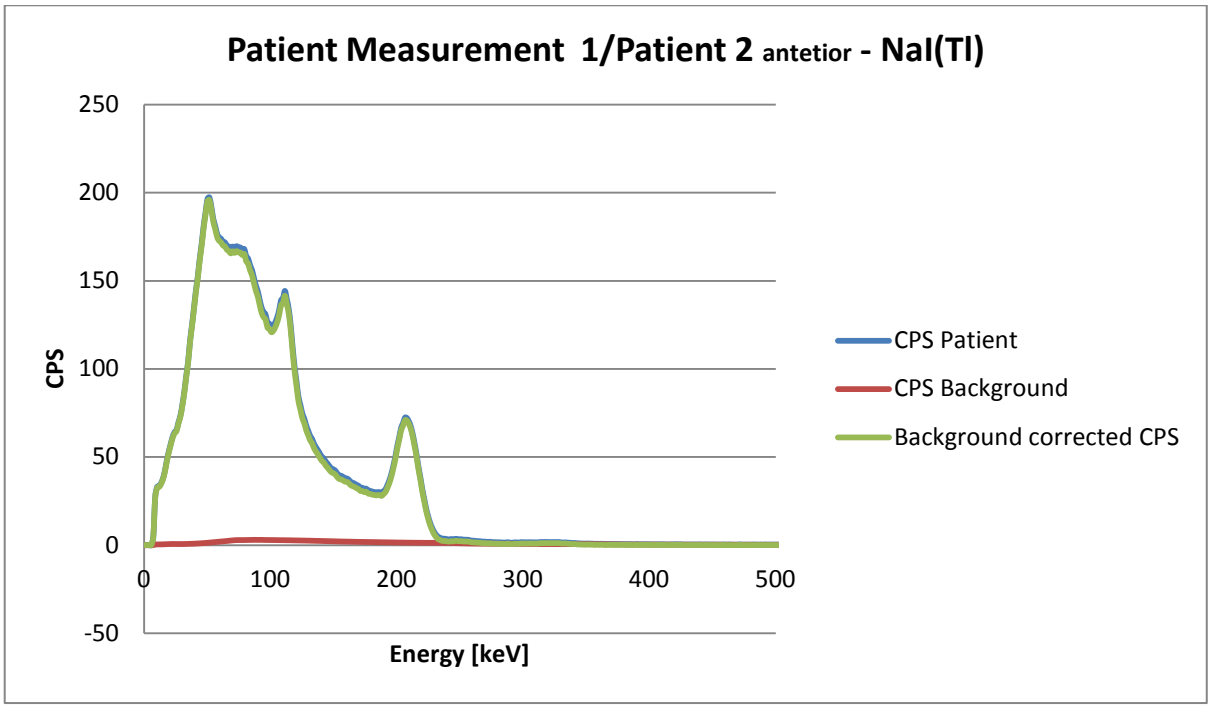

b) Patient Measurement – An example from Patient no.2 in anterior position using NaI(Tl) detector system, 2nd measurement, 41 days after the administration date:

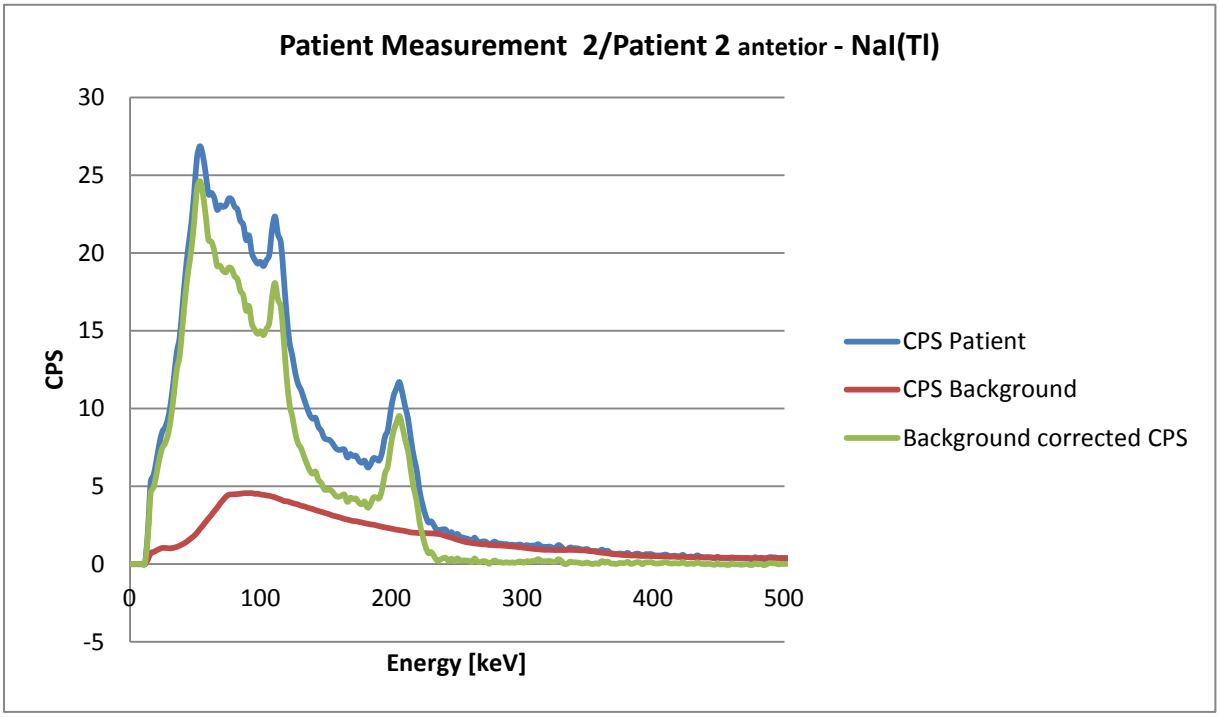

c) Patient Measurement – An example from Patient no.2 in anterior position using NaI(Tl) detector system, 3rd measurement, 70 days from the date of administration:

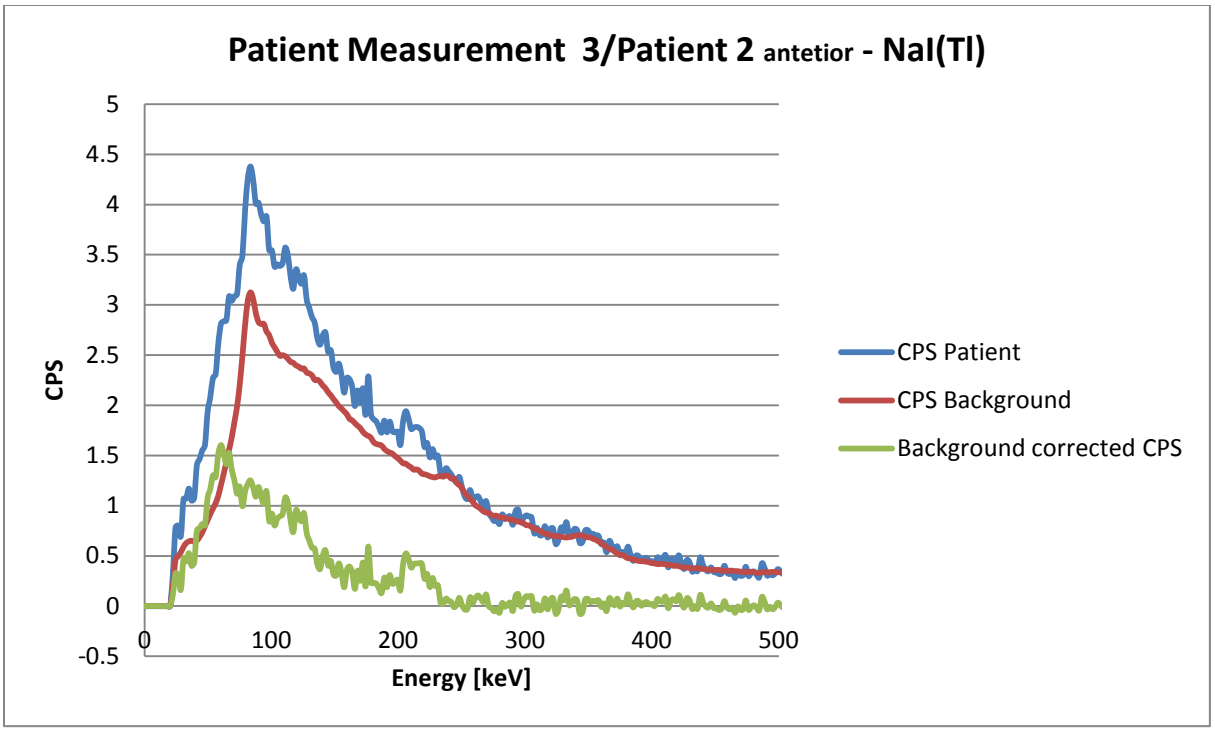

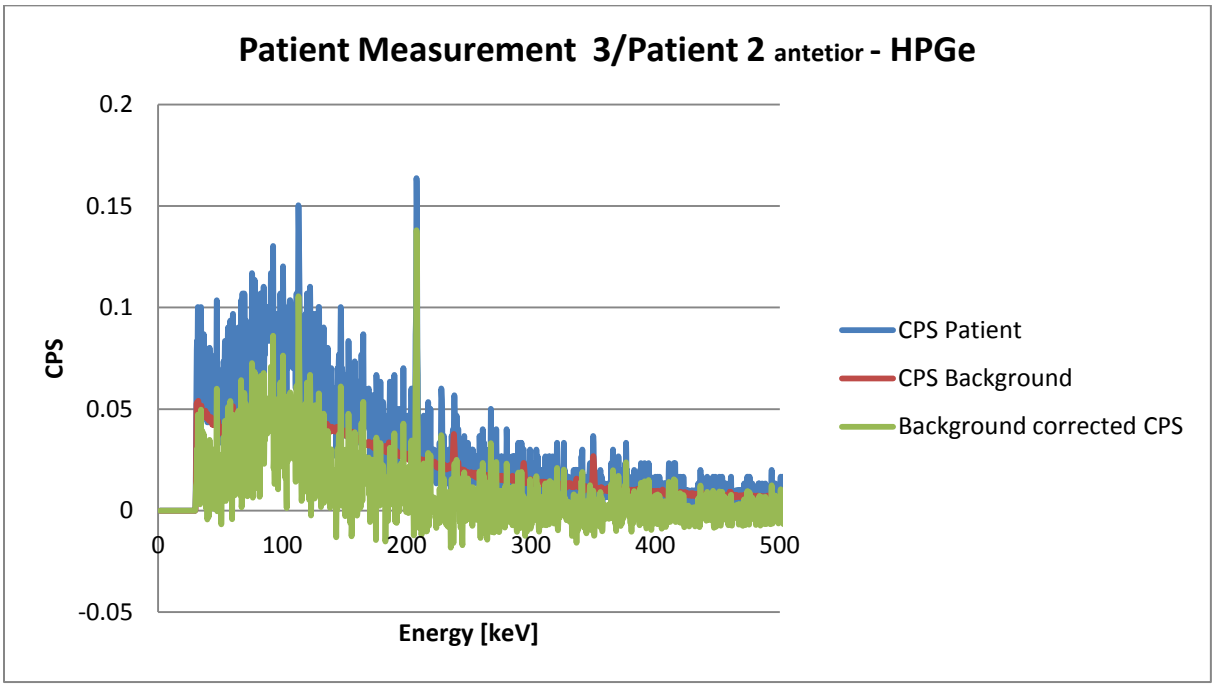

Fig. 20, Data analysis from patient measurements, example from patient number 2, anterior measurements:

For further analysis of data, a plot was obtained in order to identify the channel # in the spectrum. The background CPS was subtracted from the Patient CPS. The energy window was determined for the 208 photo-peak in order to obtain the Gross Area CPS (as a sum of the CPS

in the energy window), and the net area CPS (R_{peak}) was determined by subtraction of the scatter area, as described above. Furthermore, for purposes of stability-check of the detector system and of the results calculated by Maestro software, a determination was also made of:

- ✓ Total count rate in background in energy windows at 208 keV peak
- ✓ Sum of background CPS in energy window
- ✓ Total background count rate per channel# in the energy window at 208 keV

Total count rate in background in energy windows 208 keV peak - Number of channels for 208 keV peak

XIV. Applied Methods for TB Activity determination on Patients

For the measured data on R_{peak} the activity in the Patient TB was determined in Excel. The assumption was made that point source geometry could be applied. However, since the activity was located at an unknown depth in tissue, correction for photon attenuation in the patient body was also applied. Attenuation correction using the conjugate view method is described below.

If the activity had been only ^{177}Lu, then the detector measurements in the anterior view (the detector placed in front of the patient), the detected net count rate due to 208 keV photons was:

$$R_{peak,ant} = A_{TB} \cdot n_\gamma \cdot \frac{S}{4\pi D_{ant}^2} \cdot \epsilon \cdot e^{-\mu x} \qquad (16)$$

where x is the depth of the activity source in the patient in the direction from the front. Here n_γ is the number of emitted 208 keV gammas per decay of ^{177}Lu, ϵ is the detector photopeak efficiency valid for 208 keV photons. D_{ant} is the distance from the detector surface to the patient mid-point in the anterior-posterior direction, μ is the linear attenuation coefficient valid for 208 keV, and other terms are as given in the previous sections. Then in the posterior view (the detector placed behind the patient's back):

$$R_{peak,post} = A_{TB} \cdot n_\gamma \cdot \frac{S}{4\pi D_{post}^2} \cdot \epsilon \cdot e^{-\mu(T-x)} \qquad (17)$$

where T is the total patient thickness, and D_{post} is the distance to the patient midpoint as measured from the back. By applying the geometric mean for both anterior and posterior views:[43]

$$\sqrt{R_{peak,ant} \cdot R_{peak,post}} = \sqrt{A_{TB} \cdot n_\gamma \cdot \frac{S}{4\pi D_{ant}^2} \cdot \epsilon \cdot e^{-\mu x} \cdot A_{TB} \cdot n_\gamma \cdot \frac{S}{4\pi D_{post}^2} \cdot \epsilon \cdot e^{-\mu(T-x)}} =$$

$$A_{TB} \cdot n_\gamma \cdot \epsilon \cdot S \cdot \frac{1}{4\pi D_{ant} D_{post}} \cdot \sqrt{e^{-\mu T}} \qquad (18)$$

The TB Activity could be determined using the equation: [43]

$$A_{TB} = \sqrt{R_{peak,ant} \cdot R_{peak,post}} \cdot \frac{4\pi D_{and} D_{post}}{n_\gamma \cdot \epsilon \cdot S} \cdot \frac{1}{\sqrt{e^{-\mu T \cdot}}} = \sqrt{R_{peak,ant} \cdot R_{peak,post}} \cdot \frac{4\pi D_{and} D_{post}}{n_\gamma \cdot \epsilon \cdot S} \cdot \sqrt{e^{\mu T \cdot}} \quad (19)$$

Here the only term that is specific for a particular radionuclide is n_γ, while other terms relate to the measurement geometry, detector or the photon energy 208 keV. To take the different sources of 208 keV photon emissions into account (^{177}Lu1, ^{177m}Lu and ^{177}Lu2), the calculation of the activity has been made in different steps:

First the measured values of R_{peak} were corrected for the distance *(D)*, the photo-peak efficiency *(ϵ)* and the detector surface *(S)*. This gave a value $R_{corr,ant}$:[43]

$$R_{corr,ant} = R_{peak,ant} \cdot \frac{4\pi D_{ant}^2}{\epsilon \cdot S} \quad (20)$$

And the corresponding calculation to obtain $R_{corr,post}$. Then attenuation correction was made. The patient thickness (cm) was measured in CT images, in transaxial slices over the kidney-liver area. For this purpose, the Xeleris imaging station was used, and measurement using a caliper in the images. The linear attenuation coefficient for 208 keV was determined from reference values (NIST). An attenuation-corrected count rate was obtained as: [43]

$$R_{att-corr} = \sqrt{R_{corr,ant} \cdot R_{corr,post}} \cdot \sqrt{e^{\mu T}} \quad (21)$$

From the detected count-rate we wanted to determine the activities from the different sources (^{177}Lu1, ^{177m}Lu and ^{177}Lu2). In order to determine the count rate from the different sources of 208 keV gammas, a theoretical relationship was applied, as supplied by supervisors (Appendix V). A basic assumption in this relationship was that the radionuclide purity was known, meaning the amount of the radioactive solution that is ^{177}Lu at the time of production. Since the producer states that <0.05% of the total activity is in the form of ^{177m}Lu, we have assumed 0.05% as a worst case scenario.

From the theoretical relationship (depicted in the figures 11 and 12 in section VIII) an expression for the rate of photon emission at measurement time *(tm)* is obtained: [43]

$$N_{208,Tot}(t_m) = N_{177mLu}(t_m) + N_{177Lu1}(t_m) + N_{177Lu2}(t_m) = N_{208,Tot}(t_m) \cdot \left(\frac{N_{177mLu}(t_m)}{N_{208,Tot}(t_m)}\right) +$$

$$N_{208,Tot}(t_m) \cdot \left(\frac{N_{177Lu1}(t_m)}{N_{208,Tot}(t_m)}\right) + N_{208,Tot}(t_m) \cdot \left(\frac{N_{177Lu2}(t_m)}{N_{208,Tot}(t_m)}\right) = N_{208,Tot}(t_m) \cdot F_{177mLu}(t) +$$

$$N_{208,Tot}(t_m) \cdot F_{177Lu1}(t) + N_{208,Tot}(t_m) \cdot F_{177Lu2}(t) \qquad (22)$$

In Appendix V, derivations are given of fractions *F(t)*, of the respective term of the 208 keV photon-emission rate, in relation to the total 208 keV photon-emission rate. Using these fractions, the TB activity of the different radionuclides was then determined as: [43]

$$A_{177Lu1,TB} = R_{att-corr} \cdot F_{177Lu1}(t)/n_{\gamma,208,177Lu}$$

$$A_{177mLu,TB} = R_{att-corr} \cdot F_{177mLu}(t)/n_{\gamma,208,177mLu}$$

$$A_{177Lu2,TB} = R_{att-corr} \cdot F_{177Lu2}(t)/n_{\gamma,208,177Lu} \qquad (23)$$

The values on TB Activity have been compared with the results obtained from dosimetric images using gamma camera.

XV. Absorbed Dose Calculation in Organs

From the measurement using the NaI(Tl) and HPGe detector systems, it is only the TB activity that can be determined. In order to make dosimetric calculations in organs, some further assumptions are necessary. For this purpose, the image-based estimates of the activity were taken as baseline. From the images taken on last day (on day 7) a comparison was made of the TB activity determined from the detector measurements and the images to assure a good correspondence. At this time (day 7) the main radionuclide component is still ^{177}Lu as can be seen in figure 10. Therefore, based on the images, the fraction of TB activity located at different organs was determined, for liver, spleen, kidneys and remainder of body (which is the TB activity minus the activity in the other organs). The detector measurements at the late time point (approximately 1.5 month) were then analyzed by the assumption that distribution within the patient body was the same as on day 7. This means that from the images a fractional activity was determined as: [43]

$$FA_{organ}(day7) = A_{organ}(day7)/\, A_{TB}(day7) \text{ only } ^{177}\text{Lu} \qquad (24)$$

Then, the activity in an organ at the late time point was determined from the detector measurements as:

$$A_{organ}(detector\ @\ late\ time\ point) = FA_{organ}(day7) * A_{TB}(detector\ @\ late\ time\ point) \qquad (25)$$

This last analysis was made with regard to the different amounts of the source components (^{177}Lu1, ^{177m}Lu and ^{177}Lu2) at different times after radionuclide production. In effect, the analysis was made: [43]

$$A_{177Lu1,organ}(@\ late\ time) = A_{177Lu1,TB} * FA_{organ}(day7) = R_{att-corr}(@\ late\ time) * F_{177Lu1}(@\ late\ time)/n_{\gamma,208,177Lu} * FA_{organ}(day7)$$

$$A_{177mLu,organ}(@\ late\ time) = A_{177mLu,TB} * FA_{organ}(day7) = R_{att-corr}(@\ late\ time) * F_{177mLu}(@\ late\ time)/n_{\gamma,208,177mLu} * FA_{organ}(day7) \qquad (26)$$

$$A_{177Lu2,organ}(@\ late\ time) = A_{177Lu2,TB} * FA_{organ}(day7) = R_{att-corr}(@\ late\ time) * F_{177Lu2}(@\ late\ time)/n_{\gamma,208,177Lu} * FA_{organ}(day7) \quad (27)$$

Dosimetry was then performed in the OLINDA dosimetry software. Different sets of data were analyzed for this purpose.

"Set 1": Input to OLINDA was the activity data for each organ, at the imaging times (approximately 0.5h, 24h, 96h (day4) and168h (day7), only ^{177}Lu. This represents the data set that is included as part of routine dosimetry in the clinic.

"Set 2": Input to OLINDA was in addition to Set 1, the activities determined from the detector measurements i.e. $A_{organ}(@\ late\ time)$. This was then separated into different components, as described above, because OLINDA has different DFs for ^{177}Lu and ^{177m}Lu.

XVI. Results

As already mentioned part of the study was in total 7 patients, 4 female and 3 male. Anterior and Posterior measurements were performed for each patient, excluding patient no.1 who was only measured in anterior position. The data analysis performed for both positions were further used for determination of TB activity for each patient. In order to determine the Activity of different contributing components, the R (net area under the curve) was determined for the measurements in anterior and posterior, and it was corrected for distance, detector surface, efficiency (cps) for both measurement positions, and with this value the determination of the geometric mean has been determined. The mass attenuation coefficient μ/ρ for 208 keV photons in soft tissue was used based on the ICRP-44, estimated to be 0.134 g/cm^2 and ρ =1 g/cm^3. By also knowing the patient thickness the attenuation correction value was determined as $\sqrt{e^{\mu T}}$. The activity values determined from image based (Planar and SPECT), were used in combination with those measured from the detector systems. Furthermore, the activity in different organs was also determined, mainly kidneys, liver and spleen, while the remainder activity is assumed to be evenly distributed. The Activity of each organ was divided into the activity of particular contributing components ^{177}Lu1+^{177}Lu2 and ^{177m}Lu as a percent injected dose (%ID), to be used for further determination of the absorbed dose to each organ. The absorbed dose was estimated using the DFs (dose factors), from OLINDA software. A combination of several methods for determination of the activity in the total body and different organs, especially to the kidneys (considered to be the main organ at risk) was applied. Thus, this implies the method from Image base method, Planar and SPECT (%ID) for different time points, referred to as *"Case 1"*, ^{177}Lu1+^{177}Lu2 referred to as *"Case 2a"* and only ^{177m}Lu *"Case 2b"* Furthermore the ^{177}Lu1 activity, ^{177m}Lu and ^{177}Lu2 contribution at different time points has been estimated.

Because of the fact, that patient measurements were performed at different time points, the outcomes show different values for the activities. Furthermore, the radionuclide purity is an important factor for a safe administration of the radiotherapy in Patients treated with ^{177}Lu.-DOTATATE. In the following tables, details on patient included in the research project, their gender, administered activity and date of administration, therapy cycle as well as the details related to their weight and thickness are presented. Moreover, the TB corrected count rate from anterior and posterior measurement, and detector systems used, are listed in the following table:

Patient	Initials	Gender	Cycle no	Administration date [MBq]	Administered Activity [MBq]	Weight [kg]	Thickness [cm]
1	AA	F	4	4/19/2012	7435	57.4	18.8
2	TA	M	2	4/26/2012	7480	65	21.9
3	CK	M	1	5/31/2012	7235	99.8	27.4
4	MC	F	4	5/31/2012	7145	60.8	19.1
5	UH	M	4	6/7/2012	7460	77.3	24.3
5	UH	M	5	8/16/2012	7395	74	24.3
6	SG	F	2	6/14/2012	7545	70	20
7	IN	F	6	6/14/2012	7435	61.3	22.7

TB Corrected Count Rate

	Measurement 1			***Measurement 2***			***Measurement 3***		
	Rcorr, ant-upper; post-lower			***Rcorr, ant-upper; post-lower***			***Rcorr, ant-upper; post-lower***		
P	***NaI(Tl)***	***HPGe***	***Distance***	***NaI(Tl)***	***HPGe***	***Distance***	***NaI(Tl)***	***HPGe***	***Distance***
1	187.69		340	N/A	N/A	310			
	N/A			N/A	N/A	290			
2	276.62		321	3.74		121	0.26	0.07	151
	246.34		308	3.15		121	0.33	0.16	151
3	147.56		310	1.67	1.26	143	N/A		89
	125.19		300	1.63	1.75	138	N/A		100
4	107.12		300	1.62	1.31	165			
	73.49		298	0.87	0.81	165			
5	113.83		310	1.74	1.28	173			
	79.28		300	1.11	1.52	173			
5									
		0.14	15						
6	100.30	86.32	310	0.07		120	N/A		
	101.42	85.97	290	0.23		124	N/A		
7	235.09	194.17	310	0.15		125			
	205.53	174.87	290	0.25		120			

Table no. 4 Details on measured Patient measurements and obtained corrected count rate from TB measurements with detector systems

In more details this chapter of the report will address the outcomes from the TB Activity and Kidney Activity determination for each of the measured Patient.

PATIENT 1

The 1st measurement has been performed 7 days after the 4th radiotherapy administration with the activity of 7435 MBq. The first measurement was only performed in anterior position at distance 340 cm from the center of body using NaI(TI) detector system. The data acquisition time was set 305.2 *s*.

The 2nd measurement was performed using both detector systems at a distance 310 cm anterior and 290 cm posterior from the center of body to the detector systems. The data acquisition time for both detectors was 299 *s*. Unfortunately in this specific case the data could not be analyzed and the activity determination at this time point was not possible, because ROI was difficult to be identified.

The data analysis showed that the Activity in the TB after 7 days period, based on the image based method was 727.8 MBq after 165.2 hours, while based on NaI(Tl) detector system measurement it turned out to be 680.7 MBq (for both contributing terms ^{177}Lu1 and ^{177}Lu2). The Activity for each contributing term: ^{177}Lu1, ^{177m}Lu, ^{177}Lu2 and ^{177}Lu1+ ^{177}Lu2, is shown in the table below:

TOTAL BODY ACTIVITY (MBq)					
Image based	**Time p.i. [h]**	**^{177}Lu1**	**^{177m}Lu**	**^{177}Lu2**	**^{177}Lu1 + ^{177}Lu2**
	0.2	7411.5	4.5	0.16	7411.7
	20.8	2369	1.6	0.08	2369
	92.7	1265.7	1.1	0.10	1265.8
	165.2	727.8	0.9	0.11	728
NaI(Tl) based					
	165.0	680.7	0.8	0.10	680.8

Table no. 5 Total Body Activity Image based and NaI(Tl) based at different time points for all contributing terms – Patient 1

The activity distribution at different time points is shown in the plot below:

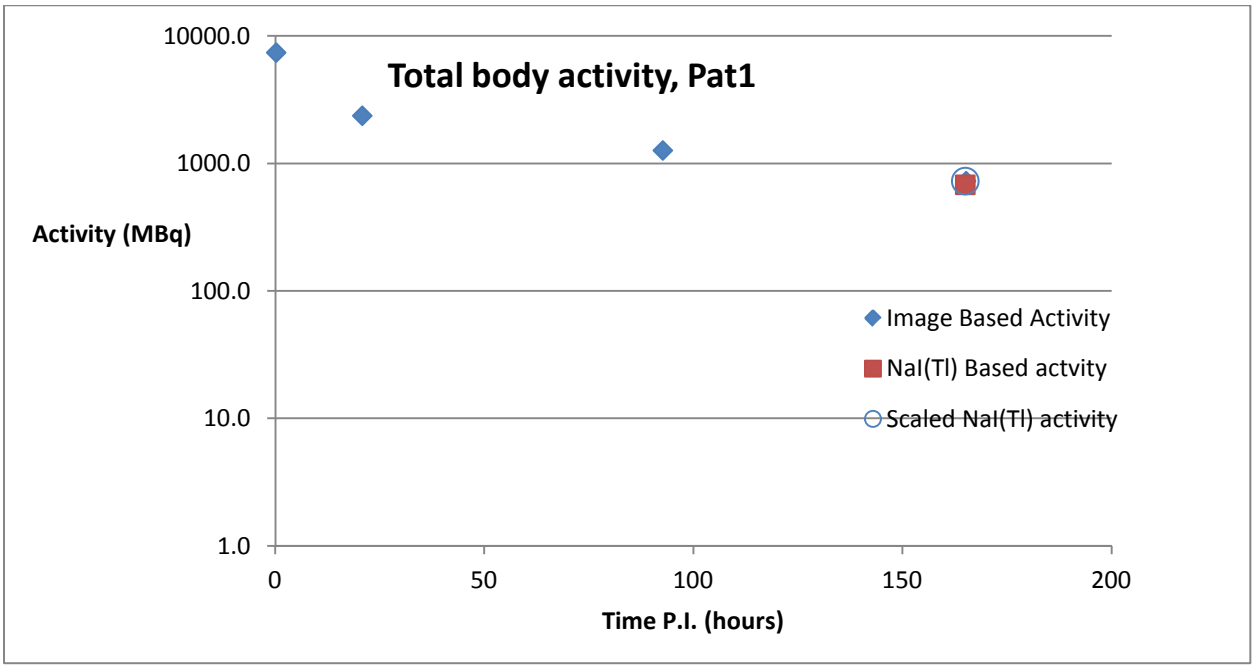

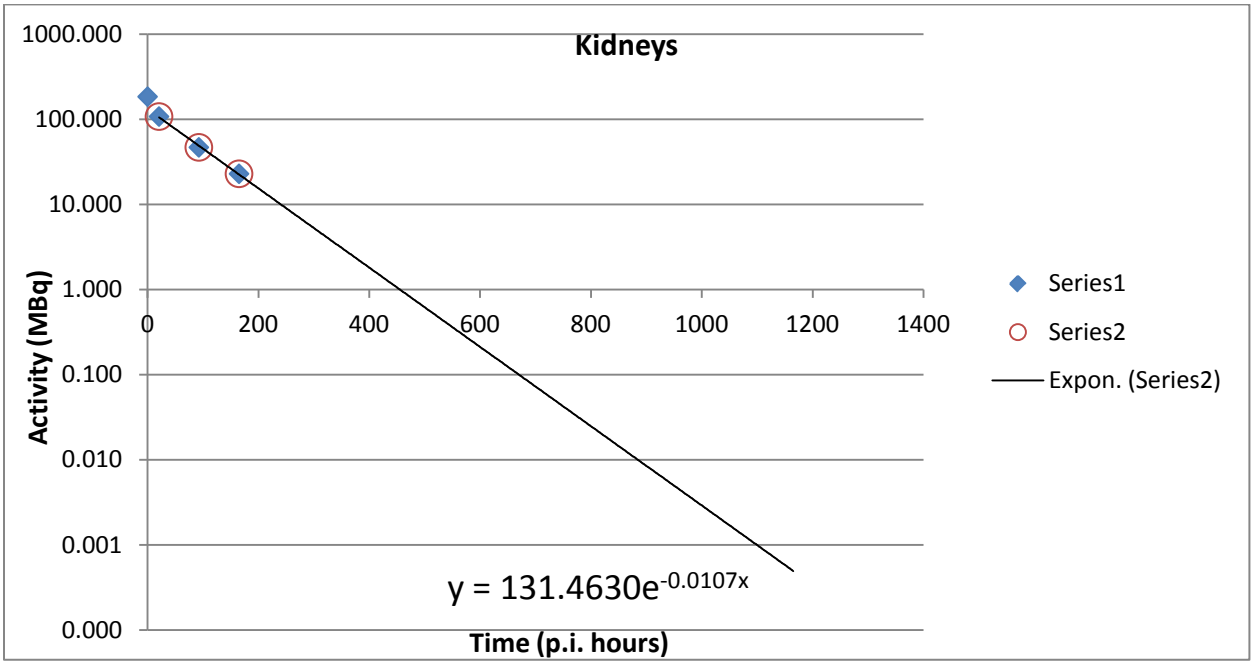

Fig. 21, Plot of results from TB activity and Kidney in Patient 1

The Activity for organs: Kidneys, Liver and Spleen at different time points is shown in the following table:

Case 1: Planar and SPECT (%ID)				
Time p.i. [h]	REMAINDER	KIDNEYS	LIVER	SPLEEN
0.2	86.5	2.5	10	1
20.8	16.6	1.5	12.8	1.2
92.7	8.6	0.6	7.3	0.6
165.2	4.8	0.3	4.4	0.4
Case 2a: ^{177}Lu1+^{177}Lu2				
Time p.i. [h]	**REMAINDER**	**KIDNEYS**	**LIVER**	**SPLEEN**
0.2	86.5	2.5	10	1
20.8	16.6	1.5	12.8	1.2
92.7	8.6	0.6	7.2	0.6
165.2	4.8	0.3	4.3	0.4
Time p.i. [h]	**REMAINDER**	**KIDNEYS**	**LIVER**	**SPLEEN**
0.283	86.5	2.5	10	1
20.867	18	1.6	13.9	1.2
92.733	12.5	0.1	10.6	0.9
165.25	9.5	0.6	8.5	0.7

Table no.6, ID% and Absorbed Dose for Kidneys and TB from: Case1: Planar and SPECT, Case2a: ^{177}Lu1+^{177}Lu2 and Case 2b: ^{177m}Lu for Patient 1

In this particular case, the absorbed dose was not determined, because of the fact that the 1st measurement was only performed in anterior position, and the curve fitting in OLIDA was not easy way to observe. Meanwhile the data obtained from the 2nd measurement could not be analyzed.

PATIENT 2

The 1st measurement has been performed 7 days after the 2nd radiotherapy administration with the activity of 7480 MBq. The first measurement was performed both in anterior and posterior position, using NaI(TI) detector at a distance from the center of body 321 cm, respectively 308 cm for the later measurement. The data acquisition time was 303.5 *s* (anterior) and 292.3 *s* (posterior).

The 2nd measurement was performed using only one detector system same as in the 1st measurement. Anterior and posterior data acquisition was obtained at 298 *s* and 298.4 *s* for the

later position of measurement. The distance from the center of body to the detector system was 121 cm for both sides of the measurements.

The 3rd measurement was performed after 70 days from the date of administration using both detector systems at a distance 151 cm from the center of body to the detector systems in both sides of the measurements. The data acquisition time for NaI(Tl) detector was 299.5 *s* for anterior and 299.5 *s* for posterior, while for HPGe detector it was 299.3 *s* for anterior and 299.2 *s* for posterior measurement.

Data analysis shows that the Activity in the TB after 7 days period, based on the image based method was 1216.1 MBq (after 165.4 hours), while based on NaI(Tl) detector system measurement it showed to be 1128.3 MBq (after 166 hours). In this particular patient the measurement was also performed at a later time point, more specifically after 61 days (approximately, 2 month after the administration). The activity shows to be 0.5 MBq for NaI(Tl) based method and 0.2 MBq for HPGe based method. In the following table the activity at different time points for used methods as well as the activity for each contributing terms, is shown:

TOTAL BODY ACTIVITY [MBq]					
Image based	**Time p.i. [h]**	**^{177}Lu1**	**^{177m}Lu**	**^{177}Lu2**	**^{177}Lu1 + ^{177}Lu2**
	0.3	7456	4.5	0.18	7456.2
	22.4	3660.8	2.4	0.13	3661
	93.3	2005.3	1.8	0.17	2005.4
	165.4	1216.1	1.4	0.19	1216.3
NaI(Tl) based					
	166.0	1128.3	1.3	0.17	1128.5
	958.7	12.8	0.4	0.09	12.9
	1462.0	0.6	0.1	0.03	0.6
HPGe based					
	1462.0	0.2	0.05	0.01	0.2

Table no. 7 Total Body Activity Image based and NaI(Tl) based at different time points for all contributing terms – Patient 2

Furthermore, the activity distribution at different time points is shown in the plot below:

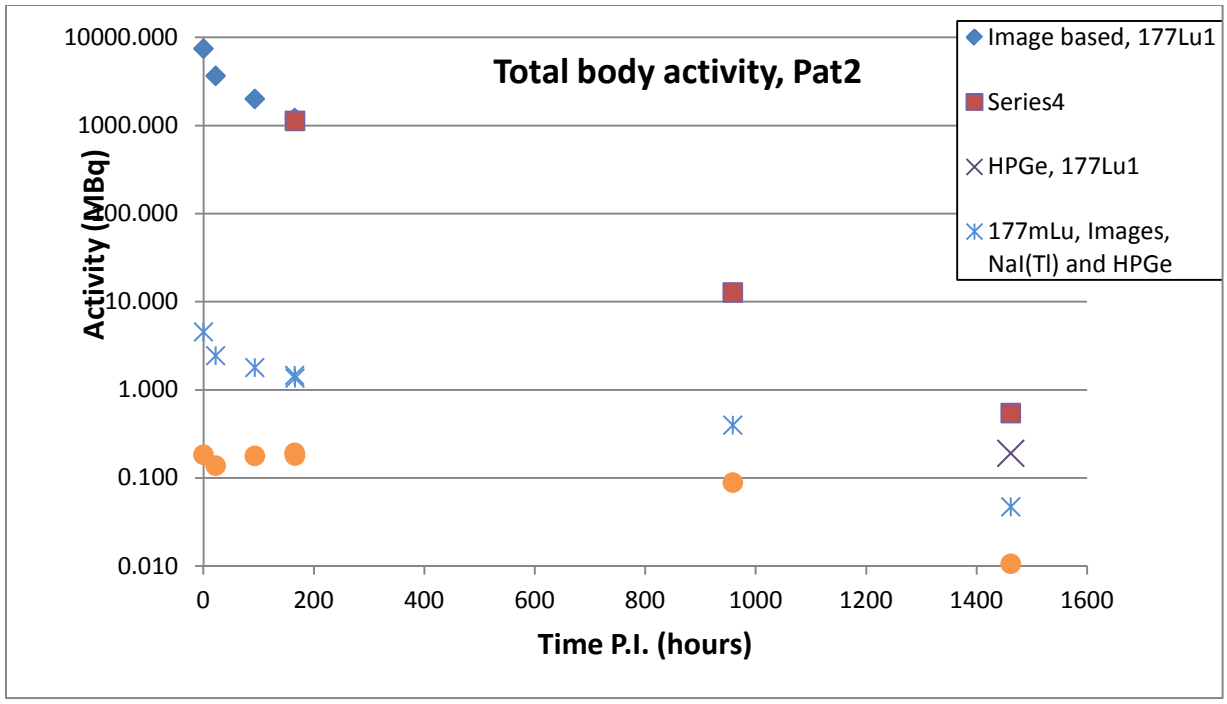

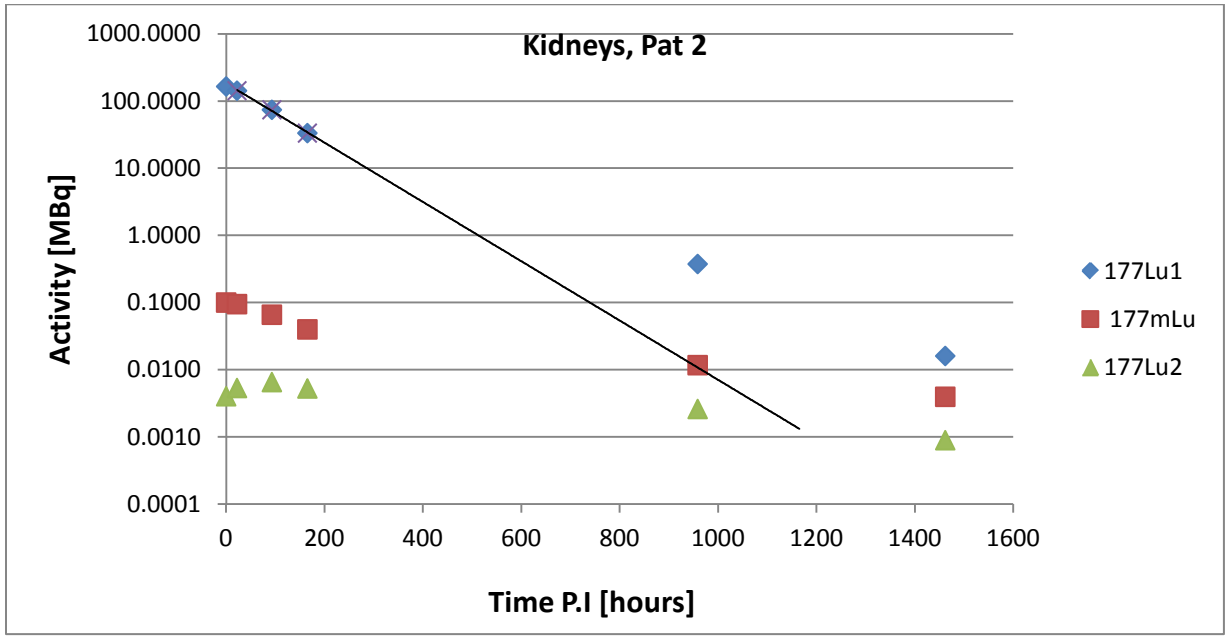

Fig 22, Plots on results from Patient 2 measurements at different time points, TB Activity and Kidneys

The data analysis shows that the TB Activity after 7 days period of time still remains high (comparing to other patient measurements), it results to be 1216.1 MBq (based on planar and SPECT), 1128.3 MBq from NaI(Tl) based measurement. The 2nd measurement was conducted after approximately 39 days and the activity results to be 12.8 MBq. This was the only patient which after the 3rd measurement the data analysis could still be performed. It was carried out

after approximately 61 days (from the date of administration) and from data analysis the Activity results to be: for NaI(Tl) based 0.5 MBq and 0.2 MBq for the HPGe based method.

Furthermore the determination of the absorbed dose was calculated by fitting the activity data to a function for each particular organ, using OLINDA software. The absorbed dose determination for each organ was made in the unit of Gy. Below is shown the %ID, which is the activity in and organ, divided by the injected amount, in percent.

In the following table the activity concentration for each particular organ is shown:

Case 1: Planar and SPECT					
Time p.i. [h]	REMAINDER	KIDNEYS	LIVER	SPLEEN	
0.3	89.4	2.2	6.5	1.9	
22.4	36	2	7.9	3.2	ABSORBED DOSE [Gy] Case 1
93.3	18.6	1	5.4	1.9	Kidneys / Total Body
165.4	11.4	0.4	3.5	0.9	5.3 / 0.7
Time p.i. [h]	REMAINDER	KIDNEYS	LIVER	SPLEEN	
0.3	89.4	2.2	6.5	1.9	
22.4	36	2	7.9	3.2	
93.3	18.6	1	5.4	1.9	
165.4	11.4	0.4	3.5	0.9	ABSORBED DOSE [Gy] Case 2a + 2b
958.7	0.1	0.00	0.03	0.01	Kidneys / Total Body
1462.0	0.00	0.00	0.00	0.00	5.6 / 0.8
Time p.i. [h]	REMAINDER	KIDNEYS	LIVER	SPLEEN	
0.3	89.5	2.2	6.5	1.9	
22.4	39.5	2.1	8.7	3.5	
93.3	27.2	1.4	7.9	2.8	
165.4	22.4	0.9	6.9	1.9	
958.7	6.6	0.2	2.03	0.6	
1462.0	2.2	0.1	0.7	0.2	

Table no.8, ID% and Absorbed Dose for Kidneys and TB from: Case1: Planar and SPECT, Case2a: ^{177}Lu1+^{177}Lu2 and Case 2b: ^{177m}Lu for Patient 2

Therefore, the absorbed dose based on the Planar and SPECT method, for the kidneys is 5.3 Gy and for the TB, 0.75 Gy. The method based on the images and NaI(Tl) based measurements the absorbed dose results to be for the kidneys 5.6 Gy and for the total body 0.8 Gy.

PATIENT 3

The 1st measurement has been performed 7 days after the 1st radiotherapy administration with the activity of 7235 MBq. The measurement has been performed in both anterior and posterior position, at a distance 310 cm, respectively 300 cm for the later measurement. The data acquisition time was 290.3 *s* (anterior) and 290.2 *s* posterior.

The 2nd measurement was performed using both detector systems, NaI(Tl) and HPGe. Anterior and posterior data acquisition were obtained at 299.04 *s* (anterior) and 298.98 *s* (posterior) for measurements performed with NaI(Tl), while the data acquisition using HPGe detector was 298.6 *s* (anterior) and 298.5 *s* (posterior). The distance from the center of body to the detector system was 143 cm for the anterior measurement and 138 cm for the posterior measurement for both detector systems.

The 3rd measurement was performed using NaITl) detector system only. The distance from the center of body was set to be 89 cm for anterior measurement and 100 cm for posterior measurement. The decision for having shorter distance was made due to the fact that we could obtain the desirable number of counts registered. In this measurement the data acquisition time was set longer at 679.4 *s* for anterior measurement and 630.7 *s* for posterior measurement. For this particular measurement the data could not be analyzed. From data analysis the TB Activity after 7 days, according to the image based method the activity is 879.1 MBq (after 164.4 h), while based on the NaI(Tl) measurement it resulted to be only 873 MBq . The activity for each contributing terms and different time points measurements are shown in the following table:

TOTAL BODY ACTIVITY [MBq]					
Image based	**Time p.i. [h]**	**^{177}Lu1**	**^{177m}Lu**	**^{177}Lu2**	**^{177}Lu1 + ^{177}Lu2**
	0.2	7214	4	0.08	7214
	23.3	2624.5	1.6	0.06	2624.5
	92.3	1434.6	1.2	0.10	1434.7
	164.4	879.2	0.9	0.11	879.3
NaI(Tl) based					
	165.1	873	0.9	0.11	873.2
	957.5	9	0.2	0.06	9.1
HPGe based					
	957.49	3.2	0.08	0.02	3.2

Table no. 9 *Total Body Activity Image based, NaI(Tl) and HPGe based respectively, at different time points for all contributing terms – Patient 3*

The TB activity at different time points is shown in the plot below:

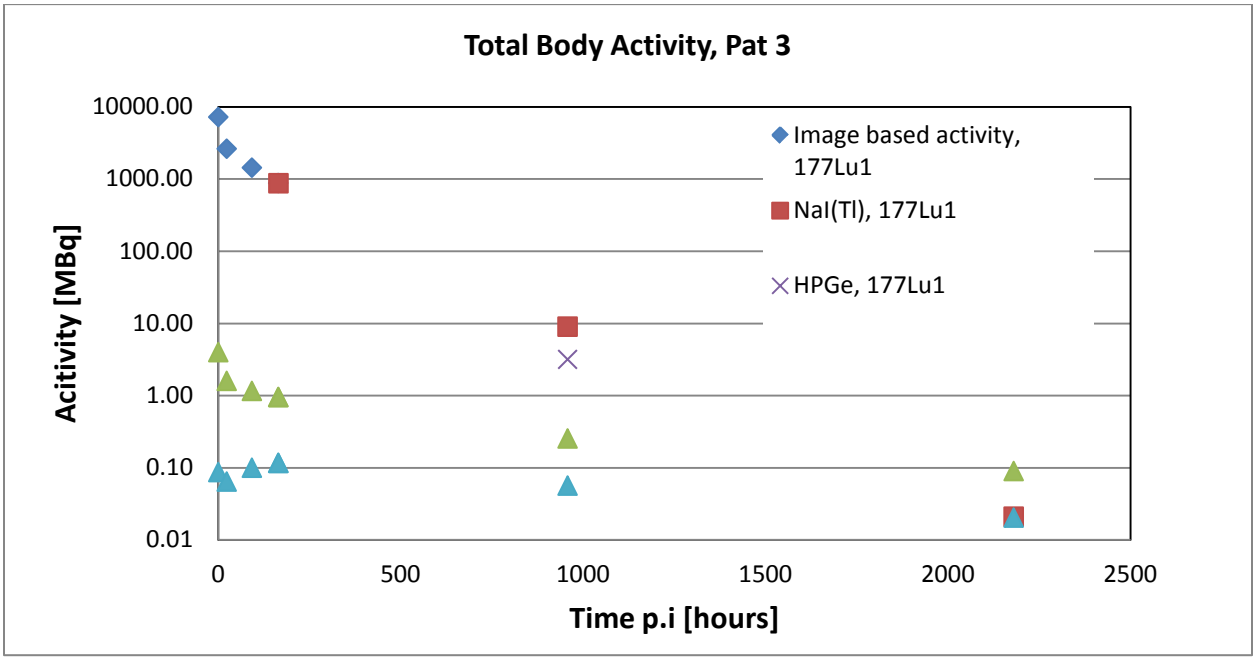

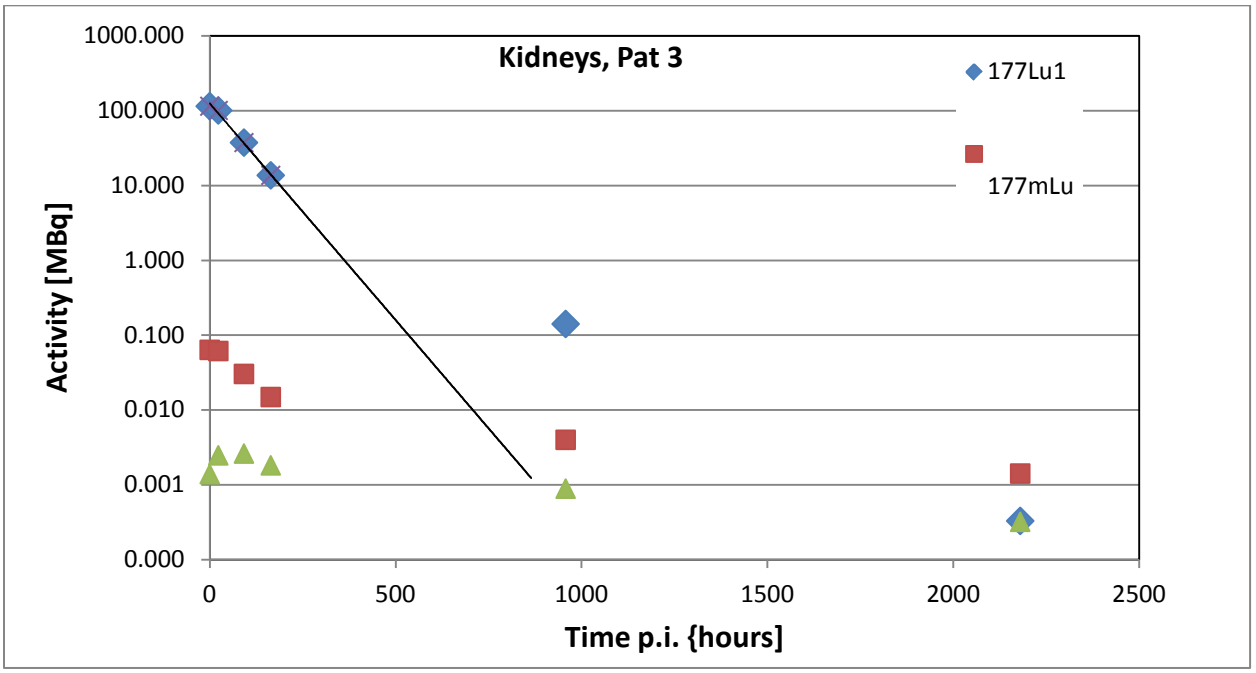

Fig. 23, Plot on results from TB activity and Kidneys in Patient 3

The data analysis on Activity determination in the TB after the 7th day of the radiotherapy administration results to be 879.2 MBq. As the 2nd measurement was performed after approximately 40 days, the activity results to be for NaI(TI) detector 9 MBq while the results from measurements performed with HPGe detector on data analysis for activity determination results to be 3.1 MBq. The 3rd measurement was performed after 52 days (from the date of administration). In this particular measurement, even though a longer acquisition time was set, it was not possible to mark the ROI therefore, no activity calculation was possible. It was mainly background interference.

Furthermore the determination of the absorbed dose was calculated by fitting the activity data to a function for each particular organ, using OLINDA software. The absorbed dose determination for each organ was made in the unit of Gy. Below is shown the %ID, which is the activity in and organ, divided by the injected amount, in percent.

Case 1: Planar and SPECT				
Time p.i. [h]	**REMAINDER**	**KIDNEYS**	**LIVER**	**SPLEEN**
0.2	89.7	1.6	8	0.7
23.3	23.7	1.4	10.2	1
92.3	12.3	0.5	6.6	0.4
164.4	7.4	0.3	4.4	0.2
Case 2a: ^{177}Lu1+^{177}Lu2				
Time p.i. [h]	**REMAINDER**	**KIDNEYS**	**LIVER**	**SPLEEN**
0.2	89.7	1.6	8	0.7
23.3	23.7	1.4	10.2	1
92.3	12.3	0.5	6.6	0.4
164.4	7.3	0.2	4.4	0.2
957.5	0.07	0.00	0.04	0.00
Case 2b: ^{177m}Lu				
Time p.i. [h]	**REMAINDER**	**KIDNEYS**	**LIVER**	**SPLEEN**
0.2	89.7	1.6	8	0.7
23.3	26.1	1.5	11.3	1
92.3	18	0.7	9.6	0.7
164.4	14.4	0.4	8.7	0.4
957.5	3.9	0.09	2.3	0.1

ABSORBED DOSE [Gy] Case 1	
Kidneys	Total Body
2.9	0.5

ABSORBED DOSE [Gy] Case 2a+2b	
Kidneys	Total Body
3.1	0.6

Table no.10, ID% and Absorbed Dose for Kidneys and TB from: Case1: Planar and SPECT, Case2a: ^{177}Lu1+^{177}Lu2 and Case 2b: ^{177m}Lu for Patient 3

Therefore, the absorbed dose based on the Planar and SPECT method, for the kidneys is 2.9 Gy and for the TB, 0. 5 Gy. The method based on the images and NaI(Tl) based measurements the absorbed dose results to be for the kidneys 3.1 Gy and for the total body 0.6 Gy.

PATIENT 4

The 1st measurement was performed 7 days after the 4th cycle radiotherapy administration with the activity of 7145 MBq. The measurement was performed both in anterior and posterior position, at a distance 310 cm, respectively 298 cm for the later measurement. The data acquisition time was 293.9 *s* (for anterior measurement) and 293 *s* (for posterior measurement).

The 2nd measurement was performed using both detector systems, NaI(Tl) and HPGe. Anterior and posterior data acquisition was obtained at 299.3 *s* (anterior) and 299.4 *s* (posterior) for measurements performed with NaI(Tl), while the data acquisition using HPGe detector was 299 *s* (anterior) and 299.2 *s* (posterior). The distance from the center of body to the detector system was 165 cm, from both detector systems. The data analysis showed that the Activity in the TB after 7 days period, based on the image based method was 334.1 MBq (after 165 hours), while based on NaI(Tl) method it shows to be 307.7 MBq. At a later time point approximately after 32 days, the total body activity for the measurement with NaI(Tl) showed to be 4 MBq while for HPGe, 3.44 MBq.

TOTAL BODY ACTIVITY [MBq]					
Image based	**Time p.i. [h]**	**^{177}Lu1**	**^{177m}Lu**	**^{177}Lu2**	**^{177}Lu1 + ^{177}Lu2**
	0.6	7124.2	4	0.08	7124.3
	20.5	1259.8	0.7	0.02	1259.8
	92.9	605.2	0.5	0.04	605.2
	165.0	334.1	0.4	0.04	334
NaI(Tl) based					
	165.6	307.7	0.3	0.04	307.8
	790.5	4	0.06	0.01	4
HPGe based					
	790.55	3.4	0.05	0.01	3.4

Table no. 11 Total Body Activity Image based and NaI(Tl) based at different time points for all contributing terms

Furthermore, the activity distribution at different time points is shown in the plot below:

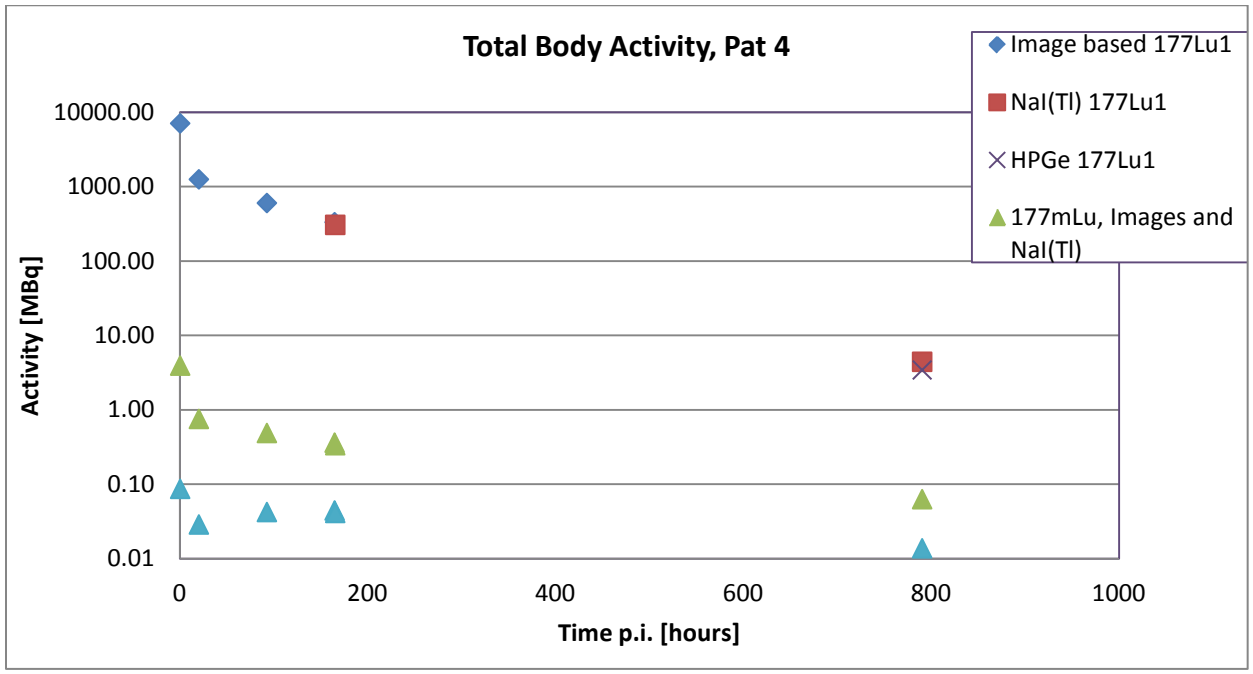

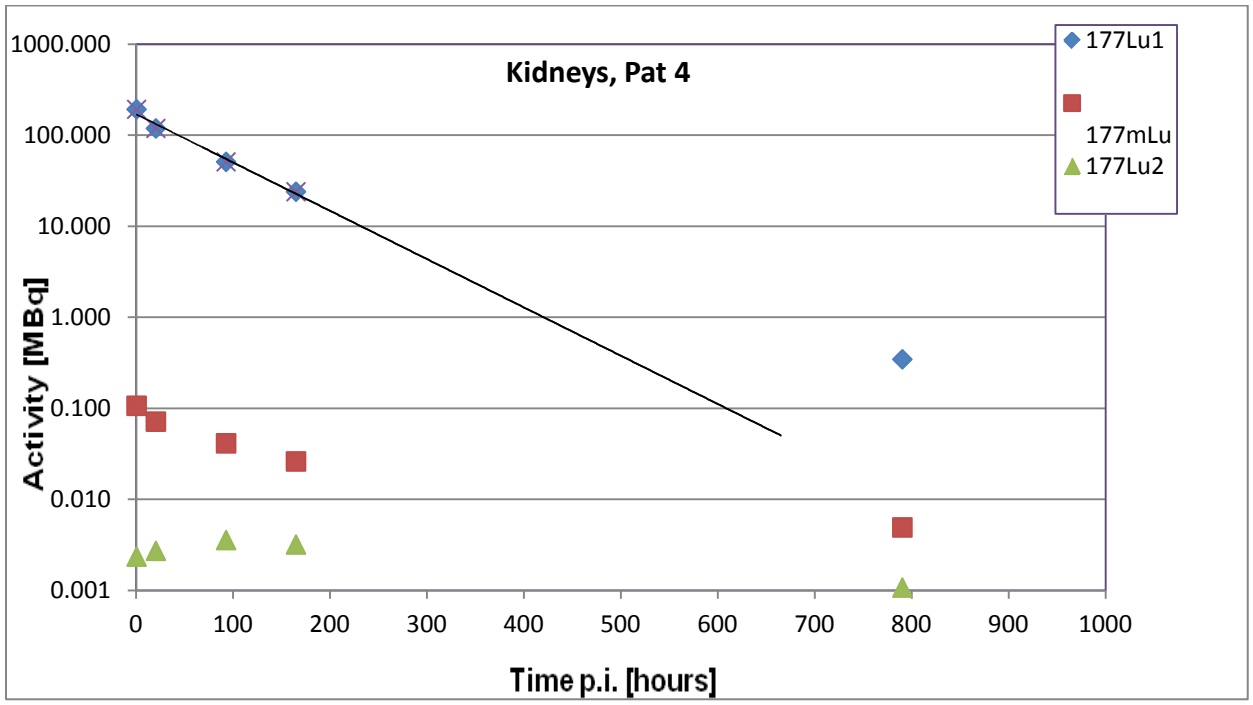

Fig. 24. Plot on results from TB activity and Kidneys in Patient 4

Furthermore the determination of the absorbed dose was calculated by fitting the activity data to a function for each particular organ, using OLINDA software. The absorbed dose

determination for each organ was made in the unit of Gy. Below is shown the %ID, which is the activity in and organ, divided by the injected amount, in percent.

Case 1: Planar and SPECT				
Time p.i. [h]	**REMAINDER**	**KIDNEYS**	**LIVER**	**SPLEEN**
0.6	92.9	2.7	3.4	1
20.5	12	1.7	2.9	1
92.9	5.8	0.7	1.4	0.5
165.0	3.3	0.3	0.8	0.3
Case 2a: ^{177}Lu1+^{177}Lu2				
Time p.i. [h]	**REMAINDER**	**KIDNEYS**	**LIVER**	**SPLEEN**
0.6	92.9	2.7	3.4	1
20.5	12	1.7	2.9	1
92.9	5.8	0.7	1.3	0.5
165.0	3.3	0.3	0.8	0.3
790.5	0.04	0.00	0.01	0.00
Case 2b: ^{177m}Lu				
Time p.i. [h]	**REMAINDER**	**KIDNEYS**	**LIVER**	**SPLEEN**
0.6	93.1	2.7	3.4	1
20.5	13.1	1.8	3.1	1.2
92.9	8.6	1	2	0.8
165.0	6.4	0.7	1.6	0.6
790.5	1.08	0.1	0.3	0.1

ABSORBED DOSE [Gy] Case 1	
Kidneys	Total Body
4.2	0.3

ABSORBED DOSE [Gy] Case 2a+2b	
Kidneys	Total Body
4.5	0.3

Table no.12, ID% and Absorbed Dose for Kidneys and TB from: Case1: Planar and SPECT, Case2a: ^{177}Lu1+^{177}Lu2 and Case 2b: ^{177m}Lu for Patient 4

Therefore, the absorbed dose based on the Planar and SPECT method, for the kidneys is 4.2 Gy and for the TB, 0. 3 Gy. The method based on the images and NaI(Tl) based measurements the absorbed dose results to be for the kidneys 4.5 Gy and for the total body 0.3 Gy.

PATIENT 5

The 1st measurement was performed 7 days after the 4th cycle of radiotherapy administration with the activity of 7460 MBq. The first measurement was performed only with NaI(TI) detector at a distance of 310 cm for anterior measurement and 300 cm for posterior measurement. The data acquisition time was 292.8 *s* (for anterior measurement) and 293.8 *s* (for posterior measurement).

The 2nd measurement was performed using both detector systems, NaI(Tl) and HPGe. Anterior and posterior data acquisition was obtained for 299.2 *s* (anterior) and 299.1 *s* (posterior) for measurements performed with NaI(Tl), while the data acquisition using HPGe detector was 298.9 *s* (anterior) and 298.74 *s* (posterior). The distance from the center of body to the detector systems was 173 cm from both detector systems.

The data analysis showed that the Activity in the TB after 7 days period, based on the image based method was 514.2 MBq (after 166 hours), while for NaI(T) based method it showed to be 482.1 MBq. At a later time point approximately after 35 days the total body activity for both NaI(Tl) and HPGe based methods resulted to be 6.4 MBq.

TOTAL BODY ACTIVITY					
Image based	**Time p.i. [h]**	**^{177}Lu1**	**^{177m}Lu**	**^{177}Lu2**	**^{177}Lu1 + ^{177}Lu2**
	0.2	7434	4.9	0.26	7434.3
	21.4	1744.2	1.2	0.08	1744.3
	94.1	843.9	0.8	0.09	844
	166	514.2	0.7	0.09	514.2
NaI(Tl) based					
	166.5	482.1	0.6	0.08	482.2
	838.4	6.4	0.1	0.03	6.4
HPGe based					
	838.4	6.4	0.1	0.03	6.4

Table no. 13 Total Body Activity Image based, NaI(Tl) and HPGe based respectively, at different time points for all contributing terms – Patient 5

Furthermore, the activity distribution at different time points is shown in the plot below:

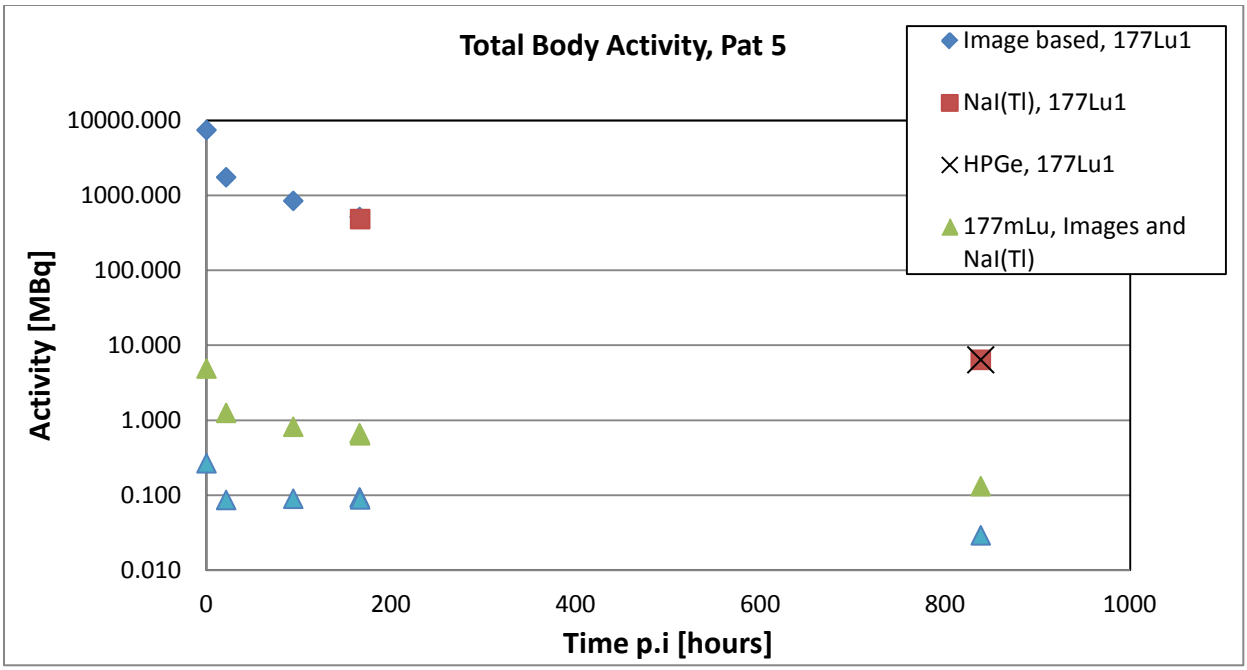

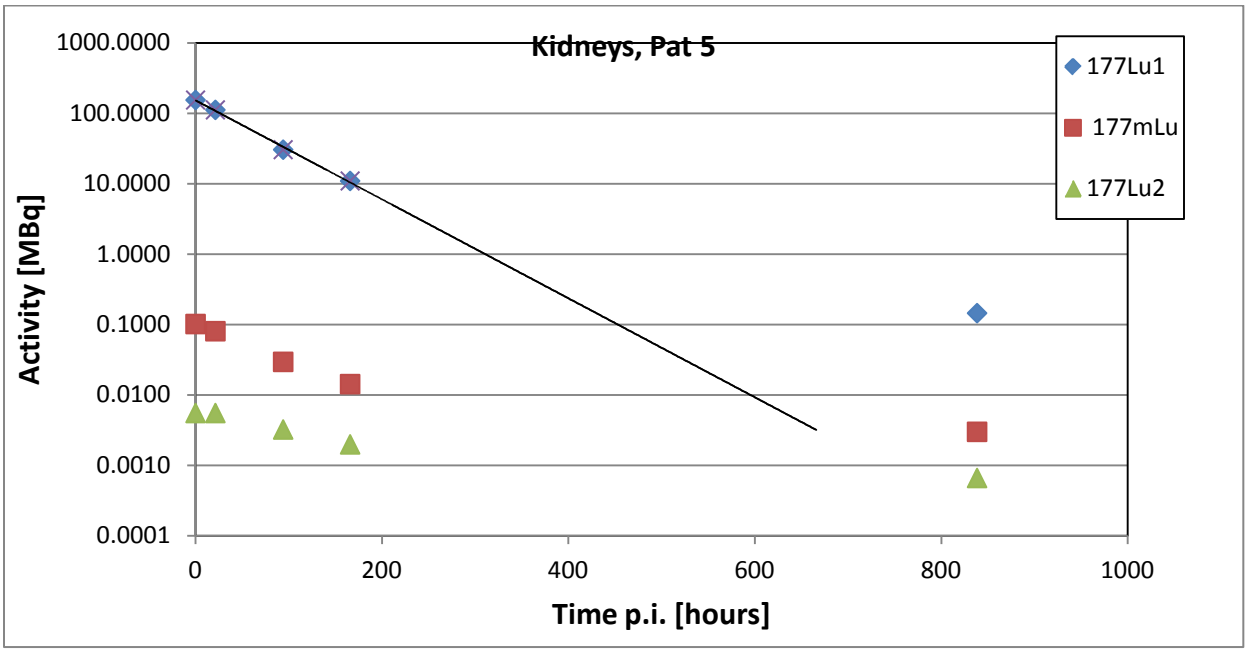

Fig. 25. Plot on results from TB activity and Kidneys in Patient 5

Furthermore the determination of the absorbed dose was calculated by fitting the activity data to a function for each particular organ, using OLINDA software. The absorbed dose determination for each organ was made in the unit of Gy. Below is shown the %ID, which is the activity in and organ, divided by the injected amount, in percent.

Case 1: Planar and SPECT				
Time p.i. [h]	REMAINDER	KIDNEYS	LIVER	SPLEEN
0.2	93.1	2	4.3	0.4
21.4	16.9	1.5	4.6	0.5
94.1	7.9	0.4	2.8	0.2
166	4.9	0.1	1.9	0.1
Case 2a: ^{177}Lu1+^{177}Lu2				
Time p.i. [h]	REMAINDER	KIDNEYS	LIVER	SPLEEN
0.2	93.1	2	4.3	0.4
21.4	16.9	1.5	4.6	0.5
94.1	7.9	0.4	2.8	0.2
166	4.9	0.1	1.78	0.1
838.4	0.06	0.00	0.02	0.00
Case 2b: ^{177m}Lu				
Time p.i. [h]	REMAINDER	KIDNEYS	LIVER	SPLEEN
0.2	93.2	2	4.3	0.4
21.4	18.4	1.6	5	0.6
94.1	11.6	0.6	4.1	0.4
166	9.6	0.3	3.5	0.2
838.4	2	0.06	0.7	0.05

ABSORBED DOSE [Gy] Case1	
Kidneys	Total Body
2.8	0.3

ABSORBED DOSE [Gy] Case 2a+2b	
Kidneys	Total Body
3.0	0.3

Table no.14, ID% and Absorbed Dose for Kidneys and TB from: Case1: Planar and SPECT, Case2a: ^{177}Lu1+^{177}Lu2 and Case 2b: ^{177m}Lu for Patient 5

Therefore, the absorbed dose based on the Planar and SPECT method, for the kidneys is 2.8 Gy and for the TB, 0. 3 Gy. The method based on the images and NaI(Tl) based measurements the absorbed dose results to be for the kidneys 3.0 Gy and for the total body 0.3 Gy.

In addition, this particular patient was measured in a very close geometry at a very late time point. His 5th cycle of treatment with administered activity of 7395 MBq. The distance from HPGe detector system to an posterior view was 15 cm. The data in this particular case could not be analyzed because it was not possible to mark the ROI therefore, no activity determination was possible. Below an illustration is presented for the very late point time measurement, when data are not possible to be analyzed:

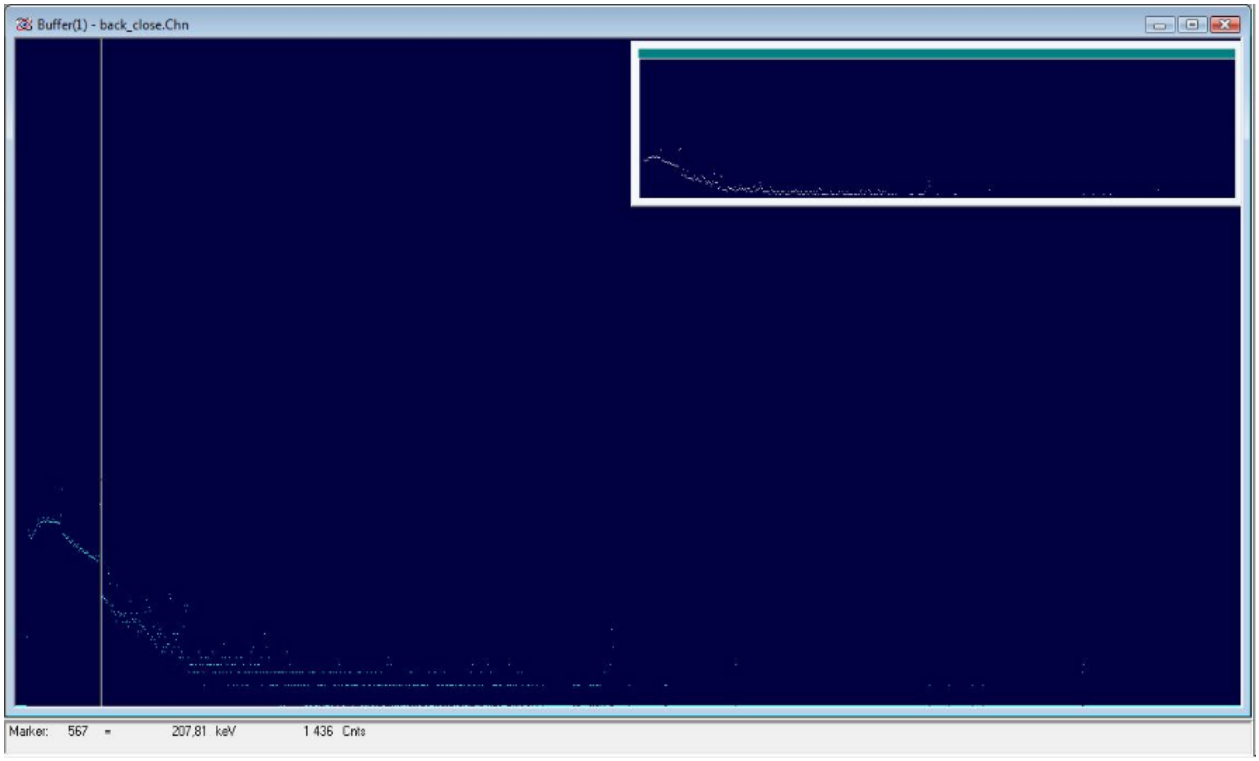

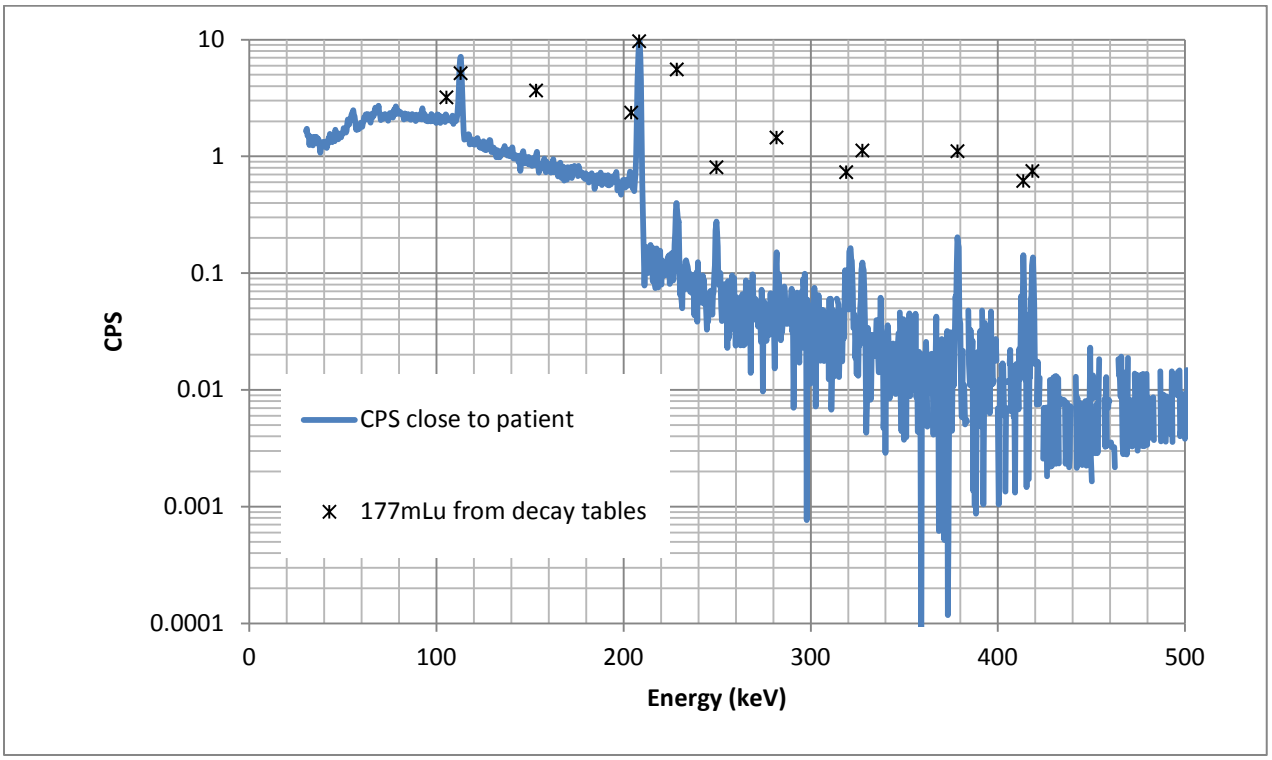

Fig. 26. Illustration from HPGe close geometry patient measurement at a late time point, upper panel from Maestro plot, lower panel the plot from the same measurement and decay of ^{177m}Lu

PATIENT 6

The 1st measurement was performed 7 days after the 2nd cycle of radiotherapy administration with the activity of 7545 MBq. using both NaI(Tl) and HPGe detector systems for anterior and posterior measurements at a distance 310 cm and 290 cm respectively. The data acquisition time for NaI(Tl) detector was 294.9 *s* (anterior) and 294 *s* (posterior). For measurements performed with HPGe the data acquisition time was 290.9 *s* (anterior) and 289.6 *s* (posterior).

The 2nd measurement was performed using only NaI(Tl) detector system for anterior and posterior measurements at a distance 120 cm and 124 cm, respectively. The data acquisition time was 299.4 *s* (anterior) and 299.3 *s* (posterior).

The 3rd measurement at a distance 133 cm for both measurement geometries was performed after 70 days from the date of administration. The data acquisition time was set to 599.2 *s* (anterior) and 599.1 *s* (posterior).

The data analysis showed that the Activity in the TB after 7 days period, based on the image based method was 465.2 MBq (after 167 hours), while for a NaI(Tl) based method it showed to be 383.8 MBq, while for HPGe, 327.8 MBq.

TOTAL BODY ACTIVITY [MBq]					
Image based	**Time p.i. [h]**	**^{177}Lu1**	**^{177m}Lu**	**^{177}Lu2**	**^{177}Lu1 + ^{177}Lu2**
	0.5	7521.4	4.5	0.15	7521.6
	23.1	1759.5	1.1	0.06	1759.6
	94.6	852.3	0.7	0.07	852.3
	167.0	465.2	0.5	0.07	465.2
NaI(Tl) based					
	166.8	383.8	0.4	0.05	383.9
HPGe based					
	166.8	327.8	0.4	0.05	327.8

Table no. 15 Total Body Activity Image based, NaI(Tl) and HPGe based respectively, at different time points for all contributing terms – Patient 6

Furthermore, the activity distribution at different time points is shown in the plot below:

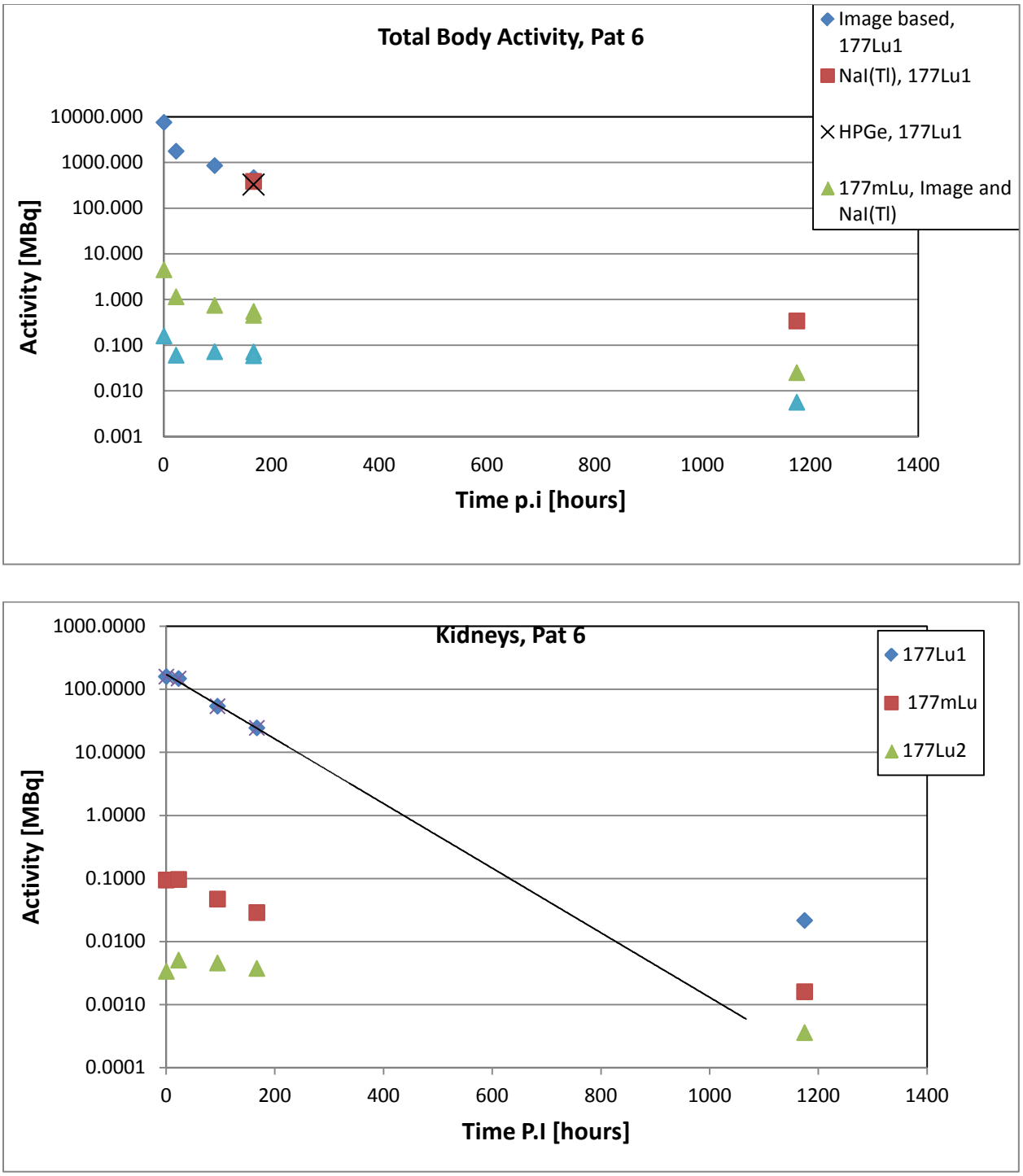

Fig. 27. Plot on results from TB activity and Kidneys in Patient 6

Furthermore the determination of the absorbed dose was calculated by fitting the activity data to a function for each particular organ, using OLINDA software. The absorbed dose determination for each organ was made in the unit of Gy. Below is shown the %ID, which is the activity in and organ, divided by the injected amount, in percent.

Case 1: Planar and SPECT				
Time p.i. [h]	REMAINDER	KIDNEYS	LIVER	SPLEEN
0.5	94.5	2.1	2.6	0.7
2317	18.4	1.2	2	1
94.6	9.2	0.7	1	0.5
167.0	5.1	0.3	0.5	0.3
Case 2a: ^{177}Lu1+^{177}Lu2				
Time p.i. [h]	REMAINDER	KIDNEYS	LIVER	SPLEEN
0.5	94.5	2.1	2.6	0.7
23.1	18.4	2	2	1
94.6	9.2	0.7	1	0.5
167.0	5.1	0.3	0.5	0.3
Case 2b: ^{177m}Lu				
Time p.i. [h]	REMAINDER	KIDNEYS	LIVER	SPLEEN
0.5	94.8	2.1	2.7	0.7
23.1	20.2	2.1	2.2	1.1
94.6	13.5	1	1.4	0.8
167.0	10	0.6	1	0.5

ABSORBED DOSE [Gy] Case1	
Kidneys	Total Body
4.8	0.4

ABSORBED DOSE [Gy] Case 2a+2b	
Kidneys	Total Body
5.2	0.4

Table no.16, ID% and Absorbed Dose for Kidneys and TB from: Case1: Planar and SPECT, Case2a: ^{177}Lu1+^{177}Lu2 and Case 2b: ^{177m}Lu for Patient 6

Therefore, the absorbed dose based on the Planar and SPECT method, for the kidneys is 4.8 Gy and for the TB, 0. 4 Gy. The method based on the images and NaI(Tl) based measurements the absorbed dose results to be for the kidneys 5.2 Gy and for the total body 0.4 Gy.

PATIENT 7

The 1st measurement was performed 7 days after the 6th cycle of radiotherapy administration with the activity of 7435 MBq using both NaI(Tl) and HPGe detector systems for anterior and posterior measurements at a distance 310 cm and 290 cm respectively. The data acquisition time for NaI(Tl) detector was 288.3 *s* (anterior) and 287.4 *s* (posterior), while for measurements performed with HPGe the data acquisition time was 279.1 *s* (anterior) and 277.6 *s* (posterior).

The 2nd measurement was performed using NaI(Tl) detector system only, for both anterior and posterior measurements at a distance 125 cm and 120 cm, respectively. The data acquisition

time was 299.5 *s* (anterior) and 299.4 *s* (posterior). The data analysis showed that the Activity in the TB after 7 days period, based on the image based method was 1081.5 MBq (after 167 hours), while for a NaI(Tl) based method it shows to be 1002.7 MBq and for HPGe, it showed to be 840.5 MBq.. For a later time point (after 48 days) the Activity for NaI(Tl) based method 0.6 MBq.

TOTAL BODY ACTIVITY [MBq]					
Image based	**Time p.i. [h]**	**^{177}Lu1**	**^{177m}Lu**	**^{177}Lu2**	**^{177}Lu1 + ^{177}Lu2**
	0.3	7411.8	4.4	0.15	7412
	20.8	4673	3	0.15	4673
	93.5	2201	1.9	0.18	2201.2
	167.7	1081.5	1.3	0.16	1081.7
NaI(Tl) based					
	167.2	1002.7	1.2	0.15	1002.8
	1164.0	0.6	0.04	0.01	0.6
HPGe based					
	167.1	840.5	1	0.13	840.7

Table no. 17 Total Body Activity Image based, NaI(Tl) and HPGe based, respectively, at different time points for all contributing terms – Patient 7

Furthermore, the activity distribution at different time points is shown in the plot below:

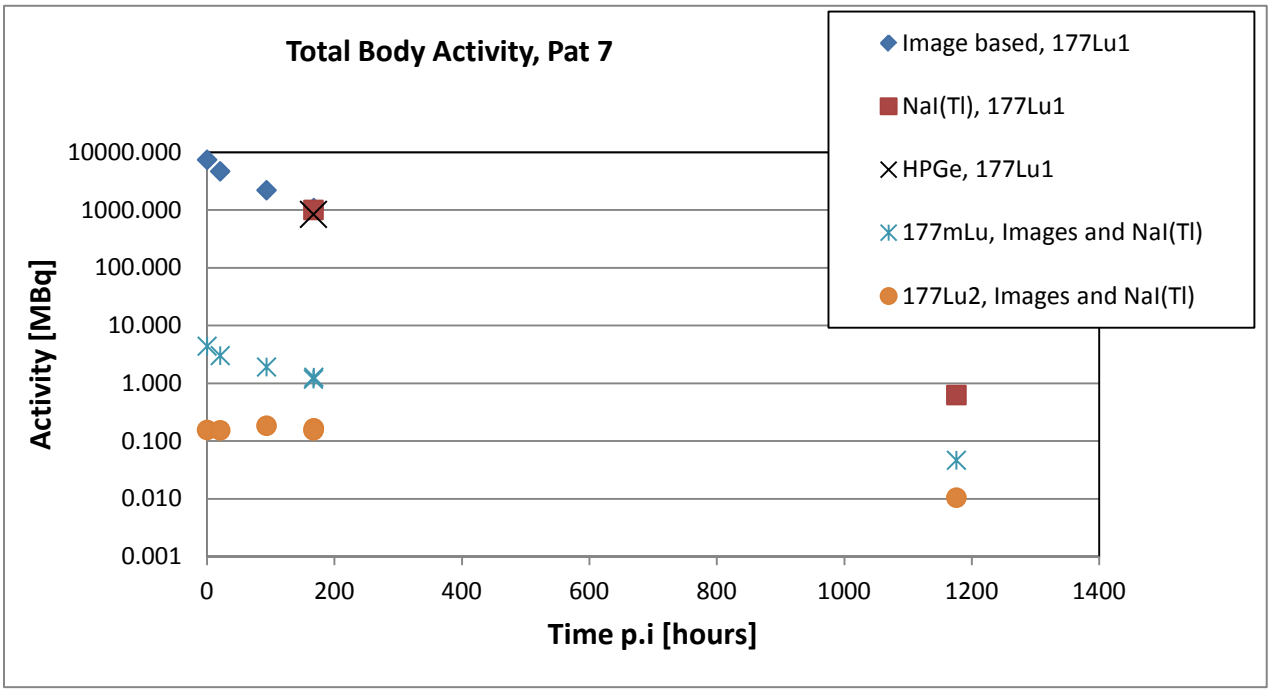

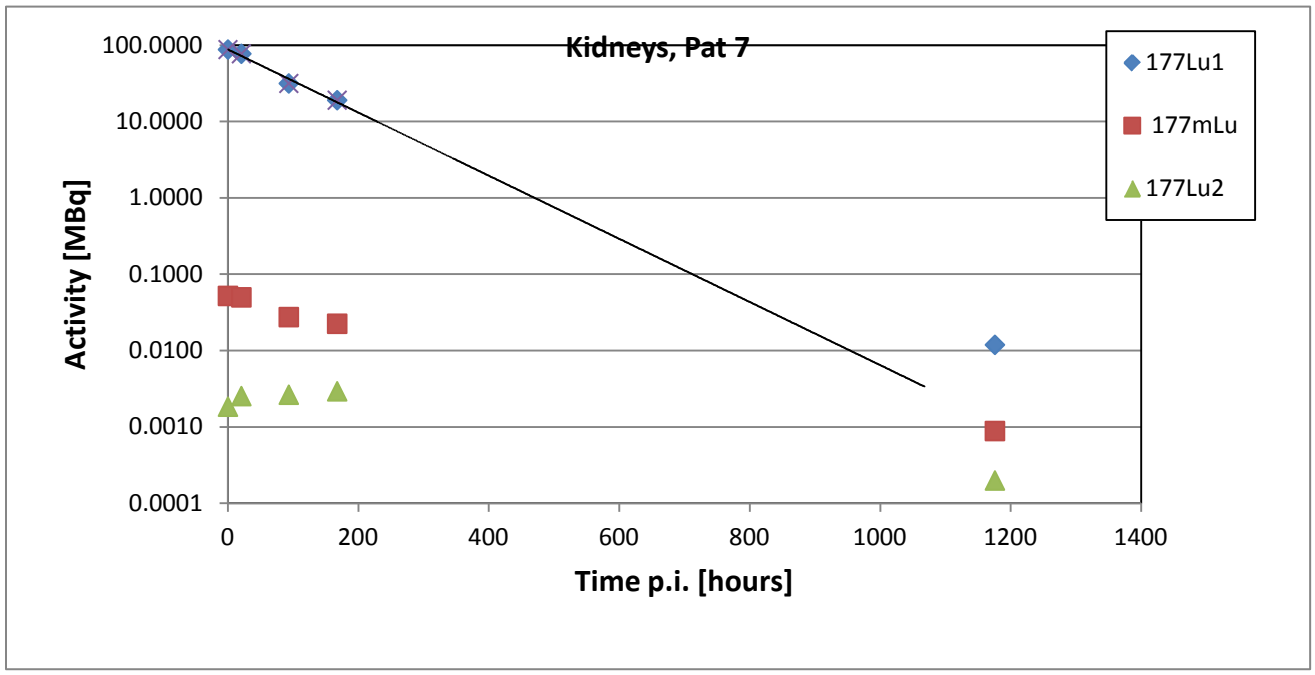

Fig. 28. Plot on results from TB activity and Kidneys in Patient 7

Furthermore the determination of the absorbed dose was calculated by fitting the activity data to a function for each particular organ, using OLINDA software. The absorbed dose determination for each organ was made in the unit of Gy. Below is shown the %ID, which is the activity in and organ, divided by the injected amount, in percent.

Case 1: Planar and SPECT				
Time p.i. [h]	REMAINDER	KIDNEYS	LIVER	SPLEEN
0.3	85.6	1.2	13.2	0
20.8	49.9	1	12.1	0
93.5	23	0.4	6.3	0
167.7	11.3	0.2	3.1	0
Case 2a: ^{177}Lu1+^{177}Lu2				
Time p.i. [h]	REMAINDER	KIDNEYS	LIVER	SPLEEN
0.3	85.6	1.2	13.2	0
20.8	49.9	1	12.1	0
93.5	23	0.4	6.3	0
167.7	11.2	0.2	3.1	0
1164.0	0.00	0.00	0.00	0
Case 2b: ^{177m}Lu				
Time p.i. [h]	REMAINDER	KIDNEYS	LIVER	SPLEEN
0.3	85.7	1.2	13.2	0

ABSORBED DOSE [Gy] Case1	
Kidneys	Total Body
2.9	0.9

ABSORBED DOSE [Gy] Case 2a+2b	
Kidneys	Total Body
3.7	1.0

20.8	54.4	1.1	13.2	0
93.5	33.8	0.6	9.2	0
167.7	22.4	0.5	6.2	0
1164.0	0.8	0.01	0.2	0

Table no.19, ID% and Absorbed Dose for Kidneys and TB from: Case1: Planar and SPECT, Case2a: ^{177}Lu1+^{177}Lu2 and Case 2b: ^{177m}Lu for Patient 7

Therefore, the absorbed dose based on the Planar and SPECT method, for the kidneys is 2.9 Gy and for the TB, 0.9 Gy. The method based on the images and NaI(Tl) based measurements the absorbed dose results to be for the kidneys 3.7 Gy and for the total body 1.0 Gy. The absorbed doses for the TB activity and for Kidneys for six (6) patients, are shown in the plots below:

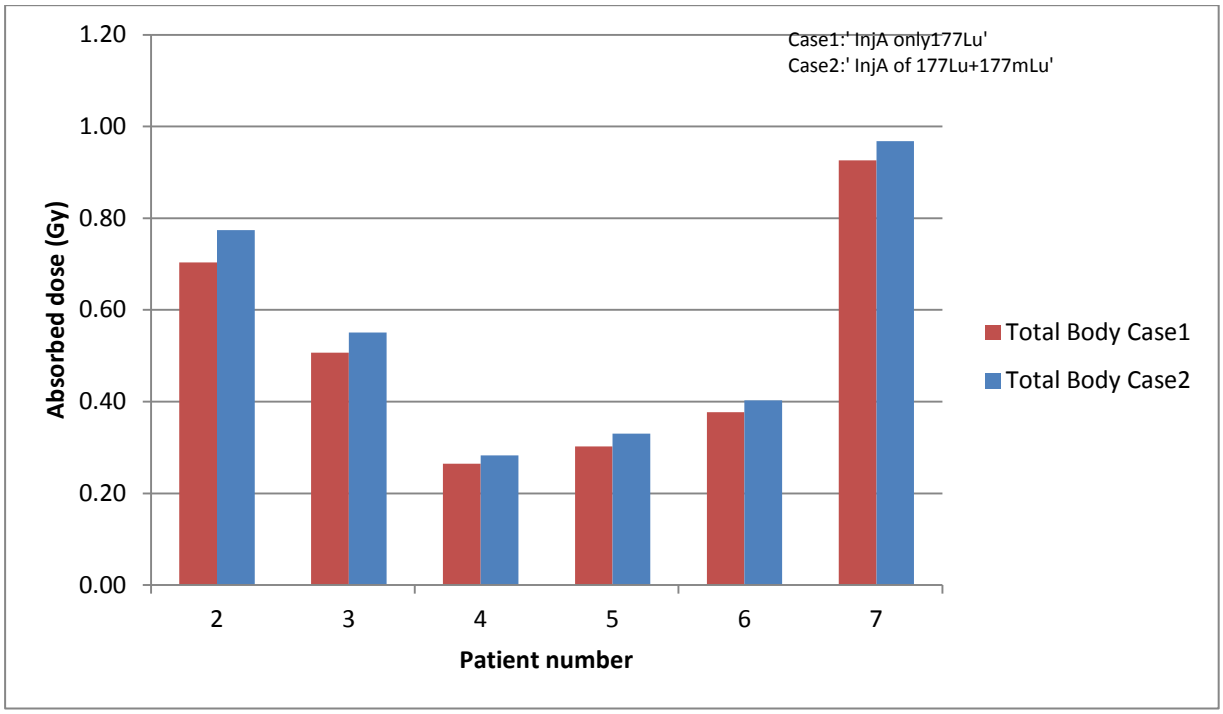

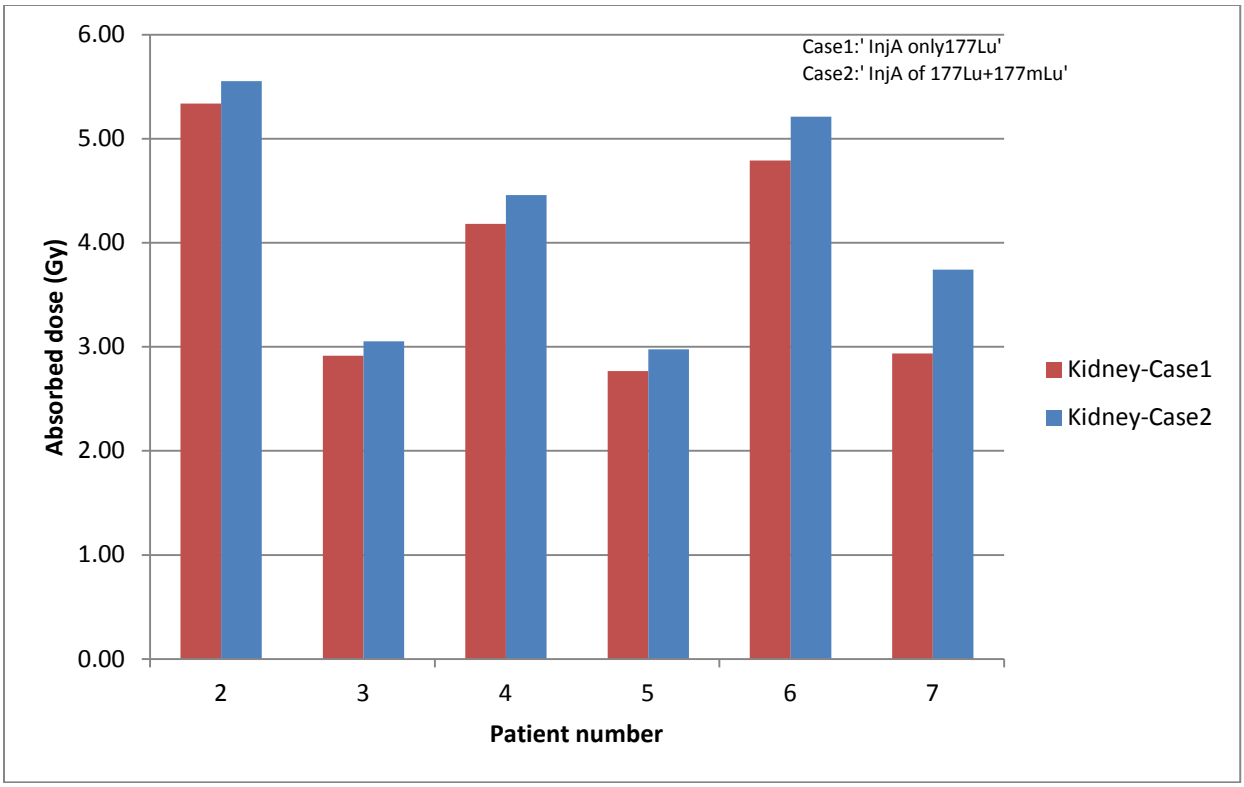

Fig.29, Plot on Absorbed doses from patients in TB and Kidneys

Thus, as seen in the plot for the "Case1" the absorbed dose for the total body shows a higher activity for Patient 7 with 0.9 Gy, Patient 2 with 0.70 Gy, Patient 3 with 0.5 Gy while comparing to the above mentioned Patient 6 and 4 the absorbed fraction ranges from 0.3-0.4 Gy. Meanwhile as regards to the kidney absorbed dose patient 2 with the highest absorbed dose of 5.3 Gy and the lowest absorbed dose for patient 5. Similarly for "Case 2".

XV. Discussion

The Activity determination for the TB for specific geometry varies and depends on the detector systems used, time point and measurement time. As seen above *(under Results Chapter)* different Activity [MBq] have been administrated to the patients who were part of this research study, ranging from the lowest of 7145 MBq to the highest Activity of 7545 MBq.

The data analysis shows that even after the 2nd time point measurement, after 34 days still there is a measurable activity in the TB, more specifically as seen in Patient no.2. Furthermore, for the same case at 3rd time point of the measurement conducted after 61 days (from the radiotherapy administration date), there is still a measurable activity.

The research addresses a question what is the impact of ^{177m}Lu fraction at this time point taking into account an approximate 2 month period from the administration?. Moreover, when would be the time point that this high activity would not be present in the TB? For this purpose a better and reliable conclusion would be to perform images at a later time point, by estimating the activity concentration, its distribution and dose organs activity.

However, taking into account that the existing activity of ^{177}Lu and ^{177m}Lu at 208 keV peak by considering the contribution of both activities as sum between each of the radionuclides and based on the decay scheme of ^{177m}Lu, it shows that the activity of ^{177}Lu is a basis generating from two sources:

- ✓ The radionuclide production of ^{177}Lu; and
- ✓ The ^{177}Lu which is build-up as a product of the decay of the ^{177m}Lu

Encountering the Activity of ^{177}Lu at injected time in MBq assuming the 0.05% impurity (as a worse case "scenario"), the ^{177m}Lu activity from total activity of the ^{177}Lu , one can estimated by the Radionuclide Purity (RNP):

$$RNP = \frac{A_{177Lu}}{A_{Total}} \cdot 100\% \qquad (28)$$

From the radionuclide administration for instance with 7400 MBq at day 30 the activity of ^{177}Lu1 is 337.23 MBq, Activity of ^{177m} Lu is 3.25 MBq, and total Activity including all the contributing terms is 341.18 MBq. Furthermore, the fraction of total Activity for ^{177m}Lu is 0.01 at day 30 and increases over time, and at day 76 it "matches" the ^{177}Lu, while being 0.43, at the time point when the activity of ^{177}Lu is only 2.96 MBq and ^{177m}Lu activity is 2.66 MBq and it starts to dominate at a later time point where the fraction of total activity will be 0.75, and the Activity of ^{177}Lu is 0.28 MBq, while the Activity of ^{177m}Lu remains 2.41 MBq. Additionally, the ^{177}Lu2 is 0 until day 40 and it increases in a small fraction over time, by *"matching"* the ^{177}Lu at day 91 when the Activity of ^{177}Lu is only 0.63 MBq and the Activity of ^{177m}Lu is 2.50 MBq. It increases in a small fraction over time.

XVI. Conclusions

Based on the key findings up to this stage of the research project, the Activity distribution at different time points and the prediction of renal retention toxicity is of complex issue. Within this context, further research is essential, by implying additional investigation methods, in order to bring the major conclusions and answer specific research questions within this frame.

Performing the measurements with both NaI(TI) and HPGe detectors for all time points would provide a better estimation and a reliable results on the measurements performed until this stage of the project. Also, a specific time point for all measurements would better address the activity distribution of ^{177}Lu. As already discussed in the chapter above (under Results) the administrated Activity with ^{177}Lu of a slight difference from patient to patient, and the 2nd time point measurement was varying between all. Therefore, having a *'fixed'* time point possibility for the measurements, for instance: one month after the treatment, would allow accurate conclusions driven by results.

By taking the long-term retention of ^{177}Lu /^{177m}Lu into account, we have estimated that the absorbed dose values for patients should be increased by on average 8±2 % for the total-body and 10±8 % for the kidneys. It is acknowledged that these estimates are based on a worst case scenario, since we have assumed that the amount of 177mLu is 0.05% of the total activity at the time of radionuclide production. Also the assumption has been made that the activity distribution at the late time point measurement is the same in the patient body, as it was on the 7th day after activity administration. An interesting future improvement may be to make an image of the radionuclide distribution at a late time point. By any means, there is still activity in the patient body that can be measured at 30 days after administration, and the current work has made calculations based on these measurements, to estimate the absorbed dose including these new long-term retention measurements.

ACKNOWLEDGEMENT

My deepest gratitude and thanks to my supervisor Mrs. Katarina Sjogreen Gleisner and co-supervisor Mr. Erik Larsson for their supervision and constructive advice and guidance during all times. I would also like to express my thanks to prof. Carl-Erik Magnusson and prof. Michael Ljungberg for their insightful comments.

My grateful acknowledgements to the Lund Hospital University personnel at the Oncology Department for their continuous help and their good understanding for my experimental work. Also, my sincere appreciation and thanks to the Patients who with no hesitation accepted to be part of this research study. Without them it would not be able for me to conduct my research.

My special acknowledgement to my family for their continuous support, encouragement and their patience.

REFERENCES

[1] *Raffaella Brone, Francoise Borson-Chazor, et* al, Renal Toxicity with 90Y DOTATOC-Relevance of Kidney Volume and Dose Rate in finding the Dose Effect Relationship vol. 46 no1, January 2005: 99s-106s

[2] *Marion de Jong, Wout A.P Breeman, Bert F. Bernard et al*,Tumor uptake of the radiolabelled somatostatin analogue (DOTAtyr3)Octreotate is dependent on the peptide amount, 26, 16 February 1999: 693-698

[3] Marison de Jong, Wout A.P. Breeman, Bert F. Bernard, et al, Tumor Response After [^{90} Y-DOTA^{0}, Tyr^{3}]- Octreotide Radionuclide Therapy in a Transplantable Rat Tumor Model Is Dependent on Tumor Size,: 42, 2001: *1841–1846*

[4] *Michael G. Stabin, A. Bertrand Brill,* State of the Art in Nuclear Medicine Dose Assessment, 0001-38, 2008: *308-320*

[5] *Stefan E Pool, Eric P. Krenning, Gerben A Koning, et al,* Preclinical and Clinical Studies of Peptide Radionuclide Therapy ,.001, 2009: *209-218*

[6] *Jason S. Lewis, Mu Wang, Richard Laforest, et al,* Toxicity and Dosimetry of ^{177} Lu –DOTA-Y3-OCTREOTATE in a Rat Model, 94, 2001**:** *p873–877*

[7] *Eric Vegt, Marion de Jong, Jack F.M. Wetzels,* et al, Renal Toxicity of Radiolabelled Peptides and Antibody Fragments: Mechanisms, Impact on Radionuclide Therapy, and Strategies for Prevention .51: DOI: 10.2967/jnumed.110.075101; *p1049–1058*

[8] *Eric Vegt, Marleen Melis, Annemarie Eek, Manique de Visser,* Renal uptake of different radiolabelled peptides is mediated by megalin: SPECT and biodistribution studies in megalin-deficient mice, DOI 10.1007/s00259-010-*1685-9*

[9] *P.J. Wallbrink, D.E. Walling, Q. He; F.Zapata (ed),* Radionuclide Measurement using HPGe Gamma Spectroscopy,*. Handbook for the assessment of soil erosion and sedimentation using environmental radionuclides,* 67–96*.* 2002 *IAEA.*

10] *S.Deepa, K. Vijay Sao, R. Gowrishankar, K. Venkataramaniah,* The 160.44 day ^{177m} Lu as a new gamma calibration standard, 2011.11.006, 81, 2012: *226–231*

[11] *Mark Konijenenberg, Marleen Melis, et al,* Radiation Dose Distribution in Human Kidneys by Octreotides in Peptide Receptor Radionuclide Therapy, 48, 2007:*134–142*

[12] *B.E. Zimmerman, T. Altzitzoglau, A.Antohe, et al,* Results of an international comparison for the activity measurement of ^{177}Lu, DoI: 10.1016 /j.apradiso.2012.02.014

[13] *Bodei L, Cremonesi M, Grana C et al,* Receptor radionuclide therapy with90Y Tyr3 Octreotide in neuroendocrine tumors, *31(7), 2004: 1038-46*

[14] Technical Reports Series no.458 – STI/DOC/010/458 ISBN 92-0-115106-3

[15] *W.H. Bakker, W.A.P.Breeman, D,J.Kwelleboom,et al,* Practical aspects of peptide receptor radionuclide therapy with [^{177}Lu][DOTA^{0} , Tyr^{3}]octreotate, , Vol50, no4, 2006; *265-71*

[16] *Zuzana Dvorakova,* Production and chemical processing of ^{177} Lu for nuclear medicine at the Munich research reactor FRM-II

[17] *B.E. Zimmerman, T. Altzitzoglou, A. Antohe et la*, Results of an international comparision for the activity measurement of ^{177}Lu, 10: 1016/japradiso.2012.02.014

[18] *S. Pomme´ n, J.Paepen, T.Altzitzoglou, R.VanAmmel, E.Yeltepe,* Measurement of the ^{177} Lu half-life :Doi:10.1016/j.apradiso.2011.04.021

[19] F.G. *Kondev, I.Ahmad, M.P.Carpenter, et al,* Gamma-ray emission probabilities in the decay of ^{177m} Lu, Doi:10.1016/j.apradiso.2012.02.029 (2012)

[20] *Mauro S. Dias, Fabricio F.V. Silva, et al,* .Standardization and measurement of gamma-ray probability per decay of ^{177} Lu, doi:10.1016/j.apradiso.2009.12.023

[21] *Marta Cremonesi, Mahila Ferrari et al,* Dosimetry in Peptide Radionuclide Receptor Therapy: A review*; 47, 2006: *1467–1475*

[22] *R. Henkelmann, A.Hey, O.Buck, K. Zjernosekov, T. Nikula*, Radiation Protection Aspects related to Lutetium 177 Use in Hospitals & Products/Lu-177 Trichloride – GMP produced *ITG*

[23] *I.Hossain et al,* Efficiency and resolution of HPGe and NaI (TI) detectors using gamma-ray spectroscopy, Vol. 7(1), January 2012: p 86-89

[24] *M. Moszyński ,* Energy Resolution of Scintillation Detectors - PL 05-400 Otwock-Świerk, Poland

[25] *Hasting A Smith, Jr. and Marcia Lucas*, Gamma – Ray Detection *p.3-64*

[26] *Roelf Valkema, Stanislas A. Pauwels et al,* Long-Term Follow Up of Renal Function after Peptide Receptor Radiation Therapy with 90YDOTA, Tyr3-Octreotide and 177Lu-DOTA-Tyr-Octreotate , Vol 46, 1 suppl, 2005 83s-91s

[27] *A.L. Seidel*, ϒ-Ray Spectroscopy , Nov13,2008

[28] *Kondev. F.G. et al,* Gamma-ray emission probabilities in the decay of 177mLu Appl. Radiat.Isotopes (2012)

[29] *J.J/ Bevelacqua Bevelaqua* ,Internal Dosimetry Primer, *Resources Vol 22, No. 5 - 2005: p7-17*

[30] *Michael Lassmann, L.Strigari, Manuel Bardies,* Dosimetry is Alive and Well, Vol 25, no 5, DOI: 10.1089/cbr.2010.0874, 2010: *p.593-595*

[31] *Barry W. Wessels, Roger G. Dale, et al,* Renal Dosimetry, Vol 25, no 5; Inc. DOI: 10.1089/cbr.2010.0867, 2010: *p. 597-599*

[32] *Jeffry A. Siegel, Michael G. Stabin, Robert M. Sharkey,*Renal Dosimetry: Ready for Bilogical Effective Dose*?,* Vol 25, no 5, DOI: 10.1089/cbr.2010.0851, 2010: *p. 589-591*

[33] *Erik Vekt, et al,* Renal uptake of different radiolabelled peptides is mediated by malign SPECT and biodistribution studies in maligh deficient mice, DOI 10.1007/s00259-010-1685-9, 2010

[34] *Jeffry A. Soegel et al*, Renal Dosimetry in Peptide Radionuclde Therapy,Vol 25 n5, 2010: 581-588

[35] *Rafaela Barone, et al*, Renal Toxicity with 90Y DOTATOC-Relevance of Kidney Volume and Dose Rate in finding the Dose Effect Relationship, vol 46no1, 2005:99s-106s

[36] *Michael G. Stabin et al,* State of the Art in Nuclear Medicine Dose Assessment, 0001-2998/08/$, 2008: 308-320

[37] *Micheal G. Stabin,* Uncertainties in Internal Dose Calculations for Radiopharmaceuticals, Vol. 49, No. 5: 49:853–860 DOI: 10.2967/jnumed.107.048132 (May 2008)

[38] *Glenn F. Knoll* , Radiation Detection and Measurement - *4th Edition*

[39] Syed Naeem Ahmed , Physics and Engineering of Radiation Detection

[40] *Frank H. Attix* , Introduction to Radiological Physics and Radiation Dosimetry,

41] http://www.ohio.edu/people/piccard/radnotes/clinical.html

[42] ENSDF Decay Data in the MIRD (Medical Internal Radiation Dose) Format for ^{177}Lu

[43] Derivations from Supervisors - Medical Radiaction Physics –Lund University

[44] Advanced Technilogy for a Safer World Detective-EX and Detective-DX HPGe-based hand-held Radioisotope Identifiers (REF)

[45] Discovery VH Integrated Hubrid SPECT-PET/CT system S8005LM Millenium VG8/CoDe-VC/Hawkeye Integrated with eNTEGRA P&R workstation, GE Medical Systems

[46] Saha G, Radioactive Decay and Interaction of Radiation with Matter (in basics of PET imaging ..2005 Springer Science Business Media inc.

Further Reading:

Miclael G. Stabin et al, Radiation Dosimetry: Formulations, Models, and Measurements, DOI: 10.1007/978-3-540-85962-8-8, 2011: *p129-144*

Lisa Bodei, Marta Cremonesi, Chiara Grana, et al, Receptor radionuclide therapy with ^{90}Y-[DOTA]^{0} –Tyr^{3} –octreotide (^{90}Y-DOTATOC) in neuroendocrine tumors, Vol. 31, No. 7, July 200, 19May2004: *p1038-1046*

Jeffry A, Siegel, Micheal G. Stabin, et al, Renal Dosimetry in Peptide Radionuclide Receptor Therapy, Vol 25, no 5, 10.1089/cbr.2010.0805, 2010; *p581-589*

Raffaella Barone, Francoise Borson-Chazot, Roelf Valkema, et al, Patient-Specific Dosimetry in Predicting Renal Toxicity with ^{90} Y- DOTATOC: Relevance of Kidney Volume and Dose Rate in Finding a Dose-Effect Relationship, Vol: 46, no. 1, January 2005: *p99s-106s*

Marion de Jong, Wout A.P. Breeman, Bert F. Bernard, et la, Tumor Uptake of the radiolabelled somatostation analogue [DOTA^{0} , Tyr^{3}], octreotide is dependent on the peptide amount, 26, 1999: *p693–698*

Roelf Valkema, Stainslas A. Pauwels, Larry K. Kvols, Dik J. Kwekkeboom, et al, Long-term follow-up of Renal Function After Peptide Receptor Radiation Therapy with ^{90} Y-DOTA^{0} , Tyr^{3} – Octreotide and ^{177} Lu-DOTA^{0}, Tyr^{3}-Octreotate 46, 2005:*p83S–91S*

Kartsen Kossert, Ole J. Nahle, Oliver Ott, et al, Activity determination and nuclear decay data of ^{177} Lu, doi:10.1016/j.apradiso.2012.02.104: *p1-7*

Barry W. Vesels, Mark W. Konijenenberg, Roger G. Dale, et al, MIRD Pamphlet No.20: The Effect of Model Assumptions of Kidney Dosimetry and Response – Implications for Radionuclide Therapy*, Vol. 49 - No. 11: 2008; 49:*p1884–1899*

Wesley E. Bloch, Keith F Eckerman, George Sgouros,et al, MIRD Pamphlet No. 21: A Generalized Schema for Radiopharmaceutical Dosimetry—Standardization of Nomenclature,50, 2009: *p477–484*

ICRU REPORT 32 – Methods of Assessment of Absorbed Dose in Clinical Use of Radionuclides*(International Commission on Radiation Units and Measurements 7910 Woodmont Avenue Washington DC 20014, U.S.A)*

Robert Loevinger; Thomas F. Budinger and Evelyn E. Watson, MIRD Primer for Absorbed Dose *Calculations, 1991*

APPENDICES

APPENDIX I	Data on Measurements from Maestro (available on-line)
APPENDIX II	Radioisotope Decay, Mean energy and Frequency (available on-line)
APPENDIX III	Energy Resolution
APPENDIX IV	Activity of Reference Sources
APPENDIX V	Theoretical assumption of ^{177}Lu and ^{177m}Lu Activity
APPENDIX VI	Determination of the activity of different source activity components (177Lu and 177mLu) from gamma spectroscopy data in 208 keV photopeak window
APPENDIX VII	Photopeak Efficiency
APPENDIX VIII	Standard Deviation
APPENDIX IX	Distance Estimation for measurement with NaI(Tl)
APPENDIX X	Summary on previous measurements with HPGe
APPENDIX XI	Summary on 177Lu sheets from IDB
APPENDIX XII	Schedule on Patient Measurements

APPENDIX III ENERGY RESOLUTION

NaI(Tl) detector and HPGe detector

-Manual Calculation

NaI(Tl)										
Radioisotope	Energy KeV	Full Peak	Scatter Background	Peak height above bkg	Counts at half max	Energy @Ex1 [keV]	Energy @Ex2 [keV]	FWHM	ΔE	ΔE (%)
^{57}Co	122	3208	1626	1582	2417	114	126	12	0.098	9.84
^{133}Ba	208	3027	364.5	2662.5	1695.75	195	214	19	0.091	9.13
^{137}Cs	662	1328	168.0	1160.0	748	639	684	45	0.067	6.80
HPGE										
Radioisotope	Energy KeV	Full Peak	Scatter Background	Peak height above bkg	Counts at half max	Energy @Ex1 [keV]	Energy @Ex2 [keV]	FWHM	ΔE	ΔE (%)
^{57}Co	122	294	37	257	165.5	120	123	3	0.0245	2.46
^{133}Ba	208	7028	36.5	6991.5	3532.25	207.17	208.61	1.44	0.0069	0.69
^{137}Cs	662	310	45	265	177.5	660	663	3	0.0045	0.45

- *Maestro Calculation*

NaI(Tl)				
Radioisotope	Energy KeV	FWHM	ΔE	ΔE (%)
^{57}Co	122	13.29	0.1089	10.89
^{133}Ba	208	4.11	0.0197	1.98
^{137}Cs	662	24.35	0.0367	3.68
HPGe				
Radioisotope	Energy KeV	FWHM	ΔE	ΔE (%)
^{57}Co	121.94	1.28	0.0104	1.05
^{133}Ba	208.39	1.46	0.0070	0.70
^{137}Cs	661.65	1.65	0.0024	0.25

Model calculation from ^{137}Cs

NaI(Tl) I			
Radioisotope	Energy KeV	ΔE (%) - Manual	ΔE (%) - Maestro
^{57}Co	122	15.83	8.57
^{133}Ba	208	12.13	6.56
^{137}Cs	662	6.80	3.68
HPGe			
Radioisotope	Energy KeV	ΔE (%) - Manual	ΔE (%) - Maestro
^{57}Co	122	1.06	0.58
^{133}Ba	208	0.81	0.44
^{137}Cs	662	0.45	0.25

APPENDIX IV ACTIVITY OF REFERENCE SOURCES

Radioactive source		Original Activity	Half life	Original date	Elapsed time	Formula	Λ	Activity [MBq]	Activity [Bq]
NaI(Tl)									
^{57}Co		22.2 MBq	272 days	01.02.2006	2296 days	A=Ao*e^-λt	0.0693 days^-1	0.06	63871.29
^{133}Ba		4.31 MBq	3832.5 days	25.03.2002	3705 days			2.21	2205271.02
^{133}Ba		8.62 MBq	3832.5 days	25.03.2002	3705 days			4.41	4410542.05
^{137}Cs		346 kBq	30.7 years	8.2003	9.5 years			0.28	279205.19
HPGe									
^{57}Co		7.4 MBq	272 days	01.02.2006	2338 days	A=Ao*e^-λt	0.0693 days^-1	0.02	19129.42
^{57}Co		14.8 MBq	272 days	01.02.2006	2338 days			0.04	38258.84
^{57}Co	*	22.2 MBq	272 days	01.02.2006	2338 days			0.06	57388.26
^{133}Ba		4.31 MBq	3832.5 days	25.03.2002	3737 days			2.19	2188582.95
^{133}Ba		8.62 MBq	3832.5 days	25.03.2002	3747 days			4.38	4377165.91
^{137}Cs		346 kBq	30.7 years	08.2003	9.5 years			0.28	279205.20

APPENDIX V THEORITICAL ASSUMTION OF ^{177}Lu and ^{177m}Lu Activity determination

^{177}Lu					^{177m}Lu				
Ao ^{177}Lu [MBq]	Half-life ^{177}Lu [h]	λ [1/h]	Elapsed time[h]	A (^{177}Lu) [MBq]	Ao ^{177m}Lu [MBq]	Half-life ^{177m}Lu [hours]	λ [1/h]	Elapsed time [h]	A (^{177m}Lu) [MBq]
			24	6672.44				24	3.68
			48	6019.43				48	3.67
			72	5430.32				72	3.65
7396.3	161.52	0.00429	96	4898.87	3.7	3849.6	0.00018	96	3.64
			120	4419.43				120	3.62
			144	3986.92				144	3.61
			168	3596.73				168	3.59
			192	**3244.73**				192	**3.57**
			216	**2927.17**				216	**3.56**
			240	**2640.70**				240	**3.54**
			264	**2382.26**				264	**3.53**
			288	**2149.12**				288	**3.51**
			312	**1938.79**				312	**3.50**
			336	**1749.04**				336	**3.48**
			360	**1577.87**				360	**3.47**
			384	**1423.45**				384	**3.45**
			408	**1284.14**				408	**3.44**
			432	**1158.46**				432	**3.42**
			456	**1045.09**				456	**3.41**
			480	**942.81**				480	**3.39**
			504	**850.54**				504	**3.39**
			528	**767.30**				528	**3.36**
			552	**692.20**				552	**3.35**
			576	**624.46**				576	**3.34**
			600	**563.35**				600	**3.32**
			624	**508.21**				624	**3.31**
			648	**458.48**				648	**3.29**
			672	**413.61**				672	**3.28**
			696	**373.13**				696	**3.26**
			720	**336.61**				720	**3.25**
			744	**303.67**				744	**3.24**

APPENDIX VI

Determination of the activity of different source activity components (^{177}Lu and ^{177m}Lu) from gamma-spectroscopy data in the 208 keV photopeak window

Both ^{177m}Lu and ^{177}Lu emit 208 keV gamma photons. In addition, due to the isomeric transition in the decay of ^{177m}Lu, a secondary amount of ^{177}Lu is being built up.

The measured count ratein the 208 keV energy window is thus due to:

a. ^{177}Lu nuclei that are directly obtained from radionuclide production, whose activity at time *t* we denote $A_{177Lu1}(t)$.
b. ^{177m}Lu nuclei that are directly obtained from radionuclide production. These nuclei may decay though either β^--decay or isomeric transition. We denote the activity by $A_{177mLu}(t)$.
c. ^{177}Lu being built up in the isomeric transition branching of ^{177m}Lu. This activity we denote $A_{177Lu2}(t)$.

Directly after radionuclide production no ^{177}Lu has yet been produced by ^{177m}Lu. Let t_{ref} be the reference time for the radionuclide production of the radionuclide. The activity $A_{177Lu2}(t_{ref})$ is thus zero.If we by *RNP* denote the fraction of the total activity that is ^{177}Lu at t_{ref} (which according to the producer is > 0.9995, i.e. the amount of ^{177m}Lu < 0.0005), then for each of **a**-**c** above we get:

$$A_{177Lu1}(t_{ref}) = RNP \cdot \{A_{177Lu1}(t_{ref}) + A_{177mLu}(t_{ref})\} = RNP \cdot A_{Tot}(t_{ref}) \quad (1)$$

$$A_{177mLu}(t_{ref}) = (1 - RNP) \cdot \{A_{177Lu1}(t_{ref}) + A_{177mLu}(t_{ref})\} = (1 - RNP) \cdot A_{Tot}(t_{ref}) \quad (2)$$

$$A_{177Lu2}(t_{ref}) = 0 \quad (3)$$

At an arbitrary time, t_m, after radionuclide production we get the following activities:

$$A_{177Lu1}(t_m) = RNP \cdot A_{Tot}(t_{ref}) \cdot \ exp(-\lambda_{177Lu} t_m) \quad (4)$$

$$A_{177mLu}(t_m) = (1 - RNP) \cdot A_{Tot}(t_{ref}) \cdot exp(-\lambda_{177mLu} t_m) \quad (5)$$

$$A_{177Lu2}(t_m) = \frac{0.217\ A_{177mLu}(t_{ref})\ \lambda_{177Lu}}{\lambda_{177Lu} - \lambda_{177mLu}} \cdot \{exp(-\lambda_{177mLu} t_m) - exp(-\lambda_{177Lu} t_m)\} \quad (6)$$

where the latter equation results since the rate of decay of $^{177}Lu_2$ is governed by the rate of decay of ^{177m}Lu, as can be seen by solving the differential equations governing serial decay. The factor 0.217 is the probability that ^{177m}Lu decays by isometric transition.

The measured count rate from a point source in air, at time t_m, in the 208 keV photopeak energy window is a sum of the count rates due to each component:

$$R_{208}(t_m) = R_{208,177mLu}(t_m) + R_{208,177Lu1}(t_m) + R_{208,177Lu2}(t_m) = \quad (7)$$

$$= \{A_{177mLu}(t_m) \cdot\ n_{\gamma,208,177mLu} + A_{177Lu1}(t_m) \cdot\ n_{\gamma,208,177Lu} + A_{177Lu2}(t_m) \cdot\ n_{\gamma,208,177Lu}\} \cdot \epsilon_{208} \cdot \frac{S}{4\pi D^2}$$

We now describe the relative contribution to the count rate from the different sources of 208 keV photons. Since the energy is the same (208 keV), and since measurement of these 208 keV photons is made in one geometry, we will further on omit the factors $\epsilon_{208} \cdot \frac{S}{4\pi D^2}$ and write the equations in terms of fractions of the total photon emission rate$N_{208,Tot}(t_m)$ (number of emitted 208 keV photons per second), as given by:

$$N_{208,Tot}(t_m) = N_{208,177mLu}(t_m) + N_{208,177Lu1}(t_m) + N_{208,177Lu2}(t_m) \quad (8)$$

$$= A_{177mLu}(t_m) n_{\gamma,208,177mLu} + A_{177Lu1}(t_m) n_{\gamma,208,177Lu} + A_{177Lu2}(t_m) n_{\gamma,208,177Lu}$$

$$= (1 - RNP) \cdot A_{Tot}(t_{ref}) \cdot exp(-\lambda_{177mLu}\, t_m) \cdot\ n_{\gamma,208,177mLu} + RNP \cdot A_{Tot}(t_{ref}) \cdot exp(-\lambda_{177Lu} t_m)\ \cdot n_{\gamma,208,177Lu}$$
$$+ \frac{0.217 \cdot\ (1 - RNP) \cdot A_{Tot}(t_{ref})\ \cdot\ \lambda_{177Lu}\ \cdot n_{\gamma,208,177Lu}}{\lambda_{177Lu} - \lambda_{177mLu}} \{exp(-\lambda_{177mLu} t_m) - exp(-\lambda_{177Lu} t_m)\}$$

We form the ratios, *F*, of the rates of photon emission of each of the components **a**-**c**to the total photon emission rate:

$$N_{177Lu1}(t_m) = N_{208,Tot}(t_m) \cdot \left(\frac{N_{177Lu1}(t_m)}{N_{208,Tot}(t_m)}\right) = N_{208,Tot}(t_m) \cdot F_{177Lu1}(t_m) \tag{9}$$

$$N_{177mLu}(t_m) = N_{208,Tot}(t_m) \cdot \left(\frac{N_{177mLu}(t_m)}{N_{208,Tot}(t_m)}\right) = N_{208,Tot}(t_m) \cdot F_{177mLu}(t_m) \tag{10}$$

$$N_{177Lu2}(t_m) = N_{208,Tot}(t_m) \cdot \left(\frac{N_{177Lu2}(t_m)}{N_{208,Tot}(t_m)}\right) = N_{208,Tot}(t_m) \cdot F_{177Lu2}(t_m) \tag{11}$$

For source component **a**:

$$F_{177Lu1}(t_m) = \frac{N_{177Lu1}(t_m)}{N_{208,Tot}(t_m)} = \left(\frac{N_{208,Tot}(t_m)}{N_{177Lu1}(t_m)}\right)^{-1} \tag{12}$$

with

$$\frac{N_{208,Tot}(t_m)}{N_{177Lu1}(t_m)} = \Bigg[(1-RNP)\cdot A_{Tot}(t_{ref})\cdot exp(-\lambda_{177mLu}\,t_m)\cdot\ n_{\gamma,208,177mLu} + RNP\cdot A_{Tot}(t_{ref})\cdot exp(-\lambda_{177Lu}t_m)\cdot\ n_{\gamma,208,177Lu} + \frac{0.217\ (1-RNP)*A_{Tot}(t_{ref})\lambda_{177Lu}n_{\gamma,208,177Lu}}{\lambda_{177Lu}-\lambda_{177mLu}}\{exp(-\lambda_{177mLu}t_m)-exp(-\lambda_{177Lu}t_m)\}\Bigg] \Big/ \left[RNP*A_{Tot}(t_{ref})\right]\cdot exp(-\lambda_{177Lu}t_m)\cdot\ n_{\gamma,208,177Lu}$$

$$=1+\left(\frac{n_{\gamma,208,177mLu}}{n_{\gamma,208,177Lu}}\right)\left[\frac{1-RNP}{RNP}\right]\cdot\left\{exp\left((\lambda_{177Lu}-\lambda_{177mLu})t_m\right)\ +\left[\frac{\lambda_{177Lu}\ 0.217}{\lambda_{177Lu}-\lambda_{177mLu}}\right]\cdot\left[exp\left((\lambda_{177Lu}-\lambda_{177mLu})t_m\right)-1\right]\right\}$$

For source component **b**:

$$F_{177mLu}(t_m) = \frac{N_{177mLu}(t_m)}{N_{208,Tot}(t_m)} = \left(\frac{N_{208,Tot}(t_m)}{N_{177mLu}(t_m)}\right)^{-1} \quad (13)$$

with

$$\frac{N_{208,Tot}(t_m)}{N_{177mLu}(t_m)} =$$
$$1 + \left(\frac{n_{\gamma,208,177Lu}}{n_{\gamma,208,177mLu}}\right)\left\{\left[\frac{RNP}{1-RNP}\right]\cdot exp\left((\lambda_{177mLu} - \lambda_{177Lu})t_m\right) + \frac{\lambda_{177Lu}0.217}{\lambda_{177Lu} - \lambda_{177mLu}}\cdot\left(1 - exp\left((\lambda_{177mLu} - \lambda_{177Lu})t_m\right)\right)\right\}$$

For source component **c**:

$$F_{177Lu2}(t_m) = \frac{N_{177Lu2}(t_m)}{N_{208,Tot}(t_m)} = \left(\frac{N_{208,Tot}(t_m)}{N_{177Lu2}(t_m)}\right)^{-1} \quad (14)$$

with

$$\frac{N_{208,Tot}(t_m)}{N_{177Lu2}(t_m)} =$$

$$= \frac{(\lambda_{177Lu} - \lambda_{177mLu})\, exp(-\lambda_{177mLu}\, t_m) n_{\gamma,208,177mLu}}{\lambda_{177Lu}0.217\, n_{\gamma,208,177Lu}\left(exp(-\lambda_{177mLu}t_m) - exp(-\lambda_{177Lu}t_m)\right)} + \left[\frac{RNP}{1-RNP}\right]\frac{(\lambda_{177Lu} - \lambda_{177mLu})\, exp(-\lambda_{177Lu}t_m)}{\lambda_{177Lu}0.217\left(exp(-\lambda_{177mLu}t_m) - exp(-\lambda_{177Lu}t_m)\right)} + 1$$

$$= 1 + \frac{(\lambda_{177Lu} - \lambda_{177mLu})}{\lambda_{177Lu}0.217}\left\{\left(\frac{n_{\gamma,208,177mLu}}{n_{\gamma,208,177Lu}}\right)\frac{1}{\left(1 - exp\left((\lambda_{177mLu} - \lambda_{177Lu})t_m\right)\right)} + \left[\frac{RNP}{1-RNP}\right]\frac{1}{\left(exp\left((\lambda_{177Lu} - \lambda_{177mLu})t_m\right) - 1\right)}\right\}$$

The activity of each source component is then given by:

$$A_{177Lu1}(t_m) = \frac{N_{177Lu1}(t_m)}{n_{\gamma,208,177Lu}} = \frac{N_{208,Tot}(t_m)}{n_{\gamma,208,177Lu}} \cdot \left(\frac{N_{177Lu1}(t_m)}{N_{208,Tot}(t_m)}\right) = \frac{R_{208}(t_m)}{\epsilon_{208} \cdot \frac{S}{4\pi D^2}} \cdot \frac{F_{177Lu1}(t_m)}{n_{\gamma,208,177Lu}} \quad (15)$$

$$A_{177mLu}(t_m) = \frac{N_{177mLu}(t_m)}{n_{\gamma,208,177mLu}} = \frac{N_{208,Tot}(t_m)}{n_{\gamma,208,177mLu}} \cdot \left(\frac{N_{177mLu}(t_m)}{N_{208,Tot}(t_m)}\right) = \frac{R_{208}(t_m)}{\epsilon_{208} \cdot \frac{S}{4\pi D^2}} \cdot \frac{F_{177mLu}(t_m)}{n_{\gamma,208,177mLu}} \quad (16)$$

$$A_{177Lu2}(t_m) = \frac{N_{177Lu2}(t_m)}{n_{\gamma,208,177Lu}} = \frac{N_{208,Tot}(t_m)}{n_{\gamma,208,177Lu}} \cdot \left(\frac{N_{177Lu2}(t_m)}{N_{208,Tot}(t_m)}\right) = \frac{R_{208}(t_m)}{\epsilon_{208} \cdot \frac{S}{4\pi D^2}} \cdot \frac{F_{177Lu2}(t_m)}{n_{\gamma,208,177Lu}} \quad (17)$$

APPENDIX VII PHOTOPEAK EFFICIENCY

NaI(Tl) detector										
Reference source	R	Detector diameter [cm]	Source-detector distance [cm]	Photon energy [keV]	n-gamma	A [Bq]	ϵ	Radioisotope	Energy [keV]	Approx. ϵ
^{57}Co	26.03	7.62	74	122	0.856	63871.29	0.718	^{177}Lu	208	0.61
^{133}Ba(1)	387.47			356	0.621	2205271.02	0.427	^{177}Lu	378	0.419
^{133}Ba(2)	784.75			356	0.621	4410542.05	0.433	^{177}Lu	418	0.41
^{137}Ba	60.40			662	0.851	279205.19	0.384	New calibrated ^{177}Lu	208	0.649
HPGe detctor										
^{57}Co (1)	1.916	5	74	122	0.856	19129.42	0.410	^{177}Lu	208	0.293
^{57}Co (2)	3.390			122	0.856	38258.84	0.363	^{177}Lu	378	0.121
^{57}Co (3)	5.655			122	0.856	57388.26	0.403	^{177}Lu	418	0.11
^{133}Ba(1)	40.712			81	0.3406	2188582.95	0.191	New calibrated ^{177}Lu	208	0.412
	7.498			276	0.07164	2188582.95	0.168			
	18.035			302	0.1833	2188582.95	0.158			
	48.396			356	0.6205	2188582.95	0.125			
	6.283			384	0.0894	2188582.95	0.113			
^{133}Ba(2)	85.950			81	0.3406	4377165.91	0.202			
	16.624			276	0.07164	4377165.91	0.186			
	38.703			302	0.1833	4377165.91	0.169			
	106.108			356	0.6205	4377165.91	0.137			
	14.176			384	0.0894	4377165.91	0.127			
^{137}Cs	4.985			662	0.851	279205.19	0.074			

APPENDIX VIII STANDARD DEVIATION - EFFICIENCY

Determination of Standard Deviation - The standard deviation σ_ϵ shows the variation of the obtained results from measurements as an average mean. The calculation of standard deviation for performed measurements has been evaluated using the equation for the detected count rate [45]:

$$R = \frac{AUC_{net}}{t} = A \cdot n_\gamma \cdot \frac{S}{D^2 \cdot 4\pi} \cdot \in \quad \Leftrightarrow \quad \in = \frac{D^2 \cdot 4\pi \cdot AUC_{net}}{A \cdot n_\gamma \cdot S \cdot t}$$

where AUC_{net} is the net area under the peak, and t is the measurement time. The other symbols are as before: *A*=activity in sample, n_γ= the emitted number of photons per decay *S* =surface area of detector, *D*=source-detector distance, and $D^2 \cdot 4\pi$= the solid angle covered by detector.

Derivation: $$\sigma_\epsilon^2 = \left(\frac{\partial \in}{\partial\, AUC_{net}}\right)^2 \cdot \sigma^2{}_{AUC_{net}} + \left(\frac{\partial \in}{\partial t}\right)^2 \cdot \sigma_t^2 + \left(\frac{\partial \in}{\partial A}\right)^2 \cdot \sigma_A^2 + \left(\frac{\partial \in}{\partial n_\gamma}\right)^2 \cdot \sigma_{n_\gamma}^2$$

$$+ \left(\frac{\partial \in}{\partial S}\right)^2 \cdot \sigma_S^2 + \left(\frac{\partial \in}{\partial D}\right)^2 \cdot \sigma_D^2$$

Assuming that:

$$\frac{\partial \in}{\partial\, AUC_{net}} = \frac{D^2 \cdot 4\pi}{A \cdot n_\gamma \cdot S \cdot t} = \frac{\in}{AUC_{net}}$$

$$\frac{\partial \in}{\partial D} = \frac{2D \cdot 4\pi \cdot AUC_{net}}{A \cdot n_\gamma \cdot S \cdot t} = \frac{2}{D} \cdot \epsilon$$

$$\frac{\partial \in}{\partial A} = \frac{D^2 \cdot 4\pi \cdot AUC_{net}}{n_\gamma \cdot S \cdot t} \cdot \left(-\frac{1}{A^2}\right) = -\frac{1}{A} \cdot \epsilon$$

$$\sigma_t^2 = 0$$

$$\sigma_{n_\gamma}^2 = 0$$

$$\sigma_S^2 = 0$$

$$\sigma_\epsilon^2 = \left(\frac{\in}{AUC_{net}}\right)^2 \cdot \sigma^2{}_{AUC_{net}} + \left(\frac{2}{D} \cdot \in\right)^2 \cdot \sigma_D^2 + \left(\frac{\in}{A}\right)^2 \cdot \sigma_A^2 = \in^2 \left\{\left(\frac{\sigma_{\,AUC_{net}}}{AUC_{net}}\right)^2 + \left(\frac{2\sigma_D}{D}\right)^2 + \left(\frac{\sigma_A}{A}\right)^2\right\}$$

The uncertainty in the measured distance was assumed 2 cm. The uncertainty in the net area under the peak was determined from Maestro. In the following table the details of used reference sources are shown, including the reference date and uncertainty, giving σ_A/A

Nuclide	Source no	Activity (kBq)	σ_A/A (%)
^{133}Ba	LW362	368	3
^{137}Cs	LW363	346	3
^{57}Co	LW364	406	3
^{60}Co	LW365	392	3

REFERENCE DATE: 1 AUGUST 2003

Standard Deviation (for used reference sources) – NaI(Tl)							
Radionuclide	Sigma AUCnet	AUCnet	SigmaAUCnet/ AUCnet	2*sigmaD/D	SigmaA/A	Efficiency	Sigma Efficiency
^{57}Co	114	10392	0.01097	0.0541	0.03	0.72	0.045
^{133}Ba (1)	707	152850	0.00463	0.0541	0.03	0.43	0.026
^{133}Ba	1011	312614	0.00323	0.0541	0.03	0.43	0.027
^{137}Cs	271	24097	0.01125	0.0541	0.03	0.38	0.024

Standard Deviation (for used reference sources) – HPGe							
Radionuclide	Sigma AUCnet	AUCnet	SigmaAUCnet/ AUCnet	2*sigmaD/D	SigmaA/A	Efficiency	Sigma Efficiency
^{57}Co (1)	19	573	0.0332	0.0541	0.03	0.410	0.029
^{57}Co (2)	33	1014	0.0326	0.0541	0.03	0.363	0.025
^{57}Co (3)	40	1691	0.0237	0.0541	0.03	0.403	0.027
^{133}Ba (1)	118	11969	0.0099	0.0541	0.03	0.191	0.012
	43	2204	0.0195	0.0541	0.03	0.168	0.011
	70	5302	0.0132	0.0541	0.03	0.158	0.010
	123	14228	0.0086	0.0541	0.03	0.125	0.0078
	41	1847	0.0222	0.0541	0.03	0.113	0.0074
^{133}Ba (2)	186	24839	0.0075	0.0541	0.03	0.202	0.013
	70	4804	0.0146	0.0541	0.03	0.186	0.012
	106	11185	0.0095	0.0541	0.03	0.169	0.011
	173	30665	0.0056	0.0541	0.03	0.137	0.0085
	63	4097	0.0154	0.0541	0.03	0.127	0.0081
^{137}Cs	40	1490	0.0268	0.0541	0.03	0.074	0.0050

APPENDIX IX DISTANCE ESTIMATION for measurements with NaI(Tl)

Efficiency for ^{177}Lu and ^{177m}Lu (distance estimation)			
Photon energy [keV]	**ϵ (CPS/Bq)**	**n-gamma**	**S (cm^2)**
208	0.61	0.11	14.52
378	0.419	0.297	
418	0.41	0.213	

R/A (CPS/Bq)			
Distance	**208**	**378**	**418**
100	7.76E-06,	1.44E-05	1.01E-05
125	4.96E-96	9.20E-06	6.46E-06
150	3.45E-06	6.39E-06	4.49E-06
200	1.94E-06	3.60E-06	2.52E-06
250	1.24E-06	2.30E-06	1.61E-06
300	8.62E-07	1.60E-06	1.12E-06
350	6.33E-07	1.17E-06	8.24E-07
400	4.85E-07	8.99E-07	6.31E-07

Note: Based on the efficiency determination for reference sources

Efficiency for ^{177}Lu and ^{177m}Lu (distance estimation)			
Photon energy [keV]	**ϵ (CPS/Bq)**	**n-gamma**	**S (cm^2)**
208	0.650	0.11	14.52
378	N/A	0.297	
418	N/A	0.213	

Distance	**208**	**378**	**418**
100	8.26E-06	n/a	n/a
125	5.29E-06	n/a	n/a
150	3.67E-06	n/a	n/a
200	2.07E-06	n/a	n/a
250	1.32E-06	n/a	n/a
300	9.18E-07	n/a	n/a
350	6.74E-07	n/a	n/a
400	5.16E-07	n/a	n/a

Note: Based on the efficiency from the new ^{177}Lu sample

APPENDIX X Summary from previous measurements using HPGe detector (close geometry)

Sample Identification:	177Lu no1	177Lu Serie 1 B1	177Lu Serie 1B2	177Lu det 3 no.3	177Lu det 2 no.3	177Lu det 3 no.2	177Lu det 3 no.2	177Lu det 2 no.2	177Lu det 2 no.1	177Lu Serie 1 B3
Sample Description:		Burk 1/3 det 3	Serie 1 det 3							Serie 1 det 3
Sample Type:	60ml-can	60ml-can	60ml-can	1300ml-can-vatska	1300ml-can-vatska	60ml-can	60ml-can	1300ml-can-vatska	60ml-can	60ml-can
Sample size	5,700 E-02 kg	6,419 E-02 kg	6,955 E-02 kg	5,100 E-02 kg	5,100 E-02 kg	5,800 E-02 kg	5,800 E-02 kg	5,800 E-02 kg	5,800 E-02 kg	6,726E-02 kg
Sample Taken On:	2011-09-14 11:01:45	2011-09-14 12:00:48	2011-09-14 12:00:51	2011-09-14 12:54:06	2011-09-14 13:11:42	2011-09-14 12:37:46	2011-09-14 12:12:16	2011-09-14 12:53:21	2011-09-14 12:11:37	2011-09-14 12:00:51
Acquisition Started:	2011-09-08 12:04:26	2012-01-26 09:11:47	2012-01-28 09:43:29	2011-11-08 12:53:46	2011-11-08 13:11:23	2011-11-08 12:37:26	2011-11-08 12:12:58	2011-11-08 12:52:53	2011-11-08 12:12:52	2012-01-26 09:54:48
Procedure:	DET3_60ml-can 1.0 g/cm3	DET3_60ml-can 1.0 g/cm3	DET3_60ml-can 1.0 g/cm3	DET3_60ml-can 1.0 g/cm3	DET2_60ml-can 1.0 g/cm3	DET2_60ml-can 1.0 g/cm3	DET2_60ml-can 1.0 g/cm3	DET2_60ml-can 1.0 g/cm3	DET2_60ml-can 1.0 g/cm3	DET3_60ml-can 1.0 g/cm3
Detector Name:	ADC3	ADC3	ADC3	ADC3	ADC2	ADC3	ADC3	ADC2	ADC2	ADC3
Geometry:	60ml - can 1.0 g/cm3	60ml - can 1.0 g/cm3	60ml - can 1.0 g/cm3	60ml - can 1.0 g/cm3	60ml - can 1.0 g/cm3	60ml - can 1.0 g/cm3	60ml - can 1.0 g/cm3	60ml - can 1.0 g/cm3	60ml - can 1.0 g/cm3	60ml - can 1.0 g/cm3
Live Time:	87.1 s	825,2 s	584,3 s	543,7 s	344,1 s	261,8 s	129,1 s	143,5 s	127,6s	821,3 s
Real Time:	91.0 s	841,2 s	596,3 s	568,0 s	360,4 s	273,7 s	135,0 s	150,5 s	133,7 s	837,1 s
Dead Time	4.29%	1,89%	2.02%	4,28%	4,54%	4,34%	4,33%	4,64%	4,58%	1,89%
Peak Locate Threshold	2.7	2.7	2.7	2.7	2.7	2.7	2.7	2.7	2.7	2.7
Peak Locate Range (in channels):	1-4096	1-4096	1-4096	1-4096	1-4096	1-4096	1-4096	1-4096	1-4096	1-4096
Peak Area Range (in channels):	1-4096	1-4096	1-4096	1-4096	1-4096	1-4096	1-4096	1-4096	1-4096	1-4096
Identification Energy Tolerance:	1000 keV	1000 keV	1000 keV	1000 keV	1000 keV	1000 keV	1000 keV	1000 keV	1000 keV	1000 keV
Energy Calibration Used Done on:	2011-07-04	2011-07-04	2011-07-04	2011-07-04	2011-06-10	2011-07-04	2011-07-04	2011-06-10	2011-06-10	2011-07-04
Efficiency Calibration Used Done on:	2010-02-23	2010-02-23	2010-02-23	2010-02-23	2011-11-08	2010-02-23	2010-02-23	2011-11-08	2011-11-08	2010-02-23
Sample Number:	6410	6398	6405	6418	6417	6413	6412	6414	6411	6409

Sample Identification:	Lu-177 Serie 2 B1	Lu-177 Serie 2 B2	Lu-177 Serie 2B3
Sample Description:	Burk 1/3 det 2	Serie 2 det 2	Serie 2 det 2
Sample Type:	60ml-can	60ml-can	60ml-can
Sample size	6,845 E-02 kg	6,872 E-02 kg	6,816 E-02 kg
Sample Taken On:	2011-09-28 12:00:48	2011-09-28 12:00:51	2011-09-28 12:00:51
Acquisition Started:	2012-01-26 09:11:54	2012-01-26 09:43:35	2012-01-26 09:54:49
Procedure:	DET3_60ml-can 1.0 g/cm3	DET3_60ml-can 1.0 g/cm3	DET3_60ml-can 1.0 g/cm3
Detector Name:	ADC2	ADC2	ADC2
Geometry:	60ml - can 1.0 g/cm3	60ml - can 1.0 g/cm3	60ml - can 1.0 g/cm3
Live Time:	923, 9 s	573,0 s	398,1 s
Real Time:	940,9 s	584,3 s	406,4 s
Dead Time:	1,81 %	1,93%	2.03%
Peak Locate Threshold	2.7	2.7	2.7
Peak Locate Range (in channels):	1-4096	1-4096	1-4096
Peak Area Range (in channels):	1-4096	1-4096	1-4096
Identification Energy Tolerance:	1000 keV	1000 keV	1000 keV
Energy Calibration Used Done on:	2011-06-10	2011-07-04	2011-06-10
Efficiency Calibration Used Done on:	2011-11-08	2010-02-23	2011-11-08
Sample Number:	6402	6406	6407

Summary on Gamma Spectrum – Measurements of ^{177} Lu using HPGe detector *(*Reports from APEX Programme)*

Sample	Date	Time	Sample taken on:	Acquisition started:	Detector Name	Live time	Real time:	Dead time
Lu-177 no1	1/26/2012	10:17:58	9/14/2011 11:01	8-Nov-11	ADC3	87.1 s	91,0 s	4,29%
Lu-177 Serie 1 B1	1/26/2012	9:33:36	9/14/2011 12:00	26-Jan-12	ADC3	825,2 s	841,2 s	1,89%
Lu-177 Serie 1B2	1/26/2012	9:55:16	9/14/2011 12:00	28-Jan-12	ADC3	584,3 s	596,3 s	2.02%
Lu det 3 no.3	1/26/2012	10:36:35	9/14/2011 12:54	8-Nov-11	ADC3	543,7 s	568,0 s	4,28%
Lu 177 det 2 no.3	1/26/2012	10:34:20	9/14/2011 13:11	8-Nov-11	ADC2	344,1 s	360,4 s	4,54%
Lu 177 det 3 no.2	1/26/2012	10:24:36	9/14/2011 12:37	8-Nov-11	ADC3	261,8 s	273,7 s	4,34%
Lu 177 det 3 no.2	1/26/2012	10:20:20	9/14/2011 12:12	8-Nov-11	ADC3	129,1 s	135,0 s	4,33%
Lu 177 det 2 no.2	1/26/2012	10:26:32	9/14/2011 12:53	8-Nov-11	ADC2	143,5 s	150,5 s	4,64%
Lu-177 det 2 no1	1/26/2012	10:20:20	9/14/2011 12:11	9-Nov-11	ADC2	127,6 s	133,7 s	5,48%
Lu-177 Serie 1 B3	1/26/2012	10:14:00	9/14/2011 12:00	10-Nov-11	ADC3	821,3 s	837,1 s	1,89%
Lu-177 Serie 2 B1	1/26/2012	9:44:21	9/28/2011 12:00	26-Jan-12	ADC2	923,9 s	940,9 s	1,81%
Lu-177 Serie 2 B2	1/26/2012	9:58:21	9/28/2011 12:00	26-Jan-12	ADC2	573,0 s	584,3 s	1,93%
Lu-177 Serie 2 B3	1/26/2012	10:09:19	9/28/2011 12:00	26-Jan-12	ADC2	398,1 s	406,4 s	2,03 %

Measurements with HPGe detector system – Instructions from Supervisors*

The spectra from the HPGe detector system were analyzed in APEX using a radionuclide library for 177mLu. A radionuclide library is a list of gamma-peaks, their abundances, and the half-life of the radionuclide, in this case 177mLu. At measurement the detector system was energy-calibrated. Also, the detector efficiency had been previously determined for different measurement geometries. This means that the efficiency given below also encompasses the effects of the measurement geometry, so that the geometry factor that we usually put in ($S/4\pi D^2$) is a now part of the efficiency value $\in$. This thus means that we do not need this geometry factor in the equations.

Determination of activity of 177Lu

If *x* is a gamma-energy that is:

a) present in the decay scheme for 177mLu,
b) is not present in the decay scheme for 177Lu,

c) is well detectable and separable in the measured spectrum.

Its AUC is $AUC_{x,177mLu}$ (unit cps) and the detector efficiency for that energy is ϵ_x, then:

$$AUC_{x,177mLu} = A_{177mLu}(MeasDate) * n_{\gamma,x,177mLu} * \epsilon_x => \quad (1)$$

$$A_{177mLu}(MeasDate) = \frac{AUC_{x,177mLu}}{n_{\gamma,x,177mLu} * \epsilon_x}$$

This activity value is then valid for the date of measurement (MeasDate). Since APEX gives the activity for a reference date (RefDate), the value given in the "nuclide MDA report" is therefore

$$A_{177mLu}(RefDate) = \frac{AUC_{x,177mLu}}{n_{\gamma,x,177mLu} * \epsilon_x} exp(\lambda_{177mLu} * PassedTime) \quad (2)$$

Where "PassedTime" is the time between the measurement and the reference date, and

$$\lambda_{177mLu} = \ln(2)/T_{1/2\_177mLu} \quad (3)$$

So, since there are several peaks, *x*, in the spectra that fulfill the criteria (a)-(c) above, we get several estimates of the activity $A_{177mLu}(RefDate)$ from which we calculate an average to get the final value:

$$A_{177mLu}(RefDate)_{final} = \sum_x A_{177mLu}(RefDate)_x \quad (4)$$

For the 113 keV and the 208 keV peaks the measured AUC are really sums of the contributions from 177Lu and 177mLu activities. For instance for the 208 keV peak:

$$AUC_{208} = AUC_{208,177mLu} + AUC_{208,177Lu} = \quad (5)$$

$$= A_{177mLu}(MeasDate) * n_{\gamma,208,177mLu} * \epsilon_{208} + A_{177Lu}(MeasDate) * n_{\gamma,208,177Lu} * \epsilon_{208}$$

$$= \left(A_{177mLu}(MeasDate) * n_{\gamma,208,177mLu} + A_{177Lu} * n_{\gamma,208,177Lu}(MeasDate)\right) * \epsilon_{208}$$

The activity values given in the Report-list are then not correct since they are calculated by the assumption that it is only 177mLu that is present. If we call the activity value given in the Report-list as B, then according to Equation 2:

$$B = \frac{AUC_{208}}{n_{\gamma,208,177mLu} * \epsilon_{208}} exp(\lambda_{177mLu} * PassedTime) \quad (6)$$

Rearranging (6) we get:

$$\frac{AUC_{208}}{\epsilon_{208}} = B\ n_{\gamma,208,177mLu} exp(-\lambda_{177mLu} * PassedTime) \quad (7)$$

From (5) we see that:

$$\frac{AUC_{208}}{\epsilon_{208}} = \left(A_{177mLu}(MeasDate) * n_{\gamma,208,177mLu} + A_{177Lu}(MeasDate) * n_{\gamma,208,177Lu}\right) \quad (8)$$

This gives:

$$B\ n_{\gamma,208,177mLu} exp(-\lambda_{177mLu} * PassedTime) = \left(A_{177mLu}(MeasDate) * n_{\gamma,208,177mLu} + A_{177Lu}(MeasDate) * n_{\gamma,208,177Lu}\right) \quad (9)$$

Solving for $A_{177Lu}(MeasDate)$ this gives

$$A_{177Lu}(MeasDate) = \quad (10)$$

$$= \frac{1}{n_{\gamma,208,177Lu}}\left(B\ n_{\gamma,208,177mLu} exp(-\lambda_{177mLu} * PassedTime) - A_{177mLu}(MeasDate) * n_{\gamma,208,177mLu}\right)$$

$$= \frac{n_{\gamma,208,177mLu}}{n_{\gamma,208,177Lu}}\left(B\ exp(-\lambda_{177mLu} * PassedTime) - A_{177mLu}(MeasDate)\right)$$

In this equation we can use the value $A_{177mLu}(RefDate)_{final}$ to determine $A_{177mLu}(MeasDate)$. However, we must calculate it to the MeasDate.

$$A_{177Lu}(MeasDate) =$$

$$= \frac{n_{\gamma,208,177mLu}}{n_{\gamma,208,177Lu}}\left(B\ exp(-\lambda_{177mLu} * PassedTime) - A_{177mLu}(RefDate)_{final}\ exp(-\lambda_{177mLu} * PassedTime)\right)$$

$$= \frac{n_{\gamma,208,177mLu}}{n_{\gamma,208,177Lu}} exp(-\lambda_{177mLu} * Passed_{Time})\left(B\ - A_{177mLu}(RefDate)_{final}\ \right) \quad (11)$$

And then we can calculate the activity of 177Lu at the Reference Date:

$$A_{177Lu}(RefDate) \quad (12)$$

$$= \frac{n_{\gamma,208,177mLu}}{n_{\gamma,208,177Lu}} exp(-\lambda_{177mLu} * PassedTime)\left(B\ - A_{177mLu}(RefDate)_{final}\ \right)exp(\lambda_{177Lu} * PassedTime)=$$

$$= \frac{n_{\gamma,208,177mLu}}{n_{\gamma,208,177Lu}} exp\left((\lambda_{177Lu} - \lambda_{177mLu}) * PassedTime\right)\left(B\ - A_{177mLu}(RefDate)_{final}\ \right)$$

APPENDIX XI SUMMARY ON IDB ^{177}Lu SPECIFICATION SHEETS

IDB Radiopharmacy bv					
	1	2	3	4	5
Lot number	12062012A	04062012A	30052012A	24042012B	17042012A
Client code	24012-1	24012-1	24012-1	24012-1	24012-1
Destination			LU Hospital, Sw		
Required Activity (GBq)	18.5	9.3	18.5	9.3	9.3
Required Calibration Date	14.06.2012 (12:00 C.E.T)	07.06.2012 (12:00 C.E.T)	31.05.2012 (12:00 C.E.T)	26.04.2012 (12:00 C.E.T)	19.04.2012 (12:00 C.E.T)
Required Volume (mL)	0.7	0.4	0.7	0.4	0.4
Reference Date	12.06.2012 (19:08 C.E.T)	04.06.2012 (17:00 C.E.T)	30.05.2012 (12:19 C.E.T)	24.04.2012 (12:46 C.E.T)	17.04.2012 (16:21 C.E.T)
Lu-177 activity on reference date (GBq)	23.7	13.6	20.7	15.8	16
Chemical form			LuCl3 Lutetium Trichloride		
Solvent			0.05 M HCl Ph Eur. In WFI		
pH Value	1.4	1.5	1.3	1.5	1.3
Expiration date	26.06.2012 (19:08 C.E.T)	18.06.2012 (17:00 C.E.T)	13.06.2012 (12:19 C.E.T)	08.05.2012 (12:46 C.E.T)	01.05.2012 (16:21 C.E.T)
Lu mass (µg)	31.2	17.7	23.5	17.5	17
Total Volume (mL)	0.7	0.4	0.7	0.4	0.4
Volumetric Activity (GBq/mL)	33.6	38.9	29.5	45.1	45.5
Specific Activity (GBq/mg)	762	770	880	903	938
Lu-177m impurity (act.Lu-177m over Lu-177)			<0.05%		
Other radionuclidic impurities			<0.01%		
Date:	12.06.2012	04.06.2012	30.05.2012	24.04.2012	17.04.2012

APPENDIX XII SCHEDULE ON PATIENT MEASUREMENTS

			MONTHS AND WEEKS																												
			April				May					June					July					August					September				
Initials	PATIENT	M	14	15	16	17	18	19	20	21	22	22	23	24	25	26	27	28	29	30	31	31	32	33	34	35	36	37	38	39	
AA	PATIENT 1	1				X																									
		2														X															
		3																													
TA	PATIENT 2	1					X																								
		2											X																		
		3															X														
CK	PATIENT 3	1											X																		
		2																X													
		3																								X					
MC	PATIENT 4	1											X																		
		2															X														
		3																													
UH	PATIENT 5	1												X																	
		2																X													
		3																						X						X	
SG	PATIENT 6	1													X																
		2																				X									
		3																							X						
IN	PATIENT 7	1													X																
		2																				X									
		3																													

X	measurement performed
X	planned measurement for the week no.
1	measurement done
2	measurement no. example 2 to be performed
3	last measurement not performed